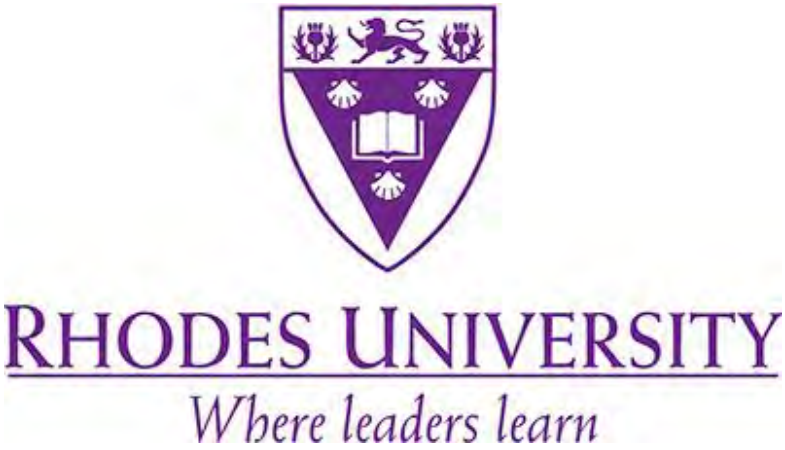

The development of a plate-based assay to detect the activation status of ARF1 GTPase in *Plasmodium falciparum* parasites

Skye du Toit

August 2022

Department of Biochemistry and Microbiology

Abstract

The exponential rise in antimalarial drug resistance in the most infectious malaria species, *Plasmodium falciparum,* has emphasised the urgency to identify and validate novel drug targets that decrease parasite viability upon inhibition. In addition to several publications indicating that the regulation of human Arf1 GTPase activity (mediated by ArfGEFs and ArfGAPs) serves as a pertinent drug target for cancer research, the identification of Arf1 and its regulatory proteins in *Plasmodium falciparum* led to the question whether these protein homologs could be exploited as drug targets for anti-malarial drug therapies. To investigate this prospect, the establishment of a novel *in vitro* colorimetric ELISA-based assay was needed to be able to detect changes in the activation status of *P. falciparum* Arf1 (*Pf*Arf1) in parasite cultures exposed to potential Arf1 inhibitors. By exploiting the selective protein interaction that occurs between active GTP-bound Arf1 and its downstream effector, GGA3, an assay protocol was established that could be used to detect the activation status of purified, truncated *Pf*Arf1 obtained from *E. coli* and endogenous *Pf*Arf1 sourced from parasite lysates. The assay relies on the use of anti-Arf1 antibodies to detect the binding of active *Pf*Arf1 in the lysates of inhibitor-exposed cultured parasites to GST-GGA3 immobilised in glutathione-coated plates. The results from chemical validation experiments conducted using the novel assay developed in this study, using the known ArfGEF inhibitor brefeldin A (BFA) and ArfGAP inhibitors Chem1099 and Chem3050, yielded the anticipated results: decrease in active *Pf*Arf1 after parasite incubation with the ArfGEF inhibitor, and increased active *Pf*Arf1 after ArfGAP inhibition. The results confirmed *Pf*Arf1 as a potential anti-malarial drug target and encourages the further development of this assay format for the identification of subsequent inhibitors in library screening campaigns. Additional pilot experiments were conducted to further explore whether the assay could detect the activation status of human Arf1 using HeLa cell lysates and to provide further evidence that the assay could be exploited as a tool in the identification of Arf1 GTPase inhibitors with BFA and the known ArfGAP inhibitor, QS11. The results suggested that, while the assay can detect the increase in active cellular Arf1 due to the inhibition of human ArfGEF following BFA treatment, subsequent treatment with QS11 showed no evidence of a reduction in active human Arf1 due to ArfGAP inhibition. Further experimentation is required to investigate the ability the assay to confirm inhibition of human Arf1 deactivation by ArfGAP inhibitors and develop the assay as a useful tool to support cancer drug discovery, in addition to antimalarial drug discovery projects aimed at Arf1.

Dedication

I am dedicating this thesis work to my beloved late mum, Stella Swanepoel.

Although you are no longer of this world, it was through your uncompromising faith in my abilities and your relentless encouragement to pursue my Master's that I am where I am today.

I hope I've made you proud.

Acknowledgments

I would like to express my sincerest gratitude to my supervisor, Professor Heinrich Hoppe, for his invaluable encouragement and guidance throughout my post-graduate studies. Not only were you the driving force behind this project, but you have also taught me to find purpose in failure and to interrogate success. I am honoured to have been a part of your research team and am indebted to you for helping me grow into the scientist I am today.

To the present and past research group members, thank you for making the lab a second home and for providing emotional and intellectual support throughout the duration of this project. I would like to extend a special thanks to Tarryn Swart for mentoring me throughout my research and aiding me in the cultivation of several technical skills, including culturing procedures. I could not have completed my research without you. Thank you to the technical administrators and cleaning staff of the Biochemistry and Microbiology department at Rhodes University, your contribution to my academic experience does not go unnoticed.

A heartfelt thanks to my family, near and far, for their faith in my academic ambitions and for their unceasing emotional support in what was to be a taxing couple of years. A special thanks to my dad and little brother, Fanus and Frederik Swanepoel, for always being a phone call away and never failing to lift my spirits. To my loving aunt, Helen Kruuse, thank you for inspiring me to become a Rhodent and for providing me with a surplus of home-made biscuits that honestly, often kept me going. To my devoted grandmother Carol Keep, thank you for shaping me into the woman I am today and inspiring me to be the best version of myself. Finally, to my aunty Zelda du Toit, thank you for always checking in on me and reminding me how lucky I am to have your counsel.

To my partner, Nicholas McMichael, thank you for anchoring me and motivating me behind the scenes. You undoubtedly took the brunt of my frustrations following failed experiments but you never failed to cheer me on. Your unfaltering love and encouragement contributed significantly to the completion of this research project and I look forward to tackling the next chapter of my life with you.

To two of my most cherished friends, Agnese Bastide and Yuchan Park, I'm not sure if I can appropriately describe the impact you both have had on my university experience as a whole… but I will give it my best go. Agnese, my Mauritian firecracker, you have endured a lot these past two years and have remained positive throughout. You inspire me to appreciate the present

and to embrace the uncertainty of the future. In spite of the distance between us, you continue to show your never-ending support and for that, I'm eternally grateful. Mr Park, I often think back to when we first met in Stats 101 on our first day at Rhodes. I would never have imagined that that encounter would flourish into the friendship I still hold dear today. I am privileged to have beared witness to your growth as a person and as a competent biochemist. Thank you for six years' worth of memories and adventures, I have no doubt that there's plenty more to come.

A massive thank you to the National Research Foundation (NRF) for funding my post-graduate studies, I would not have been able to get to where I am today without your financial support.

Table of Contents

List of Abbreviations

WHO	World Health Organisation
GTS	Global technical strategy
Pf	*Plasmodium falciparum*
IRS	Indoor residual spraying
LLIN	Long-lasting insecticidal net
GSK	GlaxoSmithKline
ROS	Reactive oxygen species
MDR	Multidrug resistance
ATP	Adenosine triphosphate
ACT	Artemisinin-based combinational therapy
CRT	Chloroquine resistance transporter
SP	Sulfadoxine-pyrimethamine
PCT	Parasite clearance time
PI4K	Phosphatidylinositol 4-kinase
PPI	Protein-protein interactions
Arf	ADP-ribosylation factor
PLD	Phospholipase D
PI	Phosphatidylinositol
GTP	Guanosine triphosphate
GDP	Guanosine diphosphate
GEF	Guanine-nucleotide exchange factor
GAP	GTPase activating protein
ALPS	ArfGAP1 lipid-packing sensor
COPI	Coat protein complex I
EGFR	Epidermal growth factor receptor
MDCK	Madin-Darby canine kidney
ECM	Extracellular matrix

MAPK	Mitogen-activated protein kinase
EOC	Epithelial ovarian cancer
GGA	Golgi- localised, γ-ear-containing, Arf-binding proteins
AP	Adaptor protein
ER	Endoplasmic reticulum
TGN	Trans-golgi network
VHS	VPS27,Hrs and STAM
AC-LL	Acid-cluster-dileucine
BFA	Brefeldin A
GCA	Golgicide A
GBF1	Golgi BFA resistant guanine nucleotide exchange factor 1
PPI	Protein-protein interaction
BFA	Brefeldin A
MD	Molecular/modelling dynamics
PV	Parasitophorous vacuole
GRASP	Golgi reassembly stacking protein
IC_{50}	Half-maximal inhibitory concentration
GST	Glutathione S-transferase
ELISA	Enzyme-linked immunosorbent assay
E.coli	*Escherichia coli*
OD	Optical density
HEPES	4-(2-hydroxythyl)-1-piperazineethanesulfonic acid
g	Gravitational force
IPTG	Isopropyl β-D-1-thiogalactopyranoside
Hz	Hertz
SDS-PAGE	Sodium dodecyl sulphate–polyacrylamide gel electrophoresis
Ni-NTA	Nickel nitrilotriacetic acid
PBS	Phosphate-buffered saline
PMSF	Phenylmethylsulfonyl fluoride

BSA	Bovine serum albumin
TBS	Tris-buffered saline
His	Histidine
IgG	Immunoglobin G
DTT	Dithiothreitol
EDTA	Ethylenediaminetetraacetic acid
CBNB	1-chloro-2,4-dinitrobenzene
HRP	Horseradish peroxidase
RPMI	Roswell Park memorial institute
RBCs	Red blood cells
DMEM	Dulbecco's modified eagle medium
BCA	Bicinchoninic acid assay
Abs	Absorbance
Da	Dalton
RF-1	Release factor 1
TEMED	Tetramethylethylenediamine
ISF	Induced soluble fraction
IIF	Induced insoluble fraction
USF	Uninduced soluble fraction
UIS	Uninduced insoluble fraction
M	Molecular weight marker
FL	Filtered lysate
FT	Flow through
W1/2	Wash step one or two
EP	Eluted protein
DP	Desalted protein
ELISA	Enzyme-linked immunosorbent assay

List of figures

Chapter 1: Literature review

The development and progression of drug resistance and the consequent need for new antimalarial drugs with emphasis placed on ADP-ribosylation factor 1 as a prospective drug target

Malaria, which has been deemed as one of the most devastating communicable diseases in terms of morbidity and mortality incidence, currently affects 80 countries. Consequently, it remains a central focal point in scientific research. The latest World Health Organisation report on malaria determined that the number of cases rose from 227 million in 2019 to 241 million in 2020 with a concomitant increase in the number of deaths by 69 000 over one annum. Notably, two-thirds of these supplemental deaths were largely dependent on disruptions in procurements for malaria prevention, diagnosis, and treatment during the SARS-CoV-2 pandemic. The African continent is by far most affected by this epidemic as it still accounts for 95% of total malaria-related deaths globally. The majority of these deaths, approximately 80%, are accounted for by children below the age of 5 (Who. int, 2021). A significant amount of funding has been allocated to researching methods to control, prevent and eliminate malaria with an estimated amount of approximately $ 3.5 billion in 2020. Despite this, it is still deficit in the estimated $6.8 billion necessary to remain on target in meeting the global technical strategy (GTS) for malaria which plans to reduce global malaria incidence and mortality rates by a minimum of 90% by 2030. (Who.int, 2021).

1.1. Life cycle of the malaria parasite

The causative agents for malaria are apicomplexan protozoan parasites belonging to the *Plasmodium* genus (Josling and Llinás, 2015). The life cycle of malaria is particularly complex and can be categorised into several stages. Notably, malaria requires both an invertebrate and vertebrate host to maintain infections. Specialised protein expression is thus vital for the invasion of various cell types as well as the evasion of its host's immune responses. The female *Anopheles* mosquito is the primary invertebrate host and vector for this eukaryotic single-celled microorganism and is responsible for its transmission to humans. There are approximately 400 species of *Anopheles* globally, of which 70 are vectors for malaria under natural circumstances (Sinka *et al*., 2012). The malaria protozoan parasites can infect several animal species which include mammals, reptiles, and birds. Notwithstanding, only four species of malaria parasites

naturally infect *Homo sapiens*, namely *Plasmodium falciparum*, *Plasmodium vivax*, *Plasmodium ovale* and, *Plasmodium malariae* (Sato, 2021). However, the primate parasite *Plasmodium knowlesi* can also cause zoonotic infections in humans (Ramasamy, 2014, Larson, 2019, Sato, 2021). Of the parasite species, *P. falciparum* is the most virulent and responsible for the majority of infections and deaths, particularly in Africa (Larson, 2019). It is also the easiest to maintain in routine laboratory cultures (Schuster, 2002), and hence the focus of the majority of malaria research projects. It is through the understanding of malaria's life cycle and ecology that we may develop new and improved strategies aimed at the prevention, control, and elimination of this disease.

1.1.1. Liver stage

Once infective sporozoites are injected into a human host by the *Anopheles* mosquito, the sporozoites are slowly released into the host's bloodstream from the site of injection (Yamauchi *et al*., 2007). Once in circulation, the sporozoites travel to and penetrate hepatocytes (located in the host's liver) using thrombospondin domains found on the circumsporozoite protein and thrombospondin-related adhesive protein (Tateja, 2007). They remain in the hepatocytes for approximately 9-16 days, where the sporozoites migrate through several hepatocytes and undergo asexual replication (Mota, *et al*., 2001). The sporozoites mature into schizonts during this migration and subsequent replication. Additionally, each schizont can produce thousands of merozoites and upon the rupturing of the infected hepatocytes, each merozoite can theoretically invade an erythrocyte once discharged from the liver.

1.1.2. Blood stage

The resulting merozoites produced during the liver stage penetrate erythrocytes in four phases. The first stage includes the recognition and reversible attachment of the merozoite to the erythrocyte membrane, followed by the reorientation and the formation of an intercellular bridge between the apical end of the merozoite and the erythrocyte. This allows for the release of enzymes from the rhoptry and microneme organelles at the apical end of the merozoite to form a nascent parasitophorous vacuole in the erythrocyte (Haldar and Mohandas, 2009). The penultimate phase involves the repositioning of the intercellular bridge and the invagination of the erythrocyte membrane around the merozoite to engulf the parasite. Finally, the parasitophorous vacuole, as well as the erythrocyte membranes, are resealed after the successful invasion of the merozoites into the erythrocyte (Miller *et al.,* 2002). Once inside the

erythrocyte, the parasites undergo a second cycle of asexual division with their own set of developmental stages. The first is the early trophozoite stage, which has a ring-like morphology and is thus also referred to as the 'ring stage'. The early trophozoite matures into a late trophozoite and at this stage, the parasite has a highly active metabolism. As a result, there is an increase in glycolysis using large amounts of imported glucose, the ingestion of its host erythrocyte's cytoplasm as well as proteolysis of the ingested host haemoglobin into amino acids (Tuteja, 2007). The end of trophic development is indicated by numerous rounds of nuclear division in the absence of cytokinesis resulting in the formation of multinucleated schizonts. This is followed by cytokinesis to form merozoites. A mature schizont can form up to 20 merozoites, which are responsible for the further infection of uninfected erythrocytes once the infected red blood cell is lysed. In humans, *P. falciparum* parasites complete this cycle of erythrocyte infection in a synchronized fashion every 48 hours. To keep the cycle of population transmission going, a small number of merozoites that have invaded erythrocytes differentiate into male and female gametocytes that serve to transmit the infection to new hosts via the *Anopheles* mosquito (Aly *et al*., 2009).

1.1.3. Anopheles mosquito stage

The gametocytes produced in an infected host are ingested by a mosquito and move to its midgut to further produce microgametes (male) and macrogametes (female) (Han *et al*., 2000). Fertilisation ensues when the gametes fuse to form a zygote. The zygote matures into an ookinete and penetrates the cell wall of the midgut and consequently produces an oocyst (Al-Olayan *et al*., 2002). Mitosis and sporogony occurring within the oocysts produce numerous sporozoites which are released when the oocyst ruptures. The sporozoites then travel to the salivary glands of the *Anopheles* mosquito in preparation for transmission into another human host (Pimenta et al., 1994). The lifecycle of malaria as described above was illustrated by Maier *et al*., 2019 in their "Trends in Parasitology" Review, and can be seen in **Figure 1.**

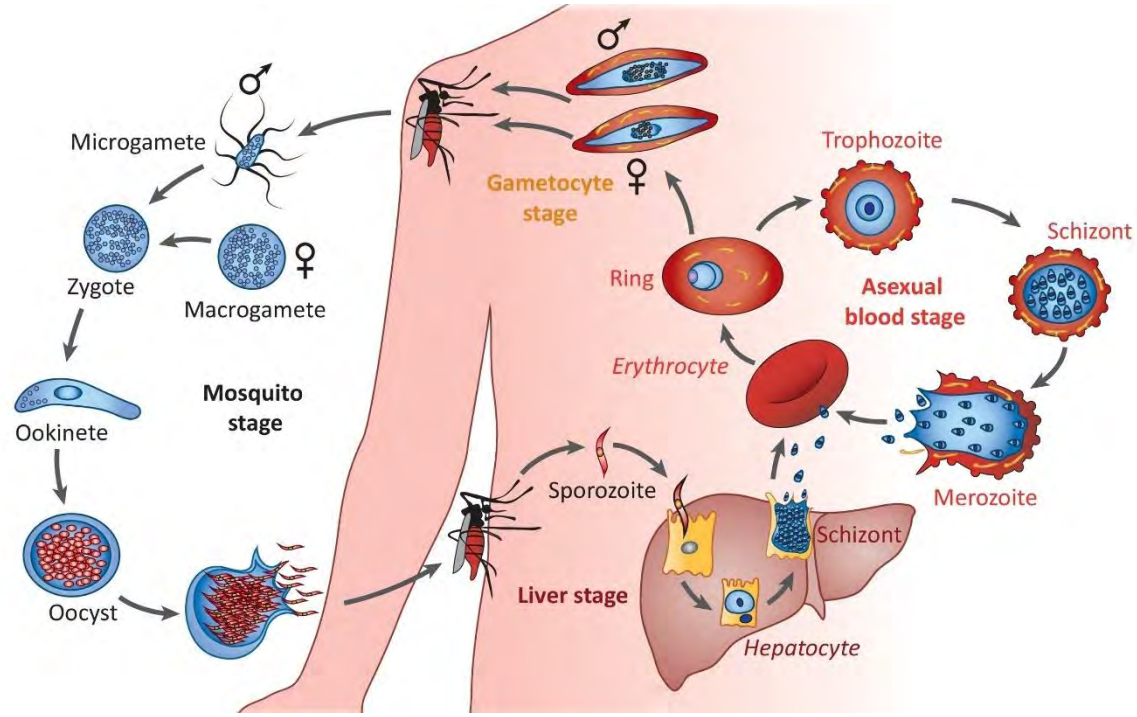

Figure 1: A visual depiction of the complete life cycle of *Plasmodium falciparum* (Taken from Maier *et al*., 2019)

1.1.4. Clinical features of P. falciparum

The initial symptoms that manifest in an individual infected with malaria are often non-specific and can easily be misdiagnosed due to the commonality of the symptoms across several possible medical conditions including influenza. Such symptoms include fever, chills, headache, jaundice, anaemia, nausea, vomiting, and diarrhoea. Less common symptoms manifested from cases of severe malaria include convulsions, haemoglobinuria, hypoglycaemia, and metabolic acidosis ("Severe falciparum malaria. World Health Organization, Communicable Diseases Cluster," 2000). The onset and progression of symptoms differ between species of infecting parasites. *P. falciparum* presents the shortest incubation period ranging from 9-14 days and is most likely to result in complicated cerebral malaria and possibly death if left untreated (Laishram *et al*., 2012). Children under the age of 5 as well as pregnant women are among those that are at high risk for the development of complications if infected (Bartoloni and Zammarchi, 2012).

1.2. Preventative strategies to combat malaria

Despite a significant reduction in the global socio-economic burden of malaria over the past decade, malaria has continued to ravage through developing countries – especially those in sub-Saharan Africa (Mbacham *et al*., 2019). This is owed to the fact that the majority of the population in these countries are impoverished and are therefore unable to invest in available preventative measures and/or are unable to seek the necessary treatment upon being infected (Tizifa *et al*., 2018). Ergo, the central focus is heavily placed on the prevention and eradication of malaria using cost-efficient strategies that can benefit developing nations in malaria endemic regions.

1.2.1. The use of insecticides as a front-line defence against malaria

Considering that malaria relies on mosquitoes to act as a vector for their transmittance, one can easily gauge the benefit of implementing interventions that reduce the populations of mosquitos in malaria endemic countries. Such strategies include swamp drainage, oiling/covering surfaces of large bodies of water and finally, the use of insecticides (Keiser *et al*., 2005). To this day the primary methods utilised in malaria prevention include the use of insecticides, mainly in the form of indoor residual spraying (IRS) and long-lasting insecticidal nets (LLINs) (Corrêa *et al*., 2019). Four main lethal insecticide classes have shown an effective response in vector control, namely: pyrethroids, organochlorines, carbamates, and organophosphates (Killeen *et al*., 2017). Notably, the only suitable class of insecticides that can be used on LLINs are pyrethroids as they are the only class of insecticides that do not threaten public health with long-term usage (Quiñones *et al*., 2015). Though, with increased exposure to this class of insecticides over the past two decades, there has been a widespread surge in pyrethroid resistance and has thus caused concern surrounding the diminishing effectiveness of LLINs (Toé *et al*., 2014). This has resulted in recommendations being made to populations that are at risk to make use of IRS or IRS in combination with LLINs, given that IRS can combine the four different classes of insecticides and slow the spread of pyrethroid resistance (West *et al*., 2014). Another way to slow down the rise in pyrethroid resistance includes the alternation of different classes of insecticides by putting the active ingredients in rotation (Pennetier *et al*., 2008). This does, however, come with its own set of barriers which includes the high cost of insecticide development and implementation. And since the majority of malaria incidence occurs in impoverished and under-developed countries, the necessity for an affordable and long-term strategy in malaria prevention is dire in the ongoing fight against malaria.

1.2.2. Malaria vaccination as an intervention strategy

The development and widespread accessibility of an effective malaria vaccine has long been a goal for scientists involved in malaria research. Finally, after 35 years of intensive study, a promising malaria vaccine by the name of RTS,S/AS01 (RTS,S) has been developed by a group of researchers at the Walter Reed Army Institute of research in partnership with GlaxoSmithKline (GSK) (Laurens, 2020). In October of 2021, it became the first parasite vaccine to obtain regulatory approval and was subsequently endorsed by WHO (D'Souza and Nderitu, 2021). The vital phase 3 trials took place in several African countries endemic to malaria from 2009-2014 (Targett, 2015). The results were published in 2015 and approximated that children between 17 months and 5 years of age who received three doses and a subsequent booster shot of this vaccine would have a 29% reduced risk of severe malaria which requires hospitalisation (Moorthy and Okwo-Bele, 2015). Further evidence from the study showed that when used in combination with LLINs and IRS, the vaccine can decrease mortality caused by malaria by as much as 70%. The development of RTS,S is a milestone reached in the advancement of malaria control and prevention. Regardless of the complexities surrounding the vaccination schedule, widespread implementation seems probable even in sub-Saharan African countries that have poor healthcare and limited resources. The RTS,S vaccine contains epitopes of the circumsporozoite protein of *P. falciparum* sporozoites and was designed to target the sporozoite phase of the parasite's lifecycle and ultimately block the consequent infection of its host's liver following the bite of an infectious mosquito (Jelínková *et al*., 2021). Despite this breakthrough in malaria research, the vaccine does not provide complete protection and comes with its list of shortcomings. When used independently, the full dosage of the RTS,S vaccine is still only 30% effective in preventing death upon infection (Samarasekera, 2021). Another disadvantage is that in its current form the vaccine is only sufficiently effective in children below the age of five. Moreover, of the five species of malaria parasites that infect humans, the RTS,S vaccine is only effective against *P. falciparum* (Samarasekera, 2021). These challenges validate the continual necessity for a multi-faceted approach to the prevention and eradication of malaria by using preventative, control, and treatment strategies in combination.

1.3. Traditional monotherapies as a treatment strategy against malaria

In conjunction with preventive and control interventions mentioned in section 1.2, it is also necessary to have treatments readily available for those who have already been infected with malaria. This predominantly includes the administration of anti-parasitics either as monotherapies or as a combination of drugs. There is a noticeable pattern observed throughout the history of traditional monotherapies where an effective drug was discovered/synthesised followed by the development of antimalarial drug resistance and finally the rapid spread of resistance by natural selection. This has resulted in the need for new and effective alternatives.

1.3.1. The history of quinine as the first antimalarial

The oldest compound that was first documented to be effective against malaria is known today as quinine. This alkaloid is naturally sourced from the bark of evergreen trees belonging to the *Cinchona* and *Remijia* species which are indigenous to the eastern slopes of the Andes mountains, extending from Bolivia to Venezuela. The bark was originally introduced as a remedy for malaria by the Jesuits in the 17th century and the active compound, quinine, was first isolated in a crystalline form by two French pharmacists in 1820 which was subsequently utilised in the standardised treatment method for malaria. Biochemically, quinine belongs to a group of drugs that are classified as aryl amino alcohols and is very basic in nature. It was originally theorised that the compound's lethal effects on *Plasmodium* parasites stemmed from its ability to interfere with the digestion of host cell haemoglobin by the parasite, which consequently causes toxic levels of partially degraded haemoglobin (Foley & Tilley, 1997). Later research investigating the role of heme in antimalarial modes of action provided evidence supporting Foley and Tilley's claims by showing that quinine, among other antimalarials, inhibited hemozoin (β-hematin) pigment formation which involves the conversion of heme released by haemoglobin digestion into inert hemozoin crystals (Combrinck *et al*., 2013, Herraiz *et al*., 2019, Kapishnikov *et al*., 2019, Olafson *et al*., 2015). After the large-scale production and distribution of quinine in the 1850s, it remained the standardised treatment against malaria until 1920 (Achan *et al*., 2011). Since then, quinine is now categorised as a quinolinemethanol and is deemed too toxic as a malaria prophylactic but is, however, still used as an intravenous injection for severe cases of malaria today.

1.3.2. Chloroquine and its mode of action

The next breakthrough occurred in 1934 when a group of German researchers, led by Hans Andersag, first discovered chloroquine (initially known as resochin) which showed therapeutic potential against malaria (Pou *et al*., 2012). Subsequent development by American researchers after World War II determined that chloroquine was highly effective as a prophylactic and treatment method for malaria (Pou *et al*., 2012). Chloroquine served as the primary intervention method for malaria up until the development of resistance by *Plasmodium* parasites led to its eventual dismissal in the late 1990s (Mwai *et al*., 2009). Chloroquine is categorised as a 4-aminoquinoline antimalarial due to the presence of a 7-chloroquinoline-substituted ring system that is complemented with a flexible pentadiamino side chain (O'Neill *et al*., 1998).

The mechanism of action for chloroquine was initially proposed to be due to the inhibition of heme polymerase in the trophozoite stage of the malarial life cycle, and as a result could prevent the conversion of heme to hemozoin (Slater, 1993). Yet, more recent studies found that chloroquine inhibits cellular hemozoin formation in the parasite by binding directly to free heme and forming a heme-chloroquine complex (Combrinck *et al*., 2013). This is clinically effective since it inhibits a vital metabolic process within the parasite where heme is released by the digestion of the host cell's haemoglobin after being ingested by the intra-erythrocytic parasite and polymerises to form an inert hemozoin crystal in the parasite's digestive vacuole (Goldberg and Slater, 1992). The accumulation of heme due to chloroquine's action is highly toxic to malaria parasites, consequently killing them. Chloroquine can passively diffuse through cell membranes into the parasite's acidic digestive vacuole where it is protonated and consequently trapped (Goldberg and Slater, 1992). Based on its half-life of 20-60 days, studies suggested that malaria patients required fewer administered doses as it remained in the bloodstream for a prolonged length of time which made it an effective and affordable antimalarial at the time (Sullivan *et al*., 1996*)*.

1.3.3. Mefloquine and its mode of action

In the early 1970s, mefloquine was synthesised by the United States military to treat soldiers suffering from malaria upon returning from the Vietnam War and subsequently became the choice antimalarial for the U.S military (Martins *et al*., 2021). Several mechanisms of action for mefloquine have been proposed over the years. Sullivan and colleagues hypothesised that mefloquine's antimalarial properties are caused by its ability to bind to heme and form a heme-mefloquine complex, consequently damaging the parasite's food vacuoles (Sullivan *et al*.,

1998). Another proposed mode of action stipulates that mefloquine's clinical effectivity is owed to the fact that it generates reactive oxygen species (ROS) within *Plasmodium* parasites (Gunjan *et al*., 2016). The most recent proposition relating to mefloquine's antimalarial mechanism of action suggests that it may target three vital parasitic proteins/co-enzymes, namely: the 80S ribosome, dolichol kinase, and finally acyl-CoA binding proteins (Wong *et al*., 2017, Ghosh *et al*., 2021). There has been a lot of speculation regarding the clinical toxicity resulting from mefloquine treatment in malaria patients over the past decade. This led to the discontinuation of mefloquine as a monotherapy in the treatment of malaria with increased reports of severe neuropsychiatric episodes that have either led to psychiatric disorders, self-harm, hospitalisation, or even disability (Eaton, 2009). It is, nonetheless, still used as a partner drug in combination therapy and is prescribed in much lower doses (Davis *et al*., 2005).

1.3.4. Fansidar and its mode of action

The antimalarial sulfadoxine-pyrimethamine (Fansidar) was developed within a similar time frame as chloroquine but only became available as a treatment method in 1981 due to the significant increase in drug resistance against chloroquine (Menard *et al*., 2005). Ironically, within a few years resistance developed against sulfadoxine-pyrimethamine and spread rapidly. Both sulfadoxine and pyrimethamine are folic acid antagonists that target the parasite folate biosynthesis pathway where sulfadoxine inhibits the activity of dihydropteroate synthase and pyrimethamine inhibits dihydrofolate reductase (Pearson & Hewlett, 1987). This makes Fansidar active against the asexual erythrocytic stages in the *Plasmodium* life cycle. However, due to the high levels of resistance, Fansidar is no longer used as a preventative drug. It is only administered for severe cases of malaria.

1.4 The implementation of artemisinin combination therapies (ACTs)

1.4.1. Discovery of artemisinin and its mechanism of action

Artemisinin was first discovered by a Chinese research group in the early 1970s led by Professor Youyou Tu (Su and Miller, 2015) where it was sourced as a herbal extract from the leaves of wormwoods called *Artemisia annua* (Weathers *et al*., 2011). It was then successfully purified in 1972, whereafter clinical trials began. By 1980, it became widespread as a treatment method in China for multidrug-resistant (MDR) strains of *Plasmodium falciparum*. Its clinical effectiveness soon gained interest from European and Asian countries (O'Neill et al., 2010).

The artemisinin compound has been classified as a sesquiterpene lactone and contains an endoperoxide bridge (Abdin *et al*., 2003), which has proven to play a crucial role in its antimalarial mode of action. A study conducted by Meshnik in 2002 proposed that artemisinin's mechanism of action is due to the decomposition of the endoperoxide bridge, a process that is mediated by heme, which leads to the accumulation of carbon-centered free radicals within the parasite's food vacuole (Meshnick, 2002). A decade later, a research group contested Meshnik's hypothesis and proposed rather that artemisinin is activated by iron and the resulting Fe-artemisinin targets the *Pf*ATP6 calcium pump by closing key domains via conformational changes, namely the phosphorylation, nucleotide binding, and actuator domains. As a result, the calcium binding site located on the *Pf*ATP6 calcium pump becomes inaccessible thus inhibiting its functionality, and ultimately leading to parasite death (Shandilya *et al*., 2013). However, advancements in the field have allowed scientists to conclude that the activation of artemisinin is, in fact, dependent on the presence of heme and have identified 124 artemisinin protein targets (Yang *et al.,* 2020). This suggests that artemisinin's mechanism of action kills malaria parasites by binding numerous parasite proteins that interfere with enzyme activity, cause protein damage, and disrupt vital cellular functions (Mbengue *et al*., 2015). Nonetheless, the individual roles played by these drug targets are yet to be elucidated.

1.4.2. ACT development

The emergence of partial artemisinin-resistant strains of *Plasmodium falciparum* was first documented in 2009 in Pailin, western Cambodia, with a 100-fold reduction rate in parasite clearance (Fairhurst and Dondorp, 2016). Since then, artemisinin resistance has also been reported in other areas of Southeast Asia as well as in sub-Saharan Africa (Owoloye *et al*., 2021). As a countermeasure to the gradual progression of drug resistance, scientists have limited the use of artemisinin as a monotherapy and started combining two or more antimalarials that varied in structure and followed different modes of action that target the same stage of the parasite's lifecycle to slow the progression of resistant strains. This proved to be highly effective and fast-acting in patients with resistant infections. The most effective drug combinations to date involve artemisinin or an artemisinin derivative (i.e., dihydroartemisinin, artesunate, and artemether) together with a partner drug that has a longer half-life such as mefloquine, lumefantrine, amodiaquine or piperaquine (Tilley *et al*., 2016). This form of treatment became widely known as artemisinin-based combination therapy (ACT), which remains the recommended treatment method for malaria today.

1.4.3. Advantages and challenges faced in the implementation of ACTs

The preference of ACTs over other combination therapies such as atovaquone-chloroguanide is a result of several factors. Firstly, ACTs act quickly and can significantly reduce the number of parasites within only 3 days (Yeung, 2018). Moreover, the companion drug is often eliminated slowly which prevents another onset of parasitic growth by targeting blood-stage schizonts. Finally, the co-administration of two different drug classes reduces the chance of resistant strains emerging (Baird, 2005). There are, however, several obstacles faced in the implementation of ACTs. The first challenge involves the high cost involved in drug development and operational expenses associated with ACTs in a clinical setting. Developing countries are the most affected by this and often opt for treatment using monotherapies since they are 20 times less expensive (Mutabingwa, 2005). Another major challenge includes the inappropriate usage of ACTs which is owed to poverty, ignorance, and the absence of drug regulatory bodies. This consequently increases the chances of resistance emergence. Since ACTs are given in multiple doses, if a patient stops taking the medication for any amount of time and reverts back to it, it will expose the parasites to the co-administered drugs in low enough doses to allow natural selection to take effect. This means that the probability of parasites becoming resistant to one or both drugs is increased.

1.4.4. The anticipated development of ACT resistance

As mentioned before, ACTs are still the main treatment method for both uncomplicated and complicated malaria as they are the most effective of all the available antimalarials. Unfortunately, ACTs are not completely invulnerable to drug-resistant strains of *Plasmodium*. It is believed that ACTs may not remain effective in the next 50 years (Sayang *et al*., 2009). A status report on ACT efficacy released by WHO in August of 2018 already confirmed that certain ACT treatments have a delayed parasite clearance rate but are fortunately still effective (WHO, 2018). The imminent threat of resistance against ACTs is further increasing the need for new drug compounds as well as new and efficient drug targets.

1.5. Mechanisms of resistance in malaria parasites

1.5.1. Rapid spread of antimalarial resistance

Despite the noticeable decline in malaria cases due to global support through the implementation of control programs, improved diagnosis, and modern intervention tools, there

is still a way to go before reaching the goal of sustained eradication in endemic countries. Resistance mechanisms evolved by malaria parasites are fast becoming a cause for concern. The mechanisms of action previously mentioned involving several antimalarial drugs are no longer as effective as they once were as there is a noticeable rise in clinical failure after treatment. **Figure 2** below demonstrates the wide distribution of resistance against chloroquine, sulfadoxine/pyrimethamine, and artemisinin in Africa and Southeast Asia – both of which are endemic to malaria (Haldar *et al*., 2018). Subsequent evaluations of this phenomenon have suggested that several artemisinin, mefloquine, and quinine-resistant lineages have also emerged independently in endemic countries while others were transmitted through human hosts as a consequence of traveling or immigration (Blasco *et al*., 2017).

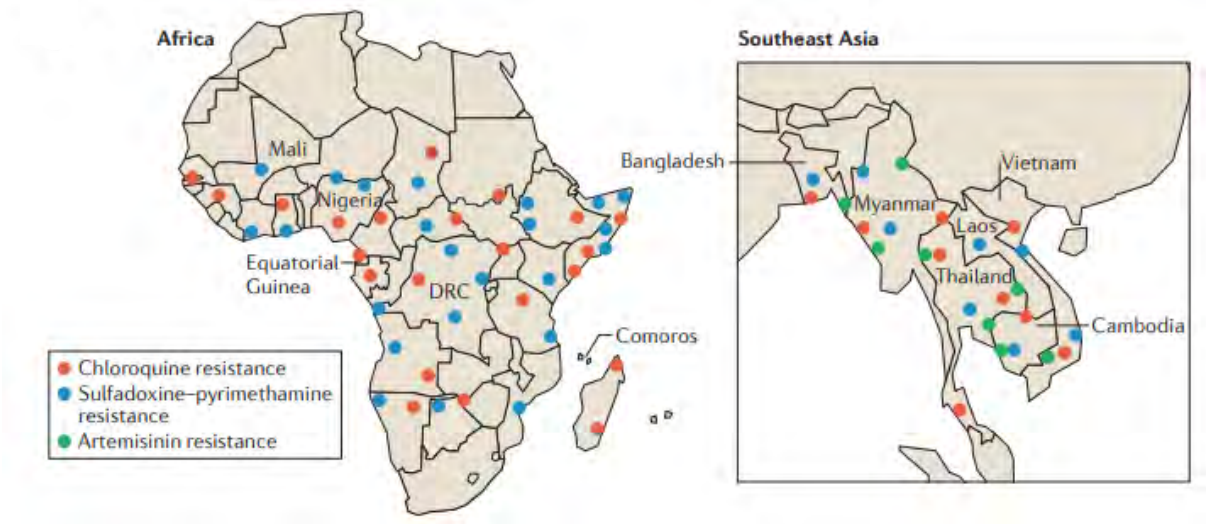

Figure 2: Detailed maps showing the distribution of *P. falciparum* resistance to chloroquine, sulfadoxine-pyrimethamine and artemisinin in Africa and Southeast Asia. Artemisinin resistance is based on two criteria: clearance and *Pf*Kelch13-associated mutation. Resistance to chloroquine and sulfadoxine-pyrimethamine (but not artemisinin) has emerged in the Amazon basin of South America (not shown). Resistance of *P. vivax* to chloroquine is emerging (not shown). Each dot represents a region of the emergence of drug resistance (Haldar *et al*., 2018).

1.5.2. The evolution of resistance mechanisms by Plasmodium species.

The phenomena surrounding the development of drug resistance are based on increased drug degradation due to increased enzymatic activity, mutation or altered expression of the drug target and lastly the modification of cellular transport of the drug itself (Haldar *et al*., 2018). Mutations that result in altered gene expression occur most often in highly polymorphic genes. This can potentially lead to the acquisition of advantageous traits (Gurwitz, 2009).

1.5.2.1. Chloroquine resistance mechanism

The development of chloroquine resistance, for instance, has been found to be a result of mutations in the chloroquine resistance transporter gene (CRT) which encodes an efflux protein (Baird, 2005). In wild-type strains, the efflux of chloroquine (which is positively charged in the parasite food vacuole) is limited by the positive charge of K76 in the efflux protein, but the mutation resulting in K76T replaces the positive charge by an uncharged side chain (Martin and Kirk, 2004). Consequently, this allows chloroquine to move along the concentration gradient through the CRT and diffuse through the transporter and out of the parasite's food vacuole, its site of action, into the cytoplasm. This results in the reduction in chloroquine concentration within the parasite's food vacuole, ultimately hindering its antimalarial ability.

1.5.2.2. Quinine resistance mechanism

Quinine and other quinoline derivatives have been found to lose efficacy when mutation(s) occur in the *Pfmdr1* gene. The exact native function of the protein encoded by this gene within *P. falciparum* is unknown, but since it is localised to the membrane surrounding the food vacuole – a common target for multiple antimalarials - it is believed to function as a drug transporter (Ibraheem *et al*., 2014). Experimental evidence obtained from A. Sidhu *et al.,* 2006 did show that *Pfmdr1* amplification does lead to a significant decrease in sensitivity to quinine, lumefantrine and artemisinin during treatment (Sidhu *et al*., 2006). This suggests that it plays a role in the acquisition of drug resistance over a range of different antimalarials. Additionally, alterations in the *Pfmdr1* gene sequence have shown to increase parasite efflux activity, which ultimately causes the drugs to be removed from the parasite at a much faster rate (Petersen *et al*., 2011).

1.5.2.3. Sulfadoxine/pyrimethamine resistance mechanism

The emergence of resistance against the combinational administration of sulfadoxine and pyrimethamine (SP) has been ascribed to point mutations occurring in genes encoding enzymes that play a key role in the obligatory parasite folate biosynthesis pathway. Increased levels of resistance have been associated with an increase in the number of mutations located in parasite genes encoding the enzymes dihydrofolate reductase (*dhfr*) and dihydropteroate synthase (*dhps*), the targets of pyrimethamine and sulphadoxine, respectively (Mbugi *et al*., 2006). Hence, it is believed that the main cause of resistance development against SP is due alterations in the sequences of both drug targets that reduce the affinity of the enzymes for sulfadoxine and pyrimethamine. This weakens the drug's recognition and binding to the parasitic targets, ultimately decreasing its efficacy.

1.5.2.4. Artemisinin resistance mechanism

Studies have suggested that mutations in either *Pf*ATPase6 or *Pf*PI3K are linked to the reported decrease in artemisinin's clinical effectiveness (Afonso *et al*., 2006; Paloque *et al*., 2016). This may seem significant in the emergence of resistance to artemisinin, however, this antimalarial has numerous drug targets which leads some researchers to believe it unlikely that point mutations occurring in one of artemisinin's numerous drug targets to be the cause for the emergence of partial resistance against this front-line antimalarial (Wang *et al*., 2017). Rather, a more accepted hypothesis suggests that the *Plasmodium* species gain tolerance to artemisinin by capitalising on its short half-life in the treated individual's bloodstream. Notably, the concentration of heme changes throughout the parasite lifecycle. Heme is at its lowest concentration during the parasite's ring-stage form because of limited haemoglobin uptake and digestion, whereas during its trophozoite stage the heme concentrations are exponentially increased (Klonis *et al*., 2011). Since heme activates artemisinin (Wang *et al*., 2015), ring-stage parasites are more capable of minimising the damage caused by artemisinin's mode of action (Witkowski *et al*., 2010). This theory supports evidence obtained by Straimer (2015) that showed that mutations occurring in the *kelch13* (K13) gene were associated with delayed parasite clearance time (PCT) after treatment (Straimer *et al*., 2015). This could explain how mutations in the K13 protein protects immature parasites by decelerating ring-stage progression. Although this doesn't completely inhibit artemisinin's action, it limits its activation and consequently restricts its antimalarial activity (Codd *et al*., 2011). Subsequent investigation on the topic also indicates that malaria parasites have enhanced cellular stress response pathways that help them counteract protein damage caused by artemisinin (Dogovski *et al*., 2015). Nonetheless, these mutations still only provide a limited amount of protection against this antimalarial. So regardless of mutations occurring in K13 genes, malaria parasites remain vulnerable to artemisinin when in the trophozoite stage of their lifecycle (Witkowski *et al*., 2013).

1.6 The need for new drugs and drug targets

Due to this rapid progression of resistance, the development of new and effective malaria drugs is a central objective for many research groups. Phenotypic screening is currently the easiest and most effective approach in the identification of antimalarial compounds that are effective against drug resistant parasites (Gamo *et al*., 2010). However, a more target-based approach in preventing the parasite's life cycle could be a more fruitful expedition for several reasons.

Firstly, through genome-wide mutagenesis studies, there are multiple genes that are already known to be essential for parasite survival (Zhang, *et al*., 2018), and there is a growing list of protein targets that are known to be druggable with inhibitors that have antimalarial activity. Several novel antimalarial drug targets have been identified by homing in on vital metabolic pathways within the *Plasmodium* species, some of which include oxidative stress, heme detoxification, synthesis of nucleic acids as well as lipid and fatty acid synthesis (Colvin and Cordy, 2020). Some promising targets include glucose transporter *Pf*HTI, which provides intra-erythrocytic parasites with glucose (primary source of energy for malaria parasites), various protein kinases involved in cell cycle progression and differentiation, apicoplast enzymes essential in several metabolic pathways (including heme synthesis), isoprenoid and fatty acid synthesis, proteases (particularly those involved in haemoglobin digestion or parasite egress from infected erythrocytes), kinases involved in lipid modification or ion transport - e.g. *Pf*ATP4 and *Pf*PI4K, and aminopeptidases, which are responsible for catalysing the cleavage of amino acids from the terminus of peptides/proteins and may also be involved in the digestion of haemoglobin-derived peptides (Kumar *et al*., 2018, Shibeshi *et al*., 2020). The discovery of new drug targets is continuing to pave the way for more efficient and effective antimalarial treatments. Due to the increasing cases of malarial resistance, it may be easier to discover compounds that are effective against the mutant target instead of screening against the entire organism. Unlike phenotypic screening, which requires large amounts of infectious malarial parasites and specialised tissue culture equipment and facilities, the methods and reagents required for target-based screening may be more tractable in standard molecular biology/biochemistry laboratories (Croston, 2017). Most importantly, it enables the *in silico* discovery and optimisation of inhibitory compounds using the tools of structural bioinformatics and computer-aided drug discovery (Croston, 2017). In this way, target-based screening is not only easier and cheaper when screening for potential drug compounds against malaria, but it also enables rational drug design.

1.7 Protein-protein interactions: Its relevance in novel target-based drug discovery

There has been a noticeable decline in the release of new and effective drugs into the market which could be a call to explore alternative types of drug targets in future research. Pharmaceutical companies and target-based discovery programs tend to focus on protein-ligand interactions when developing new drugs as they have a distinct ligand-binding site that

small molecules can interact with (Diedrich *et al*., 2020). However, there is evidence suggesting that the discovery of protein-protein interaction (PPI) modulators could broaden the categories of targets that are available for exploitation due to their vital role in both physiological and pathological processes. This makes them promising candidates as intervention targets in novel treatments. Recent target-based studies that have focused on protein-protein interactions have found it to be an effective, yet challenging strategy for novel drug development. PPIs have long been considered as "undruggable targets" for several reasons (Sawyer, 2020). The first challenge faced is the location of PPI sites as they are often found on large and hydrophobic interfaces (Mabonga & Kappo, 2019). Conceptually, these large binding surfaces are inadequate as effective drug targets due to the difficulty in finding a matching binding molecule that retains its drug-like properties. Additionally, the interfaces of PPIs are often flat with few grooves and pockets which ultimately makes it difficult to design small drug molecules that can bind to them with high affinity (Arkin *et al*., 2003). Moreover, the high-affinity binding that occurs between proteins in PPIs makes it difficult for small molecular compounds to inhibit such an interaction (Lu *et al*., 2020).

Unlike traditional ligand-binding targets, such as enzymes and receptors, PPIs lack endogenous small ligands that can be used as a reference template for inhibitor design, thus making drug development that much more complex. Drugs that have been developed to target PPIs have also generally been found to have a higher molecular weight (>400 Da) than traditional small molecule drugs (200>500 Da). This makes meeting Lipinski's 'rule of five' which stipulates the characteristics of 'druggable' compounds that much more difficult (Feng *et al*., 2017). Despite these challenges, the discovery of 'hot-spots' in the larger interaction surfaces of PPI's have made it possible to design drugs that can accurately target them. These 'hot-spots' are segments of amino acid residues on the interface of PPIs that contribute to the binding free energy (Cukuroglu *et al*., 2014). Therefore, the greater the PPI area the more 'hot-spots' will be observed. This means, theoretically, even though there is a large interface area, small molecule drugs can be designed in such a way as to act specifically on these regions of amino acid residues to inhibit/intervene in high affinity PPIs.

1.8. ADP-ribosylation factor (Arf) GTPases:

Arf GTPases are soluble proteins that are ubiquitous in nature as they are found across a wide range of eukaryotes, including *Plasmodium* parasites. These proteins act as molecular switches

that regulate essential cellular processes by interchanging between inactive (GDP-bound) and active (GTP-bound) conformations which will be further elaborated on below. Given their status as key players in signal transduction, Arf GTPases are subject to a variety of protein-protein interactions that have the potential to be exploited in future drug discovery campaigns and further motivates the exploration of Arfs as potential drug targets for malaria and other diseases.

1.8.1. Cellular functions

Members belonging to the Arf family of GTPases have been determined to play indispensable roles in a diverse range of cell signalling processes and signal transduction events. Each class of Arf proteins have their own unique cellular distributions and recognise and bind to different subsets of effector molecules that together dictate their specialised biological functions (D'Souza-Schorey and Chavrier, 2006). Members of the class I Arf GTPases (Arf1, Arf2 and Arf3) are localised to the Golgi apparatus and the cytosol where they mediate the recruitment and assembly of various coat proteins onto budding vesicles occurring along the secretory pathway (Bonifacino and Jackson, 2003). In addition, class I Arf proteins also recognise and initiate the activation of lipid-modifying enzymes such as phospholipase D (PLD) and phosphatidylinositol (PI) kinases (Sztul *et al*., 2019). The specific functions conducted by class II Arf proteins are still not fully understood, however, a few studies have suggested that Arf5 is likely involved in early Golgi transport and the recruitment of coat complexes to the *trans*-Golgi membranes (Claude *et al*., 1999, Takatsu *et al*., 2002, D'Souza-Schorey and Chavrier, 2006). The only member belonging to class III is Arf6 localised to the plasma membrane and endosomal compartments. This class is responsible for the regulation of clathrin-dependent endosomal membrane trafficking events, the activation of lipid-modifying enzymes and the stimulation of actin polymerisation, vital for phagocytosis and exploited by the innate immune system (Van Acker *et al*., 2019).

1.8.2. Nomenclature and structural architecture:

The Arf family of proteins are classified as small monomeric GTPases and belong to the Ras (rat sarcoma) superfamily. A total of six mammalian ADP-ribosylation factor (Arf) GTPase isoforms have been discovered in a diverse range of eukaryotic species. These isoforms have since been categorised into three main classes – Class I (Arf1, Arf2 & Arf3), Class II (Arf4 & Arf5) and Class III (Arf6) which are grouped according to their sequence homologies (Nie, 2006). One of the main differentiating features of the Arf family of proteins compared to other

small GTPases is the presence of an N-terminal amphipathic α-helix extension (Lundmark *et al*., 2008). This helix is highly hydrophobic due to the post translational myristoylation that occurs on the second residue (glycine) of this extension. This structural feature is seen as vital in the recruitment and subsequent binding of Arf proteins to their respective sites within the membrane. Connected to the amphipathic helix of Arf GTPases is a conserved G-domain that is ubiquitous in all GTPase families. The aforementioned domain is made up of five α-helices and six β-sheets (Lundquist, 2006) and houses five relatively conserved sequence motifs (also known as 'G boxes') that function as binding sites for guanine nucleotides (Reiner and Lundquist, 2018). The G1 motif, also termed 'the P-loop', is observed in many nucleotide binding proteins and is able to recognise β-phosphate and Mg^{2+} ions on target nucleotides (Toma-Fukai and Shimizu, 2019). The G2 and G3 motifs contain the switch I and switch II regions which interact with the β- and γ-phosphate ions found on said target nucleotides, which include GDP and GTP (Osaka et al., 2021). Importantly, these switch regions display significant structural differences upon GTP binding and GTP hydrolysis that result in conformational changes that occur between a GTPase's active and inactive forms (Cabrera-Vera *et al*., 2003). This is the basis of a GTPase's primary function as a 'molecular switch' in many biological processes. Finally, the G4 and G5 motifs are essential in binding and distinguishing the guanine base from other nucleotides (Toma-Fukai and Shimizu, 2019) which makes these proteins highly specific in functionality. Remarkably, the conserved G-domain is connected to Arf's amphipathic helix through a 'linker region' which is much shorter in length compared to linker regions found in other GTPase families (Liu *et al*., 2010, Chavrier and Ménétrey, 2010). This consequently restricts Arf effectors to a position close to the membrane surface as opposed to other members of the Ras superfamily which are normally positioned further from the membrane surface (Gillingham and Munro, 2007). This makes sense when considering that the binding partners of Arf are typically coat proteins and/or lipid-modifying enzymes that shape and alter lipid bilayers.

1.8.3. Arf regulation: GEFs and GAPs

The catalytic activity imposed by both guanine nucleotide exchange factors (GEFs) and GTPase activating proteins (GAPs) in the activation and deactivation of small GTPases has been a popular topic of research due to their ability to significantly increase the rate of GTPase GDP/GTP nucleotide exchange (GTPase activation) or GTP hydrolysis (GTPase deactivation) when compared to the intrinsic rates of these reactions by unassisted GTPases. Markedly, the

specifics of Arf nucleotide exchange are vital when considering Arf proteins as possible drug targets in drug development programmes.

1.8.3.1. Arf activation by ArfGEFs

Despite significant structural variability across ArfGEFs, they all share a conserved ~200 amino acid Sec7 domain which is responsible for promoting GEF activity on Arf (Toma-Fukai and Shimizu, 2019). The catalytic mechanism of the Sec7 domain relies heavily on an invariant glutamate residue (also referred to as the 'glumatic finger') located at the hydrophilic end of the Sec7 domain (Casanova, 2007). The high affinity between inactive Arf and the Sec7 domain of ArfGEFs causes an interaction that changes the conformation of the Arf protein core. As a result, Arf-GDP associates with the deep hydrophobic pocket located on the surface of the Sec7 domain. Subsequently, the glutamic finger on the Sec7 domain enters the nucleotide-binding site where it competes with the β-phosphate on GDP electrostatically (Cherfils and Zeghouf, 2013). This causes the subsequent displacement of GDP from Arf. The second conformational change that is significant in the activation of Arf includes the remodelling of the interswitch region that is comprised of two β-sheets and is located between the Arf switch I and switch II regions (Khan and Ménétrey, 2013). A visual comparison between the two nucleotide-dependent conformational changes that determine the activation status of Arf1 is presented in **Figure 3** below (Lee *et al*., 2004). The restructuring of the interswitch region is also often referred to as 'interswitch toggle'. When Arf is inactive (-GDP bound) the β-sheets making up the interswitch region along with the α-amphipathic helix on the N-terminal extension are sheltered within a hydrophobic pocket in the Arf protein core (Jackson, 2014). This conformation prevents Arf from interacting with membranes. Upon the remodelling of the Arf protein core, changes are also initiated in the interswitch toggle which causes the release and exposure of the N-terminal α-amphipathic away from the hydrophobic pocket in the protein core thus allowing interaction with lipid membranes (Yorimitsu *et al*., 2014). Moreover, apart from their role in GDP and GTP exchange, both switch regions and the interswitch region provide a scaffolding on the surface of Arf which acts as the primary binding site for effector proteins (Donaldson and Jackson, 2011). It is important to note that the GTP-bound activated form is more favoured in the cellular context due to the presence of substantially higher concentrations of GTP in relation to GDP (Mondal *et al*., 2015).

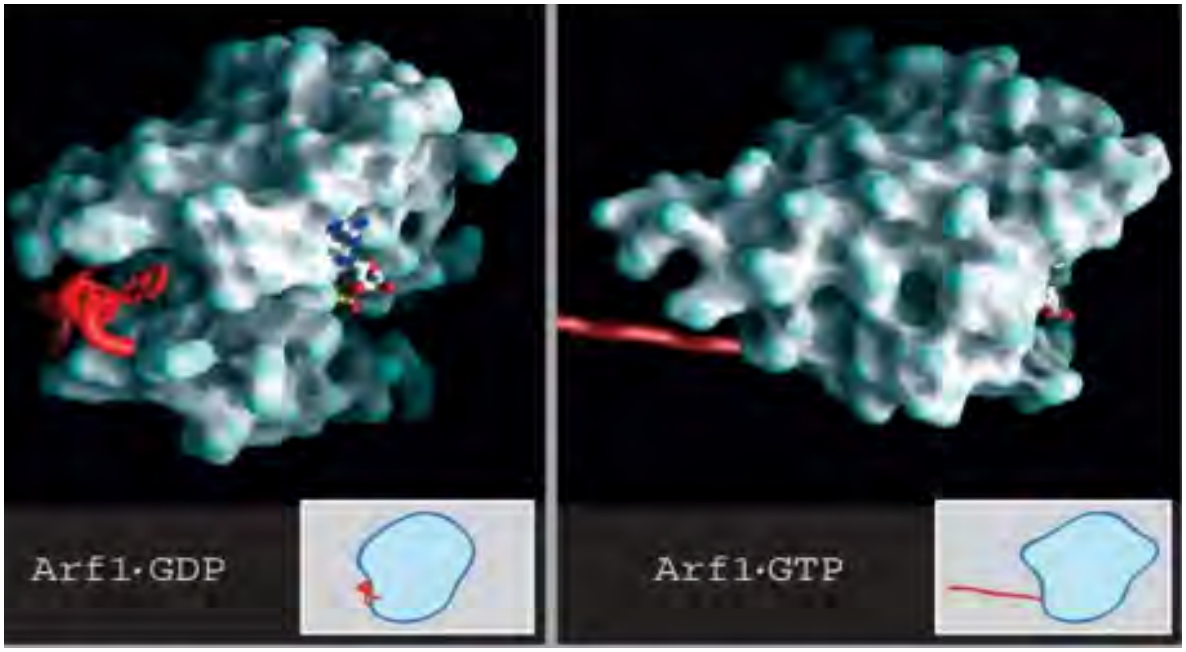

Figure 3: Conformational changes in Arf1 determined by nucleotide exchange. A structural comparison between GDP-bound and GTP-bound Arf1 where the amphipathic α-helix (red) is sheltered within a hydrophobic pocket when bound to GDP (left). Upon nucleotide exchange of GDP for GTP, the amphipathic helix is ejected due to loss of the hydrophobic pocket (right) and is subsequently inserted into the membrane bilayer (Taken from Lee *et al*., 2004).

1.8.3.2. Arf inactivation by ArfGAPs

By contrast, the ArfGAP proteins aid in the inactivation of Arf signalling by enabling the hydrolysis of GTP to GDP at an accelerated rate (Nawrotek *et al*., 2016). Initial studies looking at the general structure of GAP proteins to gain insight into the mechanisms utilised by mammalian GAPs were conducted using the RasGAP domains (Scheffzek *et al*., 1997). This study revealed the presence of an arginine (arginine finger) on the GAP protein which was determined to be responsible for orientating a conserved glutamine residue found in GTPase's switch II region to initiate the nucleophilic attack of the γ-phosphate of GTP by activating a water molecule (Scheffzek *et al*., 1997). In addition, the arginine finger was also found to stabilise negative charges present during the transition state (Scheffzek *et al*., 1997). Together, these processes result in the hydrolysis of GTP on Arf and causes its subsequent deactivation. However, more recent studies revealed that while all GAPs make use of a tandem of residues for the activation of a nucleophilic water molecule and stabilise the negative charges at the transition state, not all GAPs make use of the switch II glutamine/arginine finger tandem but rather utilise different residues in the switch I region to accomplish GTPase hydrolysis (Cherfils and Zeghouf, 2013). Approximately 31 human genes have been found to encode ArfGAP proteins (Kahn *et al*., 2008) of which the most extensively studied ArfGAP members belong to the human ArfGAP1 sub-group since its function has been investigated in context of

Arf-dependent membrane traffic. Principally, ArfGAP mediated hydrolysis is required for the disassociation of coat proteins from membranes, but the timing of hydrolysis initiation needs to be regulated as the coat protomers need time to assemble on their target membrane. Two respective regulatory mechanisms have been described for ArfGAP1. The first model suggests that GAP activity is reliant on the coat protein coatomer where GAP activity is hindered by cargo proteins. The second, more accepted model, hypothesises that ArfGAP1 can sense membrane curvature via its ALPS motifs. The ArfGAP1 lipid-packing sensor (ALPS) motifs allow it to fold into amphipathic α-helices *in vitro* when interacting with highly curved membranes that contain loosely packed lipids (specifically those found on budding COPI and clathrin coated vesicles) (Mesmin *et al*., 2007). This consequently triggers its ability to stimulate Arf GTPase activity. Moreover, these ALPS motifs are also essential in targeting Arf proteins to the Golgi (Levi *et al*., 2008) and correctly orientating ArfGAP1 so that it can efficiently carry out its regulatory function. Moreover, mammalian ArfGAP2 and 3 are believed to have emerged from a common ancestor since they have a 58% sequence identity (Kahn *et al*., 2008). Structurally, these two proteins have little in common with ArfGAP1. This is evident in the lack of ALPS motifs in ArfGAP2/3 (Kahn *et al*., 2008). Despite this, these ArfGAPs are still localised to the Golgi membrane due to high-affinity binding with the COPI coat (Frigerio *et al*., 2007). Understanding how mammalian ArfGEFs and ArfGAPs mediate Arf signalling could provide necessary insights into the mechanisms followed by the isoforms of these proteins in other eukaryotic species. The GTPase cycle regulated by GEFs and GAPs is diagrammatically illustrated in **Figure 4**.

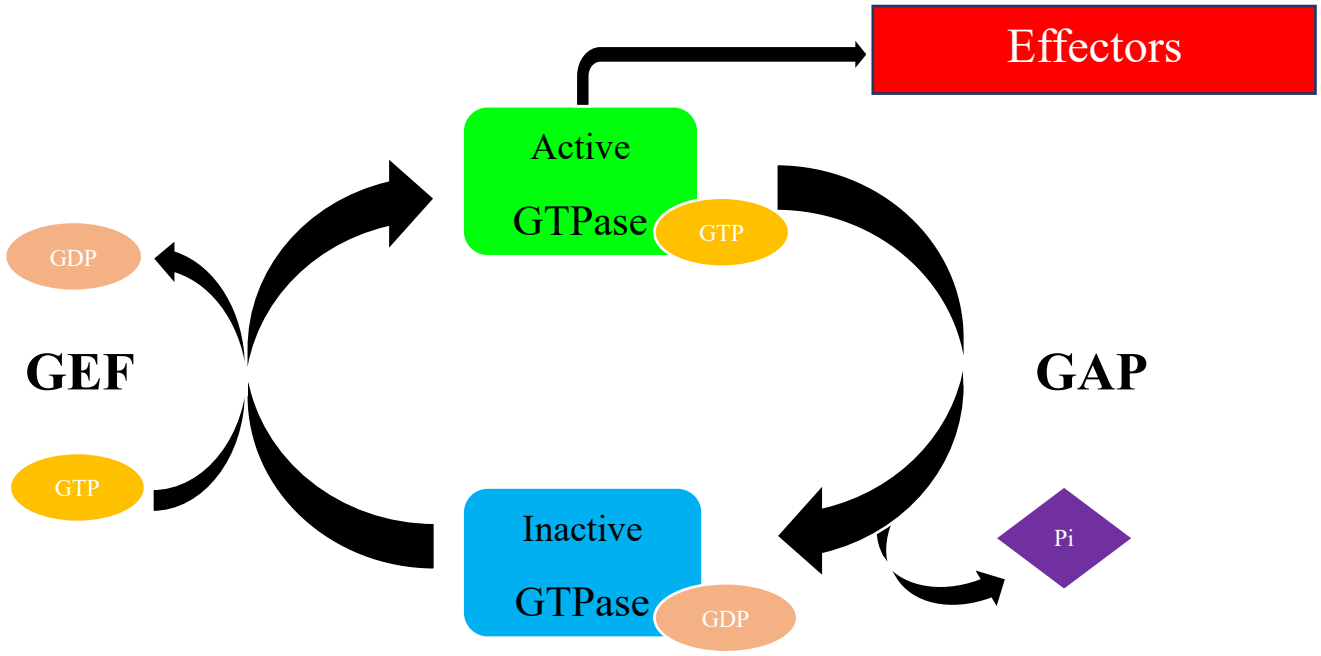

Figure 4: Mode of action for small GTPases. Since GTPases act as molecular switches, they shift between active (-GTP bound) and inactive (-GDP bound) states where nucleotide exchange is regulated by GEFs and GAPs (Adapted from Westrip *et al*., 2021).

1.10 The role of Arf GTPases in cancer

The appeal of Arf GTPases as potential drug targets arose from their indispensable roles in cancer research. Markedly, Arf1 and Arf6 have been the most extensively studied in this regard where several studies have drawn a direct correlation between the dysregulation of expression and activity of Arf proteins, their GEF and GAP regulators as well as their effectors with an increase in the proliferation and metastasis of several cancer types.

1.10.1. The role of Arf6 in cancer research

The overexpression of Arf6 and its subsequent activation of downstream signalling pathways has been directly linked to poor survival rates amongst patients suffering from one of several cancers including but not limited to breast, lung, and pancreatic cancers (Knizhnik *et al*., 2011, Morgan *et al*., 2015, Hashimoto *et al*., 2004). In order to validate the role of Arf6 in breast cancer and how its expression levels affect the cancer's invasive abilities, Hashimoto and colleagues silenced Arf6 (using siRNA-mediated knockdown methods) in mice and found that by doing this, breast cancer as well as melanoma invasion had been impaired (Hashimoto *et al*., 2004). These results suggest that Arf6 plays a significant role in cancer cell invasion and tumour angiogenesis. Moreover, the triple expression of Arf6, phosphorylated epidermal

growth factor receptor (EGFR) and the Arf6GEF BRAG2/GEP100 was found to be associated with an increased risk of mortality in cancer patients (Morishige *et al*., 2008, Casalou *et al*., 2020). To better understand the role of Arf6 in cancer metastasis, researchers looked at local tissue invasion using cancer cell lines as their model system. It is important to note that in order to initiate tissue invasion, cancer cells have to first detach from the primary tumour by dismantling their cell-cell junctions (Guan, 2015). When using Madin-Darby canine kidney (MDCK) cells, it was observed that Arf6 was responsible for inducing internalisation of the adherence molecule E-cadherin which consequently triggers the disassembly of cell-cell junctions (Xu *et al*., 2015). Furthermore, Arf6 was also found to play a key role in the degradation of extracellular matrix (ECM) barriers, which subsequently allows cancer cells to invade the surrounding stroma (Hongu *et al*., 2016). This process is mediated by Arf6 as is regulates invadopodia formation by recruiting the necessary molecules to the plasma membrane. Invadopodia are protrusive structures that are rich in actin and have the ability to degrade ECM and promote cancer cell invasion.

1.10.2. The role of Arf1in cancer

The overexpression of Arf1 has also been observed to play a pivotal role in ovarian, breast and prostate cancers (Casalou *et al*., 2020) A possible explanation for this phenomenon could be found in a study done 10 years prior where a team of researchers found that by inducing epidermal growth factor (EGF) signaling in MDA-MB-231 breast cancer cells, Arf1 was activated (Boulay *et al*., 2008). The association between EGF and the activation of Arf1 was further investigated by Boulay *et al* (2008) where they determined that Arf1 expression was directly associated with breast cancer metastasis and proliferation by contributing to the activation of the phosphatidylinositol 3-kinase (PI3K) pathway, but the detailed mechanism remains to be elucidated (Boulay *et al*., 2008). An additional study revealed that inhibition of Arf1 in MDA-MB-231 breast cancer cells increases the efficacy of actinomycin D and vinblastine which are anti-tumour drugs (Luchsinger *et al*., 2018) and further suggests a correlation between Arf1 and breast cancer cell proliferation and metastasis. Research into prostate cancer has also suggested that Arf1 plays a role in promoting tumourgenesis by stimulating the activation of the mitogen-activated protein kinases (MAPK) ERK1/2, and overexpression of Arf1 increases cell proliferation, anchorage-independent growth and tumourgenesis in prostate cancer cell lines and mouse models (Davis *et al*., 2016). In contrast, the inactivation of Arf1, by mutating its Thr48 residue, terminates Arf1's capability to activate ERK1/2 and consequently inhibits cell proliferation (Davis *et al*., 2016). This suggests that

Arf1 plays an integral part in MAPK signalling in prostate cancer. Finally, in 2017 a study linked the upregulation of Arf1 with increased cell proliferation and migration in epithelial ovarian cancer (EOC) cells, and that this effect was mediated through cell survival and proliferation promoting PI3K/Akt signalling pathway (Gu *et al*., 2017).

1.11. Downstream Arf1 effectors

Upon Arf activation via nucleotide exchange from GDP for GTP and subsequent membrane binding, Arf proteins interact with downstream effector proteins to mediate their diverse biological functions. One of the most studied and well understood functions of the Arf GTPases family is their role in regulating the assembly of various coat complexes onto budding vesicles in several membrane trafficking pathways. This section will focus primarily on Arf1 effectors involved in protein trafficking within the secretory pathway with emphasis placed on the Arf-dependent Golgi-localised, ɣ-ear containing, ADP-ribosylation factor binding (GGA) family of proteins.

1.11.1. Coat protein complex I coatomer (COPI)

The COPI complex is approximately 700 kDa in size and is comprised of seven distinct subunits (Lee *et al*., 2004) which, in a high salt environment, can separate into two subcomplexes, namely the F-COPI subcomplex (contains four components) and the coat-like B-COPI subcomplex (contains three components) (Fiedler *et al*., 1996). Additionally, the components of the F-COPI subcomplex have been shown to have a similar sequence and structure to clathrin-binding adaptor protein (AP) complexes (Bykov *et al*., 2017) which will be further elaborated on below. The COPI complex is mainly recruited to membranes involved in retrograde transport that traffics cargo from the Golgi to the endoplasmic reticulum (ER) and between the Golgi cisternae and is dependent on the activation of Arf1 (D'Souza-Schorey and Chavrier, 2006). Arf1 and COPI associate through interactions between the switch regions of Arf1 and the F-COPI subcomplex of COPI (Zhao *et al*., 1997).

1.11.2. Heterotetrameric adaptor protein (AP) complexes

The AP complexes are responsible for mediating intracellular membrane trafficking that occurs along the secretory and endocytic transport pathways. A total of five AP complexes have been identified where each is comprised of two large subcomplexes which in turn contain smaller subunits (Park and Guo, 2014). Arf1-GTP plays a pivotal role in regulating clathrin coat

recruitment to the late Golgi and endosome compartments by acting as docking sites for AP-1, AP-3 and AP-4, (Ooi *et al*., 1998, Ren *et al*., 2013). The interaction that occurs between Arf1 and the adaptor proteins initiates these adaptors to subsequently bind to other vesicular coat components including scaffolding proteins (which polymerise to form the outermost layer of budding vesicles), accessory proteins (these are responsible for mediating the different aspects of coat functioning) and lastly to sorting signals (which sorts and concentrates cargo into the appropriate vesicles) in preparation for targeted vesicular trafficking (Cai *et al*., 2007, Park and Guo, 2014).

1.11.3. The GGA family of proteins: Structural organisation and cellular utility

The GGA family members contain a carboxy-terminal domain that is homologous to the carboxy-terminal domain of the ɣ1- and ɣ2-adaptin- subunit isoforms of AP-1 and are primarily associated with the TGN and endosomes (Bonifacino, 2004). In addition, they cycle between the cytosol and the *trans*-Golgi network and endosomes via recruitment by Arf1-GTP. Once they are recruited to their targeted membranes, they interact with clathrin (to form vesicle coats) and with the cytosolic tails of various transmembrane cargo proteins and cargo receptors (Ghosh & Kornfeld, 2004). There have been 3 GGA proteins identified in humans (GGA1, GGA2 and GGA3) and they have all been observed to be made up of four domains namely, the VHS, GAT, hinge and GAE domains (Shiba *et al*., 2003, Puertollano *et al*., 2001). Two schematic diagrams representing the shared structural architecture of GGA proteins, and the variations in hinge domains are shown in **Figure 5** (adapted from von Einem *et al*., 2015).

1.11.3.1. The VPS27, Hrs and STAM (VHS) domain

The VHS domain is named after the VPS27, Hrs and STAM proteins as they were the first proteins to be identified and characterised containing this ~140 residue domain (Lohi *et al*., 2002). Since then, at least 60 additional proteins have been found to contain a VHS domain at their N-terminus (Lohi *et al*., 2002). The VHS domain has been observed to function as a recognition module for vesicle cargo proteins by specifically interacting with acidic-cluster-dileucine (AC-LL) or 'DXXLL' motifs (where the X can be interchanged with any amino acid) present in the cytoplasmic tails of vesicle cargo and transport proteins, such as those found in sortilin and M6PRs (Collins *et al*., 2003).

1.11.3.2. GGAs and TOM1 (GAT) domain

The GAT domain is separated from VHS domain by a short proline-rich sequence (Collins *et al*., 2003). GAT is named after this domain's occurrence in GGAs as well as the TOM1 protein and is responsible for GGA's specificity in binding GTP-bound active forms of Arf (excluding GDP-bound inactive forms of Arf) (Hirst *et al*., 2001). The mechanism for this high specificity involves two subdomains within the GAT domain; a N-terminal helix-loop-helix (coiled-coil) motif and a C-terminal three-helix bundle (Shiba *et al*., 2003). The N-terminal hook subdomain is responsible for the recruitment of GGAs onto the Golgi as it binds directly to Arf-GTP which acts as a molecular switch in the GGA recruiting process (Bonifacino, 2004). The three-helix bundle subdomain has a similar structural homology to a domain found in SNARE proteins that are vital in protein-protein interactions (Shiba *et al*., 2003). Additionally, it was also determined that the C-terminus of GGA1 and GGA3 bind ubiquitin and this binding is dependent on the presence of Arf-GTP bound to the N-terminus of the GAT domain (Shiba *et al*., 2003). This finding suggests that GGAs interact with ubiquitinated proteins once they have been recruited to the TGN. The structural significance of the N-terminal hook subdomain (helix-loop-helix) stems from its uniqueness as it is not found in any other Arf-binding proteins, e.g. ArfGEFs and ArfGAPs (Collins *et al*., 2003). Yet, the binding of these modules onto the surface of Arf overlap remarkably. The hook subdomain of the GGA GAT domain as well as ArfGEF bind to the switch I and switch II regions of active Arf (Arf-GTP), whereas ArfGAP binds to the Arf switch II region (Ghosh & Kornfeld, 2004, Bonifacino, 2004). Consequently, it is suggested that the GGA-GAT domain competes with ArfGAPs to bind with Arf, which ultimately maintains membrane association of both Arf-GTP and GGAs (Collins *et al*., 2003).

1.11.3.3. The ɣ-adaptin ear (GAE) and hinge domains

The GAE domain is a C-terminal appendage found in the GGA family of proteins which is comprised of approximately 120 residues. This domain is homologous to the ɣ-adaptin-subunit isoforms of AP-1, which suggests that it serves as a platform for the binding of other endocytic accessory proteins such as ɣ-synergin and Rabaptin-5 (Nogi *et al*., 2002, Miller *et al*., 2003). The GAE domain is separated from the GAT domain by a long clathrin-binding linker (also referred to as the hinge domain), which is largely unstructured and is the least conserved in terms of sequence and length when compared to the other GGA domains or other proteins (Boman *et al*., 2002, Doray *et al*., 2012). The GGA hinge region interacts directly with clathrin which subsequently couples the membrane-bound cargo to the mechanical scaffold of vesicles forming at the *trans*-Golgi network (Boman *et al*., 2002, Collins *et al*., 2003). Since the hinge

region also associates with AP-1, this suggests that AP-1 and GGAs work together in recruiting various cargo to clathrin-coated vesicles at the TGN (Lui *et al*., 2003, Bonifacino, 2004).

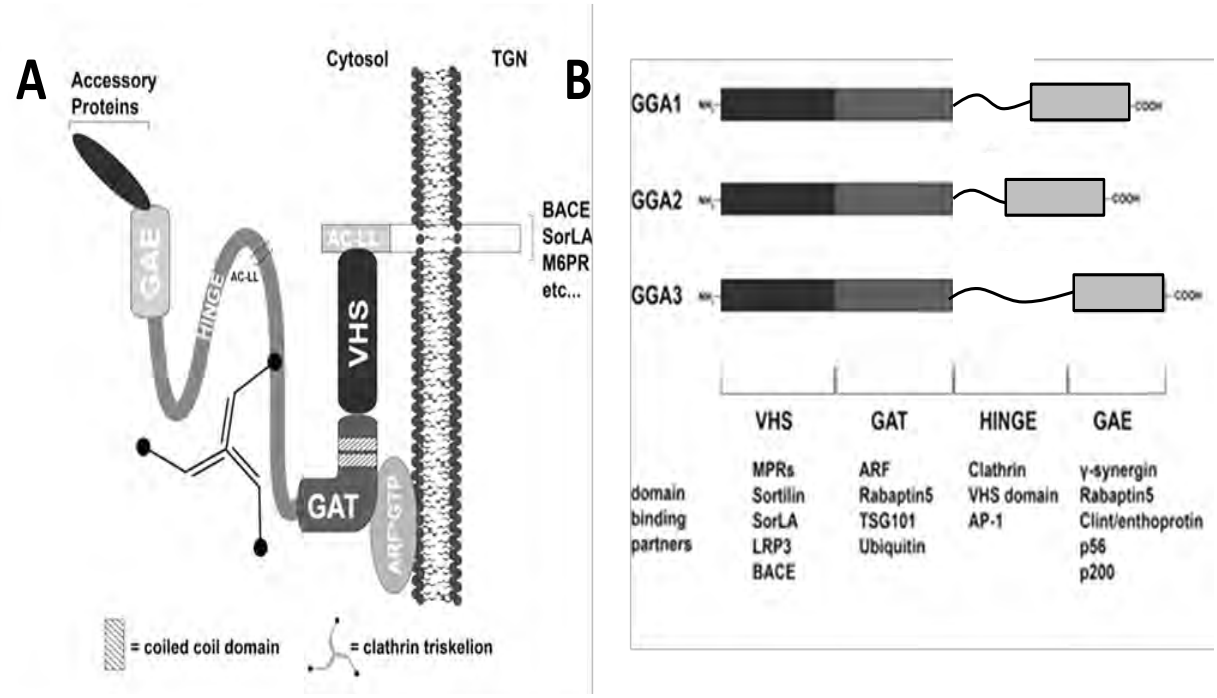

Figure 5: Structural architechture of GGA proteins. **A:** GGA's are recruited from the cytosol onto the *trans*-Golgi network where they regulate protein transport to endosomes/lysosomes. The N-terminal VHS domain recognises protein cargo and binds those that contain AC-LL (DXXLL) motifs. Linked to the VHS domain is the GAT domain (containing a coiled-coil subdomain as well as a three-helix bundle subdomain) which binds active Arf-GTP and is responsible for membrane recruitment of the GGA protein. The hinge domain contains one or more clathrin binding sites and houses an internal AC-LL motif for autoregulation. The GAE domain binds specific accessory proteins. **B:** GGA1-3 have variable hinge domains but the other three domains (VHS, GAT & GAE) are conserved and have distinct binding partners. (Adapted from von Einem *et al*., 2015).

1.12. Arf1 inhibitors

The discovery of Arf GTPase inhibitors has primarily been centralised around Arf1. While these inhibitors have been valuable in defining the functions of Arf1 in cells, their discovery has also been further motivated by the potential Arf1 has displayed as an anti-cancer drug target. Notably, the existing Arf1 inhibitors are predominantly compounds that target protein-protein interactions where they block the activation of Arf1 by ArfGEFs and, to a lesser extent, Arf1 deactivation by ArfGAPs.

1.12.1. Brefeldin A (BFA)

First described in 1958, brefeldin A is a fungal fatty acid metabolite that has become a well-established inhibitor for Arf1. This compound has demonstrated significant effects on the function and structure of intracellular organelles, more specifically the Golgi apparatus. This motivated further research into BFA so as to gain a better understanding of the mechanisms responsible for the underlying organisation of intracellular compartments and to use as a tool in target-based inhibition of secretory pathway events. The subsequent discovery that BFA specifically inhibits Golgi-localised Arf1 activation by obstructing ArfGEF activity revolutionised our understanding of BFA's mechanism of action (Helms and Rothman, 1992, Donaldson *et al*., 1992, Chardin and McCormick, 1999, Pacheco-Rodriguez *et al*., 2002). Interestingly, brefeldin A stabilises the Arf1:Sec7 domain complex instead of impeding its formation. This establishes BFA as an uncompetitive inhibitor that stimulates Arf1-GDP to act as a 'dominant negative' which traps Arf1-GEF and ultimately obstructs Arf1 activation (Peyroche *et al*., 1999, Chardin and McCormick, 1999). Despite recent evidence suggesting that BFA has remarkable antitumour and apoptosis-inducing activity (Larsson *et al*., 2006, Paek, 2018, Zhou *et al*., 2019), it is not considered a suitable drug for human administration largely because of its poor bioavailability and therapeutic index (Phillips *et al*., 1998, Ohashi *et al*., 2012). Nevertheless, multiple compounds that disrupt the Golgi by targeting Arf1 have been identified and have shown good bioavailability (Toda *et al*., 2015). This supports the hypothesis that targeting the Golgi with compounds characteristically similar to BFA may hold a lot of therapeutic potential.

1.12.2. Golgicide A (GCA)

Golgicide A was first discovered in a screening campaign for small-molecule inhibitors that obstruct the effects of bacterial toxins on host cells (Sáenz *et al*., 2009). This compound was found to effectively protect Vero cells from shiga toxin and consequently encouraged further research into its mechanism of action. By conducting immunofluorescence experiments, GCA seemed to have profound effects on the Golgi apparatus and TGN by dispersing the *medial*- and *cis*-Golgi compartments (Sáenz *et al*., 2009). Moreover, time-course experiments disclosed that the Golgi first became tubulated before it dispersed completely (Sáenz *et al*., 2009). Both the aforementioned observations drew similarities with the effects resulting from BFA treatment. It was then established that GCA is selective for GBF1 – an ArfGEF that mediates vesicular trafficking by activating Arf1 (Sáenz *et al*., 2009). This suggests that the GBF1

ArfGEF is vital in maintaining Golgi structure, enabling retrograde protein trafficking between the Golgi and TGN and that the inhibition of its functioning results in similar effects as that displayed by treatment with BFA.

1.12.3. AMF-26

Since the discovery of BFA, the interaction between Arf1 and ArfGEF has become an attractive drug target, especially in cancer research. This motivated research into the identification of inhibitory compounds that target this interaction and have BFA-like properties. A study conducted by Y. Ohashi *et al* (2012) made use of a computer modelling/molecular dynamics (MD) simulation which suggested that AMF-26 bound to the same contact surface as BFA (the Arf1-Sec7 domain). This motivated an investigation looking at the effects that this compound has on the Golgi apparatus and the activation status of Arf1. The results indicated, similarly to BFA, that AMF-26 affects membrane trafficking by disrupting the Golgi, particularly the *cis*-Golgi and *trans*-Golgi networks by inhibiting the functioning of GBF1 and impeding the activation of Arf1 (Ohashi *et al*., 2012). Moreover, treatment with AMF-26 indicated a complete regression of human breast cancer BSY-1 xenografts (Ohashi *et al*., 2012). These studies demonstrated AMF-26's antitumour properties and further displayed its promise as a novel drug candidate when targeting Arf1 activation.

1.13. Arf1 as a possible antimalarial drug target

The absence of lipid and protein trafficking machinery in mammalian erythrocytes, where malaria parasites spend the majority of their life cycle, means that the host cell cannot provide the necessary nutrients for this intracellular parasite that requires a continuous supply of energy in order replicate rapidly. In order to overcome this challenge, malaria parasites export approximately 10% of their own genome-encoded proteins into the cytosol of their host cells which is believed to include trafficking machinery that allow it to import and export proteins between its parasitophorous vacuole (PV) and the erythrocyte membrane (Dhangadamajhi *et al*., 2010). Notably, the PV provides an interface between the parasite and the host cell cytoplasm. Since malaria relies heavily on protein trafficking for its survival, an increasing number of studies have started investigating proteins that may play a pivotal role in these trafficking events. This led to the eventual discovery of an Arf1 isoform in the *P. falciparum* genome (Lee *et al.,* 1997). Despite mammalian Arf1 proteins being well characterized and thoroughly researched, relatively little is known about *P. falciparum* Arf1 (*Pf*Arf1) except that

it binds GTP, has low intrinsic GTPase activity (Stafford *et al*., 1996), has the capability to stimulate phospholipase D and phosphatidylinositol 4-phosphate 5-kinase activity (like mammalian Arf1) (Lee *et al*., 1997; Leber *et al*., 2009), co-localises with the Golgi marker GRASP in parasites (Thavayogarajah *et al*., 2015), has a high structural similarity to mammalian Arf1 (Cook *et al*., 2010) and is inhibited by the canonical Arf1 inhibitor, brefeldin A (BFA) and Golgicide A (GCA) (Crary *et al*., 1992).

Min Zhang and colleagues carried out a landmark study in which they used transposon mutagenesis of *P. falciparum* to create over 3 000 mutants in order to carry out whole-genome loss-of-function screens (Zhang *et al*., 2018). They managed to saturate the genome, define mutability of genes, and determine the fitness costs of a large proportion of the parasite genome. Their results suggested that 2680 genes are crucial for optimum growth and survival in the asexual blood stages, one of which was *Pf*Arf1 (Zhang et al., 2018). Additional essential genes included the only gene encoding a sec7-containing protein (presumably an ArfGEF), and one of the two genes predicted to encode ArfGAPs. Additional evidence for the essentiality and 'druggability' of Arf1 function is that Brefeldin A and Golgicide A – both known inhibitors of Arf1 activation in mammalian cells – rapidly disperse *Pf*Arf1 from the parasite Golgi and inhibit *P. falciparum* viability with low micromolar IC_{50} values (T. Swart, PhD thesis). In addition, a screen of compounds for inhibitors of *Pf*Arf1 deactivation by *Pf*ArfGAP1 (one of the two predicted ArfGAPs encoded by the *P. falciparum* genome) yielded GAP inhibitors that also compromise parasite viability at low micromolar IC_{50}s (Swart *et al*., 2020). From a drug discovery point of view, the high similarity in structure between human Arf1 and *Pf*Arf1 may raise concerns surrounding the selectivity with which the function of *Pf*Arf1 vs. its human counterpart could be disrupted. However, Arf inhibitors act by inhibiting the GEFs and GAPs which regulate the activation and deactivation of Arf GTPases and not Arf1 itself. This is useful because there are structural differences between GEFs and GAPs across different species (Barr and Lambright, 2010) possibly enabling increased selectivity. As an example, the abovementioned *Pf*ArfGAP1 inhibitors selectively inhibit the deactivation of *Pf*Arf1 by *Pf*ArfGAP1, not human ArfGAP1, and *vice versa* for human ArfGAP1 inhibitors (Swart et al., 2020; T. Swart, PhD thesis). The functional characterisation and the promising results obtained through the abovementioned Arf1 studies has further developed the idea that it could make a promising target when combatting malaria.

1.14. *P. falciparum* ArfGEFs and ArfGAPs

Much like their Ras-related counterparts, Arf proteins cycle between two main conformations, namely active GTP-bound and inactive GDP-bound forms. This phenomenon, as described in section 1.7.3, is assisted by two classes of regulatory proteins, ArfGEFs and ArfGAPs. This is also true for *P. falciparum* Arf1. Unlike the 31 human genes that encode proteins with ArfGAP domains, the *P. falciparum* genome only encodes two ArfGAP-like proteins (Zhang *et al*., 2018). Structural analysis of one of these *Pf*ArfGAP isoforms (also referred to as *Pf*ArfGAP1) revealed a high similarity in the catalytic domain when compared with mammalian ArfGAP domains (Cook *et al*., 2011). Despite this comparable similarity in tertiary structure, there was also an observed variance in amino acid sequence homology when compared with human ArfGAP1 (~39% identity and ~52% similarity) (Cook *et al*., 2011) which suggests that different amino acid residues in this *Pf*ArfGAP isoform interact with *Plasmodium* Arf1. Nonetheless, a study conducted by Swart *et al* (2020) confirmed that the hydrolysis of GTP and subsequent deactivation of *Pf*Arf1 could be accomplished using the GAP domain of human ArfGAP1 *in vitro*. It was also confirmed that both *Pf*ArfGAP isoforms showed catalytic GAP activity, however, contrary to *Pf*ArfGAP1, the *Pf*ArfGAP2 was superfluous for the survival of blood-stage parasites (Zhang et al., 2018). Moreover, genome analysis conducted on *P. falciparum* showed a single ArfGEF which was identified by its unusual Sec7 domain (Baumgartner *et al*., 2001). Unlike the Sec7 domains found in other eukaryotes, *Plasmodium* parasites contain an additional 146 amino acids within the Sec7 domain of its ArfGEF (Baumgartner *et al*., 2001). Despite this insertion sequence, a study done in 2004 confirmed that this domain was responsible for Brefeldin-A (BFA) sensitivity in *P. falciparum* parasites. This suggests that the *Pf*ArfGEF is similar to its mammalian counterparts, plays an essential role in *Pf*Arf1 activation and protein trafficking within the secretory pathway (Wiek *et al*., 2004).

1.15. This study's motivation, overall aim and experimental objectives

1.15.1. Motivation:

The inability of mosquito vector control measures to eradicate malaria and the absence of the widespread deployment of a highly effective vaccine entails that antimalarial drug compounds remain a principal component of malaria control measures. However, historic antimalarials have become obsolete due to parasite resistance, which is also threatening ACTs, the current

mainstay of malaria treatment. In the exploration of novel targets for the discovery of antimalarial compounds, Arf1 may be proposed as a candidate, based on the interest in Arf1 as a cancer drug target and existing Arf1 inhibitors that show anti-cancer activity in cell culture and mouse models. A challenge in the identification of Arf1 inhibitors is the lack of robust and effective plate-based assays that can be used to screen a variety of different compound libraries for Arf inhibitors. This was addressed in a study conducted by Swart et al. (2020) which described a plate-based GGA3-GST capture assay that could detect the *in vitro* deactivation of *Pf*Arf1 by *Pf*ArfGAP1. The assay involved the incubation of His-tagged *Pf*Arf1-GTP with *Pf*ArfGAP1, followed by the immobilisation of *Pf*Arf1 in nickel-coated 96-well plates. The residual active *Pf*Arf1 in the wells could then be detected by incubation with the GAT domain of GGA3 fused to GST, followed by the addition of a colorimetric GST substrate. The assay was used to screen a compound library and identify small molecule inhibitors of GAP-mediated *Pf*Arf1 deactivation. Encouragingly, the inhibitors were also found to inhibit *in vitro P. falciparum* parasite viability at low micromolar concentrations. However, it remains unclear whether the compounds are able to inhibit *Pf*Arf1 deactivation in the parasites, or whether the anti-parasitic activity of the compounds could be ascribed to unrelated off-target effects. Addressing this is the motivation of the study.

1.15.2 Overall aim of this study:

To confirm the antimalarial mode of action of *Pf*Arf1 activation or deactivation inhibitors identified in *in vitro* protein-based screens, an assay is required that is able to detect the activation status of *Pf*Arf1 in cultured parasites exposed to the compounds – inhibitors of *Pf*Arf1 activation should cause a decrease in the level of active *Pf*Arf1 in parasites, and *vice versa* for *Pf*Arf1 deactivation inhibitors. The aim of this study was to conceptualise, establish and validate an ELISA-based method for detecting changes in active *Pf*Arf1 levels in compound-exposed parasites to assist in the validation of *Pf*Arf1 as antimalarial drug target.

1.15.3 Experimental objectives:

The conceptual ELISA assay exploits the phenomenon that domains of the effector protein GGA3 bind selectively to active Arf1. To achieve the goal of developing an ELISA assay to quantify active *Pf*Arf1 in cultured parasites, the experimental objectives included:

- the heterologous expression of *Pf*Arf1, GST-GGA3^{GAT} and GST-GGA3^{PBD} in *E. coli* and purification of the proteins by affinity chromatography;

- comparing the ability of the two GST-GGA3 constructs to selectively bind to active *Pf*Arf1-GTP vs. inactive *Pf*Arf1-GDP using two assay formats – a nickel plate assay where His-tagged *Pf*Arf1 is immobilised on the plate and GST-GGA3 binding detected by GST enzyme activity, and a glutathione plate ELISA assay where the GST-GGA3 proteins are immobilised on the plate and *Pf*Arf1 binding detected by anti-Arf1 antibodies;
- determining if the glutathione plate ELISA assay can detect active vs. inactive *Pf*Arf1 present in lysates of cultured *P. falciparum* parasites;
- validating the assay by using it to detect expected changes in the levels of active *Pf*Arf1 in parasite cultures treated with an Arf1 activation inhibitor (BFA) and two experimental Arf1 deactivation inhibitors (Chem1099 and Chem3050);
- exploring the ability of the assay to detect changes in the levels of active Arf1 in human (HeLa) cells treated with Arf1 inhibitors.

A more detailed description of the ELISA assay format and the experimental objectives is presented in the introduction to Chapter 3.

Chapter 2: Methods and materials

2.1. Plasmid constructs used in this study

2.1.1. PfArf1 construct for in vitro protein interaction assays

The pET-28a (+) – *Pf*Arf1$^{N\Delta17}$ construct, lacking codons for the first 17 amino acids of *Pf*Arf1, was prepared by T. Swart by sub-cloning a codon-optimised *Pf*Arf1$^{N\Delta17}$ nucleotide sequence (Genscript) into the *Bam*HI/*Nhe*I restriction sites of the pET-28(+) plasmid (Swart *et al*., 2020). Cryopreserved glycerol stocks of T7 Express lysY/Iq *E.coli* cells (New England Biolabs) containing the construct was donated by T. Swart and subsequently used in this study.

2.1.2. GST-GGA3^{GAT} construct for in vitro protein interaction assays

The pGEX-4T-2/GGA3^{GAT} construct was used to express the GST-GGA3^{GAT} fusion protein where GST encoded by the pGEX-4T-2 expression plasmid was fused to the nucleotide sequence encoding the GAT domain of the human GGA3 (amino acids 107–286). The construct was donated by K. Nakayama (Addgene plasmid #79436). Cryopreserved glycerol

stocks of T7 Express lysY/Iq *E. coli* cells harbouring the construct were prepared and donated by T. Swart for use in this study.

2.1.3. GST-GGA3^{PBD} construct for in vitro protein interaction assays

The pGEX-4T-1/GGA3^{PBD} construct was obtained from GenScript, where the *E. coli* codon-optimised nucleotide sequence encoding the protein binding domain of human GGA3 (amino acids 1-316) was sub-cloned into the *Bam*HI/ *Xho*I restriction sites of the pGEX-4T-1 plasmid prior to delivery as a lyophilised stock. The plasmid was prepared for *E. coli* transformation by dissolving the pGEX-4T-1/GGA3^{PBD} construct in 20 µL of filter-sterilised water and storing it at 20°C until use.

2.2. Preparation of pGEX-4T1/GGA3^{PBD} *E. coli* stocks

2.2.1. Preparation of competent E. coli *cells*

Rosetta (DE3) *E. coli* cells (Novagen) and T7 Express lysY/Iq *E. coli* cells (New England BioLabs) were used in this study. Untransformed *E. coli* cells were grown in 5 mL Luria broth at 37°C for 16 hours with continuous agitation. An aliquot of 2.5 mL of the overnight culture was added to 100 mL of Luria broth (1 in 40 inoculum) and incubated at 37°C with continuous agitation until the OD_{600nm} reached 0.6 - 0.8. The cells were collected by centrifugation at 2152 x *g* for 10 minutes at 4°C and thereafter kept on ice. The cells were resuspended in 4 mL of refrigerated RF-1 buffer (100 mM KCl, 50 mM $MnCl_2$, 30 mM potassium acetate, 10 mM $CaCl_2$, 15% (v/v) glycerol, pH 5.8) and incubated on ice for 20 minutes. The cells were collected by centrifugation at 1377 x *g* for 10 minutes at 4°C and gently resuspended in 3 mL refrigerated RF-2 buffer (10 mM HEPES, 10 mM KCl, 75 mM $CaCl_2$, 15% (v/v) glycerol, pH 6.8). Aliquots of the bacterial suspensions were prepared in cryotubes and stored at -80°C.

2.2.2. Transformation of competent E. coli *cells using heat shock*

Competent *E. coli* cells were thawed on ice. To 50 µL of competent *E. coli* cells, 1 µL pure plasmid was added. The mixture was briefly and gently mixed before being incubated on ice for 30 minutes. Heat shock was conducted by incubating the mixtures in a heating block at 42.5°C for 1 minute and thereafter immediately incubated on ice for 5 minutes. Luria broth (500 µL) was added to the transformation mixture, and the solution was incubated at 37°C for

1 hour with gentle agitation. The cells were collected by centrifugation at 3099 x *g* for 3 minutes and resuspended in 100 µL Luria broth. The resuspended cells were plated on Luria-agar plates containing 50 µg.mL^{-1} kanamycin or ampicillin (depending on the construct resistance marker) and incubated at 37°C for 16 hours before being stored at 4°C. To prepare a cryopreserved stock, a single colony was picked from the plate, transferred to 5 mL Luria broth containing 50 µg.mL^{-1} ampicillin or kanamycin and propagated overnight at 37°C with gentle shaking. An aliquot of 850 µL of the overnight culture was combined with 150 µL glycerol in a cryotube and stored at -80°C.

2.3. Bacterial protein expression and purification

2.3.1. Analytical-scale bacterial expression

Scrapings from the glycerol stocks of expression constructs in transformed Rosetta (DE3) or T7 Express lysY/Iq competent *E. coli* cells were propagated in 5 mL Luria broth containing 50 µg.mL^{-1} kanamycin or ampicillin at 37°C for 16 hours with continuous agitation. An aliquot of the overnight culture (0.4 mL) was transferred to 8 mL Luria broth containing 50 µg.mL^{-1} kanamycin or ampicillin (1 in 20 inoculum) and incubated at 37°C with continuous agitation until the OD_{600nm} value reached 0.5 – 0.9. Protein expression was induced by adding 1 mM IPTG to the expression culture and incubation continued for 3 - 4 hours at 37°C. The bacterial cells were collected by centrifugation at 5 000 *g* for 10 minutes and stored at -20°C overnight. Thereafter, all steps were conducted on ice using ice-cold buffers. The frozen pellet was thawed for 10 minutes and resuspended in 1 mL wash buffer (50 mM Tris-HCl, pH 8.0). The cells were lysed by adding a final concentration of 2 mg.mL^{-1} lysozyme and incubated for 30 minutes, followed by two cycles of probe sonication at 60 Hz for 45 seconds with a 1 minute interval between cycles. The cell lysate was centrifuged at 5 000 *g* for 10 minutes to separate the soluble and insoluble fractions. The insoluble fraction was resuspended in 1 mL wash buffer and both fractions were combined with 25 µL 4X SDS-PAGE sample buffer (0.25 M Tris, pH 6.8, 4.2% (w/v) SDS, 40% (v/v) glycerol, 4% (v/v) β-mercaptoethanol, 1% (w/v) bromophenol blue in water), followed by a 5-minute incubation in boiling water. Thereafter, the fractions were stored at -20°C for subsequent SDS-PAGE analysis.

2.3.2. Preparative-scale bacterial expression

Scrapings from frozen glycerol stocks of the relevant expression constructs in transformed Rosetta (DE3) or T7 Express lysY/Iq *E.coli* cells were propagated in 5 mL Luria broth containing 50 μg.mL^{-1} kanamycin or ampicillin at 37°C for 16 hours with continuous agitation. A sample of 2.5 mL of the overnight culture was transferred to 250 mL of Luria broth containing 50 μg.mL^{-1} kanamycin or ampicillin (1 in 100 inoculum) and incubated at 37°C with continuous agitation until the OD_{600nm} value reached 0.5 - 0.9. Protein expression was induced by adding 1mM IPTG to the expression culture and incubating for 3 -4 hours at 37°C. The bacterial cells were collected by centrifugation at 5 000 *g* for 10 minutes and the pellet was resuspended and washed in 20 mL of Ni-NTA equilibration buffer (50 mM Tris-HCl, 20 mM imidazole, pH 8.0) or GST equilibration buffer (PBS containing 0.2% Triton X-100 with 1mM PMSF) for His-tagged (*Pf*Arf1$^{N\Delta17}$) and GST-tagged (GST-GGA3^{GAT} and GST-GGA3^{PBD}) fusion proteins respectively. The resuspended pellet was centrifuged again at 5 000 x *g* for 10 minutes, the supernatant discarded, and the pellet stored at -20°C overnight.

2.3.3. Cell lysis and protein extraction

Cell lysis was conducted on ice using refrigerated buffers. The frozen pellet of the preparative-scale expression culture was thawed on ice for 30 minutes before being resuspended in 10 mL Ni-NTA or GST equilibration buffer. The cells were lysed in 2 mg. mL^{-1} lysozyme in equilibration buffer for 30 minutes on ice, and by 2 cycles of sonication at 60 Hz with 1-minute resting periods on ice between each cycle. The cell lysate was centrifuged at 14 000 *g* for 30 minutes to separate the soluble and insoluble fractions. The insoluble fraction was discarded, and the soluble fraction retained on ice for subsequent affinity chromatography purification.

2.3.4. Preparation of Ni-NTA and glutathione agarose columns

All reagents and buffers used in the affinity chromatography columns were filter-sterilised using a 0.45 μm filter. Ni-NTA Fast Start kit (Qiagen) columns were stored at 4°C in storage solution (50% ethanol in water). The column was washed in one volume water and was conditioned with two volumes of Ni-NTA equilibration buffer (50 mM Tris-HCl, 20 mM Imidazole, pH 8.0) before purification. To prepare the glutathione agarose column, 3-4 mL of Pierce glutathione agarose slurry (ThermoFisher Scientific) was added to an empty column and left at 4°C for 60 min for the beads to settle. The beads were washed in 3 volumes of water and the column stored in glutathione agarose storage buffer (2 M NaCl, 1 mM sodium azide in

water) at 4°C until further use. Before purification, the column was washed in one volume of water and equilibrated with two volumes of GST equilibration buffer (PBS containing 0.2% Triton X-100 with 1mM PMSF).

2.3.4.1. Protein purification by Ni-NTA affinity chromatography

The soluble *E. coli* fraction was filtered through a 0.45 µm syringe filter. A 60 µL aliquot of the filtered lysate was collected and stored on ice (Fraction 1, F1) for subsequent SDS-PAGE analysis. The filtered lysate was applied to the equilibrated Ni-NTA column. A 60 µL aliquot of the flow-through was collected and stored on ice (F2). The column was washed twice in 5 mL Ni-NTA equilibration buffer. A 60 µL aliquot of the flow-through from each wash was collected and stored on ice (F3 & F4). Bound proteins were eluted by applying 3 mL Ni-NTA elution buffer (50 mM Tris-HCl, 500 mM imidazole, pH 8.0) to the column. A 60 µL aliquot of the eluate was collected and stored on ice in preparation for SDS-PAGE analysis (F5). The rest of the eluate was stored on ice until desalting.

2.3.4.2. Recharging the Ni-NTA column

Once protein purification was complete, the Ni-NTA column was washed with 7 mL filter-sterilised water, followed by 7 mL of stripping buffer (20 mM sodium phosphate, 500 mM NaCl, 50 mM EDTA, pH 7.4) which was left to run through the column. Another 7 mL of filter-sterilised water was added to the column before the addition of 7 mL 0.1 M nickel sulphate solution. Another 7 mL of filter-sterilised water was left to flow through the column before adding storage solution (50% ethanol in water). The recharged column was stored at 4°C until further use.

2.3.4.3. Protein purification by glutathione affinity chromatography

The soluble *E. coli* fraction was filtered through a 0.45 µm syringe filter. A 60 µL aliquot of the filtered lysate was collected and stored on ice for subsequent SDS-PAGE analysis (F1). The filtered lysate was applied to the equilibrated glutathione agarose column. A 60 µL aliquot of the flow-through was collected and stored on ice (F2). The column was washed twice in 5 mL glutathione equilibration buffer. A 60 µL aliquot of the flow-through from each wash was collected and stored on ice (F3 & F4). Bound proteins were eluted by applying 3 mL glutathione elution buffer (10 mM reduced glutathione, 50 mM Tris-HCl, pH 9.5) to the column. A 60 µL aliquot of the eluate was collected and stored on ice (F5). The rest of the eluate was stored on ice until desalting. After purification, the column was washed in two volumes of water, one volume of glutathione cleansing buffer 1 (0.1 M borate, 0.5 M NaCl,

pH 8.5), one volume of water, one volume of glutathione cleansing buffer 2 (0.1 M acetate, 0.5 M NaCl, pH 4.5), one volume of water and stored in glutathione storage buffer at 4°C until further use.

2.3.5. Protein desalting and storage

A PD-10 desalting column containing Sephadex G-25 M resin (GE Healthcare), was equilibrated with 5 volumes (7 mL each) of assay buffer (25 mM HEPES, 150 mM KCl, 1 mM $MgCl_2$, 1 mM DTT, pH 7.4). The eluate obtained by Ni-NTA or glutathione-agarose affinity chromatography was applied to the desalting column and allowed to flow through the resin. Purified proteins were subsequently eluted by adding 3.5 mL assay buffer to the column. A 60 µL aliquot of the desalted purified protein was collected and stored on ice for SDS-PAGE analysis (F6). Purified, desalted proteins were stored in 20% (v/v) glycerol at -20°C.

2.3.6. Bradford assay – Protein concentration determination

The concentration of the desalted purified protein was determined alongside a BSA protein standard curve using a Bradford assay. A two-fold dilution series ranging from 0.075 – 1.25 $mg.mL^{-1}$ BSA in assay buffer was prepared and stored at -20°C until use. Bradford reagent (Sigma-Aldrich) was equilibrated to room temperature and 250 µL was added to 5 µL of assay buffer (background), BSA protein standards and desalted purified protein samples in a 96-well plate and incubated at 25°C for 5 minutes. The absorbance at 595 nm was determined for each sample in a Spectramax M3 plate reader (Molecular Dynamics). After subtracting the Abs_{595} readings obtained with the background samples, a BSA standard curve with an R^2 value ≥ 0.99 was used to obtain the concentration of the desalted purified proteins.

2.4. SDS-PAGE and Western blotting

2.4.1. SDS-PAGE

The F1- F6 samples collected in sections 2.3.4.1 and 2.3.4.3 were combined with 20 µL of 4X SDS-PAGE sample loading buffer (0.25 M Tris, pH 6.8, 4.2% (w/v) SDS, 40% (v/v) glycerol, 4% (v/v) β-mercaptoethanol, 1% (w/v) bromophenol blue) and incubated in boiling water for 5 minutes. The samples were loaded in the wells of a 4% (w/v) acrylamide stacking gel (0.125 M Tris, pH 6.8, 0.1% (w/v) SDS, 4% (w/v) acrylamide, 0.1% (w/v) *bis*-acrylamide) alongside

a blue pre-stained protein standard broad range molecular weight marker (New England Biolabs) or a Precision plus protein all blue pre-stained protein standard (Bio-Rad) and resolved on a 12% or 8% (w/v) acrylamide resolving gel (0.38 M Tris, pH 8.8, 0.1% (w/v) SDS, 12% or 8% (w/v) acrylamide, 0.27% (w/v) *bis*-acrylamide). Electrophoresis was carried out for 90 minutes at 120V in SDS-PAGE running buffer (25 mM Tris, 192 mM glycine, 0.1% (w/v) SDS) (Laemmli, 1970). Gels were stained in Coomassie stain (0.25% (w/v) Coomassie blue R-250, 45 % (v/v) methanol, 10% (v/v) acetic acid in water) overnight at 37°C with gentle agitation. Stained gels were destained in a destain solution (40% (v/v) methanol, 10% (v/v/) acetic acid in water) until bands were visible. Gels were digitally photographed using a Chemidoc XRS+ gel documentation system and software (Bio-Rad).

2.4.2. Western Blotting

The proteins of interest were resolved on polyacrylamide gels where the Coomassie staining was omitted and proceeded to be transblotted onto a Hybond ECL nitrocellulose blotting membrane (Amersham) at 100 V (250-300 mA) for 60 minutes at 4°C in transblotting buffer (25 mM Tris, 192 mM Glycine, 20% (v/v) methanol in water) using a Mini-PROTEAN II electrophoresis apparatus (Bio-Rad). Following the transblotting, the membrane was rinsed in water. The blot was incubated with a temporary Ponceau S stain solution (0.1% (w/v) Ponceau, 1% (v/v) glacial acetic acid in water) for 5 minutes to ensure successful transfer before being destained with Ponceau-S destain solution (1% (v/v) glacial acetic acid) until the bands became visible.

2.4.2.1. Detection of His-tagged proteins

The blot was blocked with 20 mL incubation buffer (0.1% (v/v) Tween-20, 1 % (w/v) BSA, 2% (w/v) milk powder in tris-buffered saline (TBS; 40 mM Tris, 150 mM NaCl, pH 7.4) overnight at 4 °C with gentle agitation. The blot was subsequently incubated with a 1:5000 dilution of HisDetector Nickel-HRP (SeraCare) in incubation buffer for 1 hour at room temperature with gentle agitation. After three washes with incubation buffer, the blot was covered with TMB membrane peroxidase substrate (SeraCare) and rinsed immediately with water once bands were visible. An image of the blot was taken using the Chemidoc XRS + gel documentation system and software (Bio-Rad).

2.4.2.2. Detection of GST-tagged proteins

The membrane was blocked in incubation buffer (0.1% (v/v) Tween-20, 1% (w/v) BSA, 2% (w/v) milk powder in TBS) for 40 minutes with gentle agitation. For the detection of GST-

tagged proteins the membrane was incubated in a 1:1000 dilution of rabbit anti-GST primary antibodies (Sigma-Aldrich) in incubation buffer for 1 hour, with gentle agitation at room temperature. The membrane was washed four times in wash buffer (0.1% (v/v) Tween 20 in TBS) for ten minutes on each wash with gentle shaking. The blot was subsequently incubated in a 1:5000 dilution of goat anti-rabbit IgG HRP conjugated secondary antibodies (SeraCare) for 1 hour. The membrane was washed four times with wash buffer, each for 10 minutes with gently shaking, before being covered with a small volume of TMB membrane peroxidase substrate (SeraCare) and left for 5 minutes, until the bands of interest were visible. The blot was rinsed in water before an image was taken on the Chemidoc XRS system (Biorad).

2.5. *Pf*Arf1$^{N\Delta17}$ nucleotide loading and intrinsic tryptophan fluorescence

Nucleotide loading was conducted by incubating 5 µM *Pf*Arf1$^{N\Delta17}$ and 50 µM GDP or GTP in assay buffer (25 mM HEPES, 150 mM KCl, 1 mM MgCl2, 1 mM DTT, pH 7.4) containing 2 mM EDTA at 27°C for 60 minutes with gentle agitation in a black 96-well plate. The *Pf*Arf1$^{N\Delta17}$-GDP and *Pf*Arf1$^{N\Delta17}$-GTP complexes were stabilised by adding $MgCl_2$ to a final concentration of 3 mM and incubated for 10 minutes with gentle agitation at 27°C. The intrinsic tryptophan fluorescence of *Pf*Arf1$^{N\Delta17}$ was measured as both a continuous (kinetic) reading and endpoint reading at an excitation wavelength of 297 nm and an emission wavelength of 340 nm in a SpectraMax M3 plate reader (Molecular Devices) during the nucleotide loading incubation and after the addition of $MgCl_2$, respectively. Nucleotide loading was conducted in triplicate wells for each experiment.

2.6 Ni-NTA plate-based *Pf*Arf1$^{N\Delta17}$-GGA3 GST interaction assay

Pure His-tagged *Pf*Arf1$^{N\Delta17}$ GTPase pre-loaded with GDP or GTP (prepared by nucleotide loading as described in *section 2.4.*) was diluted to a final concentration of 1 µM in assay buffer (25 mM HEPES, 150 mM KCl, 1 mM $MgCl_2$, 1 mM DTT, pH 7.4) supplemented with 1% (w/v) BSA and transferred to a Ni-NTA HisSorb 96-well plate (Qiagen) with 50 µL in each well. The plate was left to incubate for 60 minutes at 4°C with gentle agitation. Purified GST-GGA3^{GAT} and GST-GGA3^{PBD} were added separately to assay buffer to a final concentration of 1 µM, 50 µL was added to the wells containing *Pf*Arf1$^{N\Delta17}$ and the plate was incubated for a further 60 minutes at 4°C with gentle agitation. The protein solutions were aspirated, and the wells washed twice with wash buffer (assay buffer containing 0.1% (v/v) Tween-20) followed

by three additional washes in assay buffer. A GST substrate solution containing 2 mM reduced L-glutathione and 1 mM 1-chloro-2,4-dinitrobenzene (CDNB) in phosphate-buffered saline, pH 7.4, was prepared and 200 µL added to each well. The absorbance was read at 340 nm as an endpoint reading after 30 minutes using a SpectraMax M3 plate reader (Molecular Devices). Each experiment was conducted in technical triplicate. Background absorbance readings were obtained from wells incubated with GST-GGA3^{GAT}/ GST-GGA3^{PBD} in the absence of immobilised *Pf*Arf1$^{N\Delta17}$ and the mean absorbance was subtracted from the absorbance values of the experimental GST-GGA3^{GAT} and GST-GGA3^{PBD} wells.

2.7. Glutathione plate-based *Pf*Arf1$^{N\Delta17}$-GGA3 GST interaction assay

2.7.1. Confirming the binding of GST-GGA3 proteins to the glutathione-coated plate

Blocking buffer (assay buffer containing1% (w/v) BSA) was added to a Pierce glutathione-coated 96-well plate (ThermoFisher Scientific) and incubated at 27°C for 1 hour with gentle agitation. The purified GST-GGA3 proteins (GST-GGA3^{GAT} and GST-GGA3^{PBD}) were diluted to a final concentration of 1 µM in assay buffer and added to the glutathione-coated plate (100 µL per well) where they were subsequently incubated for 1 hour at 27°C. The protein solutions were aspirated, and the plate was washed four times with 200 µL wash buffer (assay buffer containing 0.1% (v/v) Tween-20) in each well. Rabbit-anti-GST antibody (Sigma-Aldrich) was diluted to 1:5000 in blocking buffer and transferred to the washed wells where it was incubated for 1 hour at 27°C. The primary antibody solution was removed, and the plate was washed four times with wash buffer. Goat anti-rabbit IgG-HRP secondary antibodies (SeraCare) were diluted to 1:10 000 in blocking buffer before being added to the plate and incubated for 1 hour at 27°C. Subsequently, the plate was washed four times with wash buffer and thereafter SureBlue Reserve HRP substrate (SeraCare), which was equilibrated to 25°C, was added (200 µL per well) and left to incubate for 5-10 minutes at 27°C. Absorbance was read at 650 nm in the Spectramax M3 plate-reader. Experiments were conducted in technical triplicate. Background control wells lacked immobilised GST-GGA3 proteins, whilst the positive control consisted of wells that were incubated with purified His-tagged GST alongside the GST-GGA3^{GAT} and GST-GGA3^{PBD} wells.

2.7.2. Confirming the binding of PfArf1$^{N\Delta17}$ to the GST-GGA3 constructs using immunodetection or a HisDetector Ni-HRP reagent

GST-GGA3^{GAT} and GST-GGA3^{PBD}, respectively, were diluted to 2 µM and immobilised in glutathione-coated plate wells. After washing away unbound GST-GGA3 proteins, pre-loaded *Pf*Arf1$^{N\Delta17}$-GDP or -GTP were added to wells at a concentration of 5 µM in blocking buffer and the plate was incubated for 1 hour at 27°C. The *Pf*Arf1$^{N\Delta17}$ solutions were aspirated, and the plate wells washed four times in wash buffer. 1D9 monoclonal mouse anti-Arf1 primary antibodies (Novus Biologicals) were diluted to 1:5000 in blocking buffer (assay buffer containing 1% (w/v) BSA) before being transferred to the plate where it was incubated for 1 hour at 27°C. The primary antibody solution was aspirated, and the plate washed four times with wash buffer (assay buffer containing 0.1% (v/v) Tween 20). Peroxidase-conjugated goat anti-mouse IgG secondary antibodies (SeraCare) diluted to 1:10 000 in blocking buffer was then added to the plate and incubated at 27°C for 1 hour. The anti-mouse antibody solution was aspirated, and the plate was washed four times with wash buffer before the addition of SureBlue Reserve HRP-substrate (SeraCare) that had been equilibrated to room temperature. The substrate was left to incubate for 5-10 minutes at room temperature before the absorbances were read at a wavelength of 650 nm in an Epoch 2 Microplate Spectrophotometer (Biotek). Each experiment was conducted in technical triplicate. Negative control wells contained immobilised GST-GGA3 proteins in the absence of GDP/GTP-loaded *Pf*Arf1$^{N\Delta17}$. The same protocol was followed when using HisDetector, however, the incubations with the primary and secondary antibodies were omitted and instead the HisDetector Ni-HRP reagent (SeraCare) diluted to 1:10 000 was added in a single step after incubating with the pre-loaded *Pf*Arf1$^{N\Delta17}$-GDP/GTP solutions.

2.8. *Plasmodium falciparum* cell culturing

2.8.1. Routine cell culturing

P. falciparum 3D7 parasites were cultured in RPMI 1640 liquid medium (with 25 mM HEPES, 2.05 mM L-Glutamine; Gibco) enriched with 0.4% (w/v) glucose, 0.5% (w/v) Albumax II, 0.0176% (w/v) hypoxanthine and 0.002% (w/v) gentamicin. Cultures were maintained at 37°C in sealed flasks filled with sterile atmosphere (5% O_2 (v/v), 5% CO_2 (v/v), and 90% N_2 (v/v)) with gentle agitation. Routinely, the culture medium was changed daily, unless parasitaemia (percentage of infected red blood cells) was estimated to be below 1%. Fresh red blood cells

were added every second day. Cultures were maintained at 20-30 mL volumes in T75 flasks or 5 mL volumes in T25 flasks, with the haematocrit (content of human red blood cells (v/v)) being maintained at 3-4%.

2.8.2. Day one in routine culturing (ring stage)

The parasite culture was transferred to a sterile 15- or 50-mL tube and centrifuged at 360 x g for 3 minutes. The media supernatant was aspirated off and a Giemsa-stained thin blood smear slide was prepared from the red blood cell pellet to determine percentage parasitaemia and parasite life-cycle synchronization. Pelleted RBCs were resuspended in fresh media and returned to the culture flask where it was gassed (with the gas mixture described above) for approximately 30 seconds. Flasks were then sealed and returned to a 37°C incubator.

2.8.3. Day two in routine culturing (trophozoite /schizont stage)

The parasite culture was transferred to a sterile centrifuge tube and centrifuged, whereafter the supernatant was aspirated followed by the preparation of a Giemsa-stained slide. If the parasitaemia percentage was <5%, the pelleted RBCs were resuspended in fresh media and returned to culturing flask. If the parasitaemia percentage was >5%, approximately 12% (v/v) of the RBC pellet was returned to the flask in fresh medium, while fresh, uninfected RBCs were added to the flask to restore the haematocrit to 3-4%. The flask was then gassed and placed back into the 37°C incubator. The remaining RBC pellet was used to prepare parasite pellets for Arf1 assays by undergoing saponin lysis (*section 2.7.5*.).

2.8.4. Giemsa-stain slide preparation

After aspirating spent media, 5µL of pelleted infected RBCs from parasite cultures were transferred to the edge of a glass microscope slide. A second microscope slide was used to smear the RBCs to form a thin monolayer. The slide was left to air dry for 1 minute and then fixed by coating the RBC monolayer in methanol for 10 seconds before it was poured off and the slide allowed to air dry. Giemsa stain mix (10% Giemsa stain (v/v) solution in PBS) was prepared and was used to cover the monolayer of RBCs for 5 minutes before being rinsed off. The slide was left to air dry again before being viewed under a 100X oil-immersion objective of an upright brightfield light microscope.

2.8.5. Saponin lysis

Saponin lysis was only performed when most of the parasites were in the trophozoite stage (day two) of their life cycle. After day 2 of routine culturing as described in 2.5.3. above, the remaining pelleted RBCs were resuspended in 1 mL cooled filter sterilized saponin lysis solution (0.3% saponin (w/v) in PBS) to lyse the RBCs. Samples were centrifuged at 5000 x g for 2 minutes at room temperature and thereafter the supernatant was aspirated. Pellets containing intact parasites and RBC membrane remnants were resuspended in 1 mL cooled PBS and centrifuged again. This wash step was conducted twice. After aspiration of the supernatant following the second PBS wash, pelleted cells were stored at -80 °C until further use.

2.9. HeLa cell cultivation

2.9.1 Routine HeLa cell culturing

The HeLa (human cervix adenocarcinoma) cell line (Cellonex, South Africa) was maintained in complete culture medium comprised of DMEM with GlutaMAX and 4.5 g/L glucose (Gibco), supplemented with antibiotic-antimycotic solution (Gibco) and 10% (v/v) heat-inactivated foetal bovine serum (FBS; BioWest) in sterile T25 or T75 cell culture flasks with gas-permeable filter caps, and incubated in a 37°C incubator with a humidified atmosphere of 5% (v/v) CO_2. The cells were maintained by replacing the medium every 2 to 3 days until the cells reached a confluency of 80-90%. Once the optimal confluency was reached, the cells were diluted by discarding the spent medium from the culture flask and briefly washing the cells in filter-sterilised PBS. The cells were subsequently incubated in dissociation reagent - approximately 0.5 mL per 10 cm^2 of Trypsin/EDTA (Gibco) - for 5 minutes in a 37°C incubator. To promote cell detachment, the flask was tapped several times prior to being observed under the microscope to ensure complete cell detachment. Approx. 80-90% of the suspended cells were aspirated and discarded, and culture medium added to the remaining cells in the flask, before the flask was returned to the 37°C incubator with humidified atmosphere of 5% CO_2. Alternatively, the aspirated suspended cells were harvested by centrifugation at 181 x *g* for cryopreservation or cell lysate preparation.

2.9.2 Cryopreservation, thawing and lysate preparation of HeLa cell stocks

HeLa cells were cryopreserved by resuspending cell pellets in 1 mL ice-cold freezing medium (10% (v/v) DMSO, 90% (v/v) FBS) and stored in cryotubes at -80°C. The cryotube containing the HeLa cells was thawed at 37°C and the contents immediately resuspended and washed twice in 15 mL pre-warmed complete culture medium followed by centrifugation at 181 x *g* for 3 minutes. The pellet was gently resuspended in either 5 mL or 10 mL complete culture medium, and transferred into a T25 or T75 culture flask, respectively. The flask was incubated overnight in a 37°C incubator with humidified atmosphere of 5% CO_2 and the routine culturing procedure was continued as described in *section 2.7.1.* Whole-cell lysis was conducted in preparation for the assay described in *section 2.9.3.* where the cells were incubated with mammalian cell lysis buffer (0.1 M EDTA, pH 8.0; 0.5% (v/v) Triton X-100, 10 mM Tris, pH 8.0) prior to experimentation.

2.10. Arf1-GGA3 GST protein-protein interaction assay using *Plasmodium falciparum* parasite lysates

2.10.1. Plasmodium falciparum parasite lysate preparation.

The parasite pellets prepared by saponin lysis *(section 2.8.5*) were thawed on ice for 40 minutes before the pellet was resuspended in 900 µL lysis buffer (Arf1 assay buffer containing 0.5% (v/v) Triton X-100) for 10 minutes. The solution was then centrifuged in a bench-top microfuge at 21 330 x g for 5 minutes until the supernatant and pellet were sufficiently separated. An aliquot of 100 µL of the supernatant was set aside for protein concentration determination, while the rest of the supernatant was divided in two for the control and experiment. The parasite lysates were kept on ice until use in the Arf1-GGA3 GST interaction assay (*section 2.8.2*).

2.10.2. Endogenous PfArf1-GGA3 GST interaction assay using P. falciparum lysates.

GST-GGA3^{PBD} was diluted to 2 µM in blocking buffer made up of complete assay buffer (25 mM HEPES, 150 mM KCl, 1 mM $MgCl_2$, 1 mM DTT, pH 7.4) supplemented with 1% BSA and transferred to a glutathione-coated plate where it was left to incubate for 1 hour at 27°C. Concurrently, nucleotide exchange of endogenous *Pf*Arf1 contained in a parasite lysate divided into two equal volumes (*section 2.10.1*) was conducted by adding a final concentration of 5 µM or 25 µM GDP/GTP to the respective lysates, as well as 20 µM EDTA. After incubating at 27°C for 60 minutes, $MgCl_2$ was added to a final concentration of 25 µM. Once GST-

GGA3^{PBD} was immobilised onto the glutathione plate and the endogenous *PfArf1* was pre-loaded with GDP/GTP, the plate was aspirated and washed 4 times in wash buffer (complete assay buffer containing 0.1% (v/v) Tween-20). The GDP and GTP pre-loaded parasite lysates were transferred to the glutathione coated plate and left to incubate with immobilised GST-GGA3^{PBD} for 1 hour at 27°C before being aspirated and the wells washed four times in wash buffer. Monoclonal 1D9 mouse anti-Arf1 antibody (Novus Biologicals) was diluted to 1:5 000 in blocking buffer before being added to the glutathione-coated plate and further incubated for 1 hour at 27°C. The antibody solution was aspirated, the plate washed four times with wash buffer and a dilution of 1:10 000 of peroxidase conjugated goat anti-mouse Ig in blocking buffer was added. After incubating at 27°C for 1 hour, the antibody solution was aspirated, and the plate washed four times with wash buffer. A volume of 200 µL SureBlue Reserve HRP substrate was added to the respective wells and left to incubate for 5-10 minutes. Once colour development was observed, absorbances were read at 650 nm in an Epoch 2 Microplate Spectrophotometer (Biotek). Background absorbance readings were recorded in a total of three replicates by measuring colour development in the negative controls which contained pre-loaded *Pf*Arf-GTP and *Pf*Arf-GDP parasite lysates incubated in wells devoid of immobilised GST-GGA3. The mean absorbances from the background controls were subtracted from each of the corresponding *Pf*Arf-GDP/GTP experimental absorbance values.

2.10.3. Validation of the PfArf1-GGA3 GST interaction assay by treatment of P. falciparum cultures with Arf1 inhibitors

Plasmodium falciparum 3D7 cultures were propagated in a T75 culture flask according to the protocol described in *section 2.8*. When the parasites reached the trophozoite stage in their lifecycle, the culture was transferred to a 50 mL centrifuge tube and was centrifuged for 4 minutes at 202 x *g*. The supernatant was removed, and the infected RBC pellet resuspended in 10 mL pre-warmed complete RPMI medium. Subsequently, the resuspended culture was split into two equal parts and added to two separate T25 flasks. Brefeldin A (BFA) was added to one of the T25 flasks to a final concentration of 20 µM, whilst the other had no additions so that it could serve as an untreated control. Both T25 flasks were incubated at 37°C for 90 minutes with gentle agitation before being transferred to 15 mL centrifuge tubes and centrifuged at 202 x g for 4 minutes. The supernatants were removed from both tubes prior to resuspending the pellets in 1 mL PBS supplemented with 0.05% saponin for 5 minutes to lyse the infected RBCs. The lysates were transferred to microfuge tubes and centrifuged for 2 minutes at 1814 x g, followed by the removal of their supernatants. The parasite pellets were

resuspended in 1 mL PBS and centrifuged for 2 minutes at 1814 x g as a wash step. The *P. falciparum* cells were briefly stored on ice before lysis with 1% Triton X-100 in PBS. Once lysed, the Arf1-GGA3 interaction assay was conducted as detailed in *section 2.9.2*. The methodology described above was repeated when treating trophozoite stage parasites with 20 µM experimental *Pf*ArfGAP inhibitors, namely Chem1099 and Chem3050.

2.10.4. Validation of PfArf1-GGA3 GST interaction assay by treatment of HeLa cultures with the Arf1 inhibitor BFA

The HeLa cultures were cultivated in a T75 flask according to the protocol described in *section 2.9.1*. Once 80-90% confluency was reached, the spent medium was aspirated, and fresh pre-warmed medium supplemented with 20 µM BFA or QS11 was added to the culturing flask. The culture was returned to the 37°C incubator with humidified atmosphere of 5% CO_2 for 90 minutes. After aspirating the medium containing BFA, the flask was gently washed with 1 X PBS before adding 4 mL Trypsin/EDTA. The flask was returned to the incubator for 5 minutes. To further dislodge the cells, the flask was lightly tapped before being examined under an inverted microscope to ensure sufficient cell detachment from the surface of the flask. Fresh pre-warmed medium was added to the culturing flasks to quench the Trypsin/EDTA. The culture was centrifuged at 181 x g for 2 minutes and the medium aspirated. The pelleted cells were resuspended and washed in 1 X PBS before being centrifuged at 181 x g for 2 minutes. The pellets were lysed with mammalian lysis buffer (detailed in *section 2.8.2.*) immediately before adding the cell lysates to GST-GGA3^{PBD} immobilised in glutathione-coated plate wells and conducting the *Pf*Arf1-GGA3 GST interaction assay as described in *section 2.9.2*.

2.11. Parasite lysate protein concentration determination and data normalisation

The protein concentration of each of the parasite lysate samples used in the Arf1-GGA3 GST interaction assays was determined by the bicinchoninic acid (BCA) assay. A set of protein standards were prepared by a two-fold serial dilution series ranging from 0.025 - 2 mg/mL BSA in deionised water. In a clear 96-well plate, 25 µL of the BSA protein standards and parasite lysates were added in duplicate wells followed by 200 µL BCA reagent (Thermo Fisher Scientific). The plate was shaken briefly before being covered and incubated at 37°C for 30 minutes. The absorbance was read at 562 nm using a SpectraMax M3 plate reader (Molecular Devices). The absorbance values obtained for the standard samples were used to construct a BSA standard curve with an R^2 value ≥ 0.99, which was subsequently used to determine the

concentration of the proteins in the parasite lysate samples. To eliminate protein concentration variation occurring between the control and experimental *Plasmodium falciparum* lysates used in the Arf1-GGA3 GST interaction assays, the data was normalised. This was accomplished by dividing the Abs_{650} values obtained after adding the HRP substrate by the relevant lysate protein concentration in mg/mL.

2.12. Statistical analyses

Where applicable, unpaired t-tests were used to draw comparisons between means of datasets to calculate the resulting P-values (using GraphPad Prism). The P-values that fell below 0.05 were interpreted to indicate a significant statistical difference.

Chapter 3: The establishment of a novel ELISA-based Arf1-GGA3 interaction assay to explore the activation status of *Pf*Arf1

3.1. Introduction

As discussed in Chapter 1, the Arf family of GTPases have exhibited therapeutic potential as drug targets in cancer research. In addition, Arf may present an even broader clinical significance as a drug target unrestricted to solely cancer. Accordingly, an ongoing interest in the research group is to explore the validity of *Pf*Arf1 as a possible drug target for malaria. Hence, this chapter will be centred around the establishment of a plate-based ELISA protein interaction assay that can detect changes in the levels of active *Pf*Arf1 in parasites treated with potential Arf1 inhibitors. This is necessary to confirm the mode of action of Arf1 inhibitors found in compound screens, with the emphasis placed on compounds previously identified as *Pf*Arf1 deactivation (*Pf*ArfGAP1) inhibitors in protein-based assays conducted within our research group (Swart *et al*., 2020). In mammalian cells, this is achieved by using a GGA3 co-precipitation/pull-down assay. In the assay, beads coated with the VHS-GAT domain of GGA3 are used to selectively bind active Arf1 present in the lysate (Cohen & Donaldson, 2010). The active Arf1 pelleted with the beads is detected by SDS-PAGE followed by western blotting using anti-Arf1 antibodies where the Arf1 band intensity in treated cells is compared to untreated control cells (Cohen & Donaldson, 2010). This assay is available in kit form and can be purchased from several suppliers e.g., Abcam, Cell Biolabs and Cytoskeleton.

3.1.2. Assay format conceptualisation

In this study our research group conceptualised and explored an alternative ELISA-based assay that could be used to detect changes in the levels of active *Pf*Arf1 in *P. falciparum* cultures exposed to Arf1 inhibitors (**Figure 6**). The principle behind this assay format, similar to that of the traditional pull-down assay described by Cohen and Donaldson, relies on the protein-protein interaction between active GTP-bound Arf1 and the effector protein GGA3. By fusing $GGA3^{PBD}$ (the protein binding domain of GGA3) to GST, GGA3 could be immobilised onto a glutathione-coated 96-well plate. A parasite lysate could then be added to the plate, allowing endogenous *Pf*Arf1-GTP to bind to the immobilised GST-$GGA3^{PBD}$ while inactive GDP-bound *Pf*Arf1 remains unbound in the supernatant. After washing the plate, the amount of

active GTP-bound *Pf*Arf1 may subsequently be detected by using a primary anti-Arf1 antibody. To quantify the amount of active *Pf*Arf1, the addition of an HRP-conjugated secondary antibody should recognise and bind to any anti-Arf1 primary antibodies and produce a colour after addition of a colorimetric HRP substrate. The consequential colour development could be measured in a standard plate reader and should have a direct correlation with the activation status of *Pf*Arf1 where intense colour development indicates a higher amount of active GTP-bound *Pf*Arf1 in the original parasite lysate.

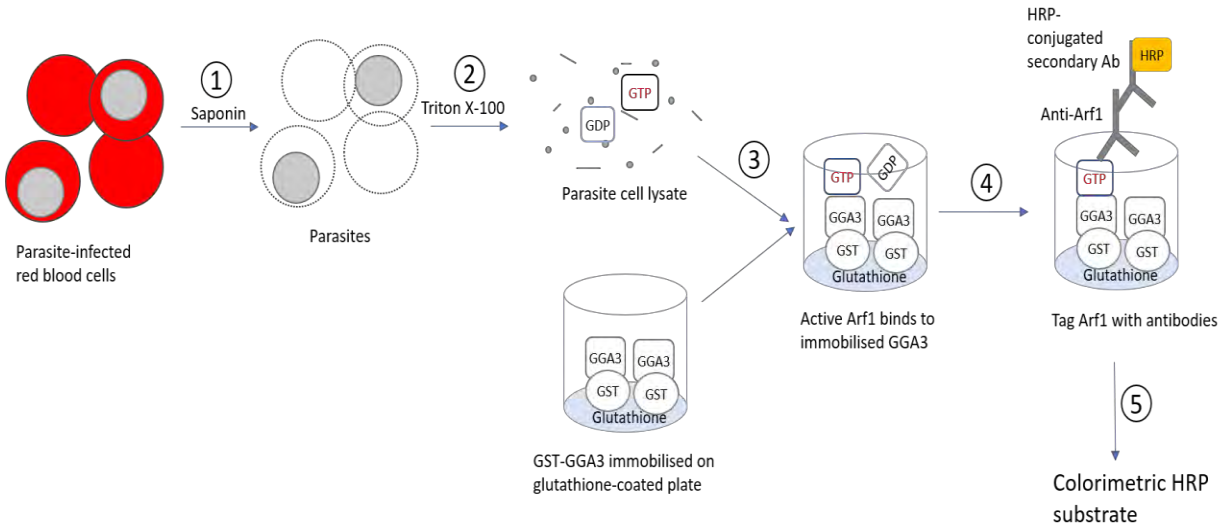

Figure 6: The principle behind the ELISA-based assay to detect active Arf1 in *P. falciparum* parasites. (1) The *P. falciparum* infected erythrocytes obtained from an *in vitro* culture are treated with saponin to permeabilise the erythrocyte membranes and remove erythrocyte cytoplasm while leaving the parasites intact. (2) The isolated parasites are treated with a homogenisation buffer containing Triton X-100, thus releasing the parasite intracellular contents (3) The resulting parasite lysate containing endogenous active (GTP-bound) and inactive (GDP-bound) *Pf*Arf1 is added to the glutathione-coated plate containing immobilised GST-GGA3, whereupon active *Pf*Arf1 binds exclusively to the immobilised GGA3 via the latter's VHS-GAT domain. (4) Primary anti-Arf1 antibodies added subsequently bind specifically to the *Pf*Arf1 captured on the GGA3-coated plate, while HRP-conjugated secondary antibodies bind to the anti-Arf1 antibodies. (5) Detection is achieved by the addition of a colorimetric HRP substrate and reading Abs_{650} on a plate reader. The amount of active *Pf*Arf1 present in the parasite lysate should thus correlate with the colour change i.e., the higher the concentration of active *Pf*Arf1 in a sample, the higher the absorbance values obtained.

3. 2. Aims and objectives

Aim of study: The motivation for this research project stems from the incontrovertible rise in antimalarial drug resistance and the consequent need for novel compounds that exhibit

auspicious antimalarial properties. A corollary of this is the search for novel druggable targets that could be exploited in target-based drug discovery projects. With the influx of literature centralised around Arf1 as a potential drug target, especially in cancer research, it is surprising that there are so few known inhibitors for this GTPase or reported drug discovery projects aimed at it. One contributory factor may be the lack of viable assay techniques that can be exploited to quantitatively measure the effects that compounds have on Arf1 in drug screening campaigns. That being said, our research group has made progress in this respect over the past few years by developing screening assays and exploring various avenues to inhibit both human Arf1 and *Pf*Arf1. One study in particular identified compounds that inhibit *Pf*Arf1 deactivation by *Pf*ArfGAP1 in an *in vitro* screening assay. In addition, the compounds inhibit the viability of cultured *P. falciparum* at low micromolar concentrations, without affecting HeLa cell viability (T. Swart, PhD). The evidence obtained in this report suggests that *Pf*ArfGAP1 could be a viable drug target for future antimalarial screening operations. It is, however, necessary to conduct a series of validation studies to authenticate that the *in vitro* antimalarial activities of the compounds are in fact due to the inhibition of *Pf*Arf1 deactivation by *Pf*ArfGAP1 and not any other unrelated effects on the parasites. Accordingly, this chapter aims to establish an ELISA-based GGA3-*Pf*Arf1 interaction assay that can be utilised to validate known *Pf*ArfGAP1 inhibitors by measuring their effects on the *Pf*ArfGAP1 deactivation of *Pf*Arf1 in *in vitro* cultured parasites. The specific experimental objectives for this study are further elaborated on below.

Specific objectives:

1. Express and purify His-tagged *Pf*Arf1 $^{N\Delta17}$, the GAT domain of human GGA3 (amino acids 107-286) fused to GST (GST-GGA3^{GAT}) and the N-terminal protein binding domain of GGA3 (amino acids 1-316) fused to GST (GST-GGA3^{PBD}) and prepare active (GTP-bound) and inactive (GDP-bound) *Pf*Arf1$^{N\Delta17}$ using *in vitro* nucleotide exchange
2. Compare the ability of the two GST-GGA3 constructs to selectively interact with *Pf*Arf1 $^{N\Delta17}$-GTP vs. *Pf*Arf1 $^{N\Delta17}$-GDP immobilised on a Ni-NTA HisSorb 96-well plate as well as a glutathione coated 96-well plate
3. Compare the ability of the two GST-GGA3 constructs immobilised on glutathione-coated plates to selectively bind *Pf*Arf1$^{N\Delta17}$-GTP vs. -GDP
4. Determine if the binding of active *Pf*Arf1 in cultured *P. falciparum* parasite lysates to immobilised GST-GGA3^{PBD} can be detected using an ELISA assay format.

3.3. Results

3.3.1. Analytical scale expression of proteins

Analytical scale expression was conducted to determine the solubility and expression levels of the recombinant proteins necessary for the ELISA-based Arf1-GGA3 assay. Glycerol stocks of T7 Express lysY/Iq *E. coli* cells transformed with the pET-28a (+)–*Pf*Arf1$^{N\Delta17}$ and pGEX-4T-2/GGA3^{GAT} plasmid constructs were donated by members of our research group. The pGEX-4T-1/GGA3^{PBD} construct was custom prepared and supplied by GenScript and used to transform Rosetta (DE3) competent *E. coli* cells. The recombinant expression cultures were propagated in Luria broth complemented with the appropriate antibiotic overnight (kanamycin for the pET-28a construct and ampicillin for both pGEX-4T constructs). Once the bacterial expression cultures reached their exponential growth phase, protein expression was induced with the addition of IPTG. Control cultures were also prepared where IPTG was excluded. Both induced and uninduced *E. coli* cells were collected by centrifugation. The cells were lysed in two steps: treatment with lysozyme, and physical lysis by sonication. The insoluble and soluble fractions were collected through centrifugation and their protein profiles analysed by SDS-PAGE. The His-tagged *Pf*Arf1$^{N\Delta17}$ construct had a predicted molecular weight of 21.1 kDa which correlated with the observed presence of an overexpressed protein band with a molecular weight of approximately 20 kDa in the induced soluble fraction (ISF) of *E. coli* cells harbouring the pET-28a (+)–*Pf*Arf1$^{N\Delta17}$ plasmid (**Figure 7A**, *arrow*), but was absent from the corresponding uninduced fraction. Similarly, the predicted molecular weights for GST-GGA3^{PBD} (62 kDa) and GST-GGA3^{GAT} (44 kDa) correlated with the protein bands observed at approximately 61 kDa and 44 kDa in the ISFs of the respective *E. coli* cultures (**Figure 7B** and **7C**, arrows), suggesting that both protein forms are soluble. Moreover, the stained protein band observed in the ISF at approximately 27 kDa (**Figure 7C**, *white arrow)* may either be due to the degradation of soluble GST-GGA3^{GAT} by proteases present in the bacterial lysate or the premature termination of protein translation given that GST has a calculated molecular mass of approximately 26 kDa.

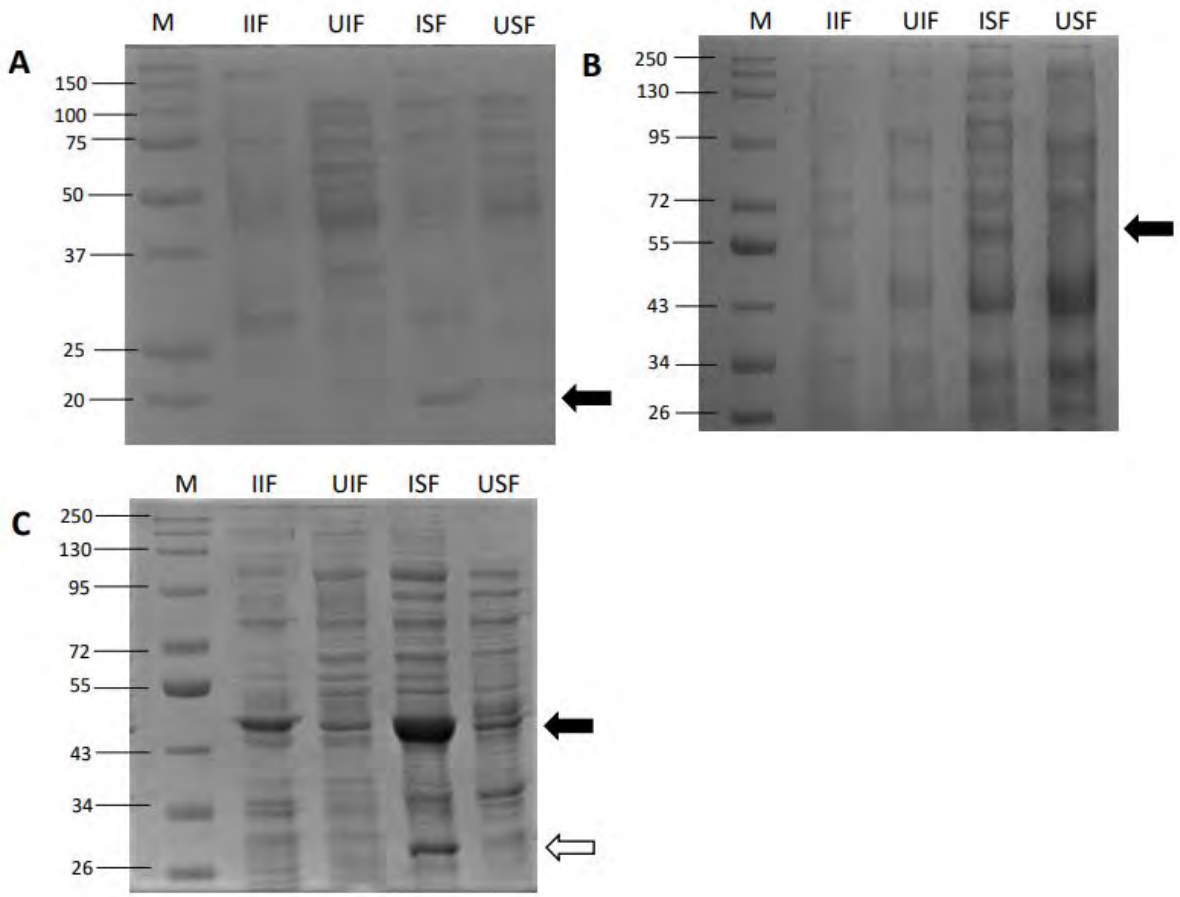

Figure 7: Analytical-scale expression profiles for the recombinant proteins necessary for the establishment of an ELISA-based Arf1-GGA3 interaction assay using *E. coli* cells. SDS-PAGE analysis of the protein profiles of *E. coli* cells expressing (A) *Pf*Arf1 $^{N\Delta17}$ (B) GST-GGA3^{PBD} (C) GGA3^{GAT} **Key.** M: Molecular weight marker in kDa, IIF: Induced insoluble fraction; UIF: Uninduced insoluble fraction; ISF: Induced soluble fraction; USF: Uninduced soluble fraction.

Initial attempts to express GST-GGA3^{PBD} using transformed T7 Express lysY/Iq *E. coli* cells at various temperatures and IPTG concentrations were unsuccessful (*results not shown*), suggesting that the Rosetta (DE3) cells used to obtain the results shown above are more appropriate for the expression of this protein. Given that the analytical-scale expression profiles for all recombinant proteins showed they were being adequately expressed in soluble forms, large-scale expression and purification of the proteins was pursued.

3.3.2. Purification of recombinant proteins

To determine whether the correct proteins had been purified, western blot analysis was conducted and the proteins under investigation were identified using antibodies specific to the proteins under investigation. In **Figure 8** the arrows labelled 'i.' indicates the respective GGA3 proteins and the arrows labelled 'ii.' indicates the proteolytic fragment or premature translation

termination product containing the GST tag. To establish the novel assay outlined in **Figure 6**, high yields of the necessary purified recombinant proteins were required. Therefore, preparative expression was conducted with the same expression parameters used in analytical-scale expression, but with a higher volume of the recombinant expression cultures. After inducing expression with IPTG, the *E. coli* cells were collected by centrifugation and lysed with lysozyme and sonication. The resulting soluble fractions were subsequently harvested by centrifugation. The *Pf*Arf1$^{N\Delta17}$ recombinant protein was purified by affinity chromatography using a Ni-NTA column, while both the GST-GGA3 fusion proteins were purified using a glutathione agarose column. Following purification, all eluted protein fractions were passed through a size-exclusion desalting column to isolate the target proteins from salts, other small molecules, and imidazole/glutathione used in the elution step. The desalting column was also necessary for buffer exchange into assay buffer. The resulting purification profiles were analysed by SDS-PAGE and the respective protein concentrations determined by a Bradford assay. *Pf*Arf1$^{N\Delta17}$ yielded between 0.9-1.5 mg purified protein per L *E. coli* culture; GST-GGA3^{PBD} yielded between 0.5-0.9 mg/L, and GST-GGA3^{GAT} yielded between 0.8-1.7 mg/L.

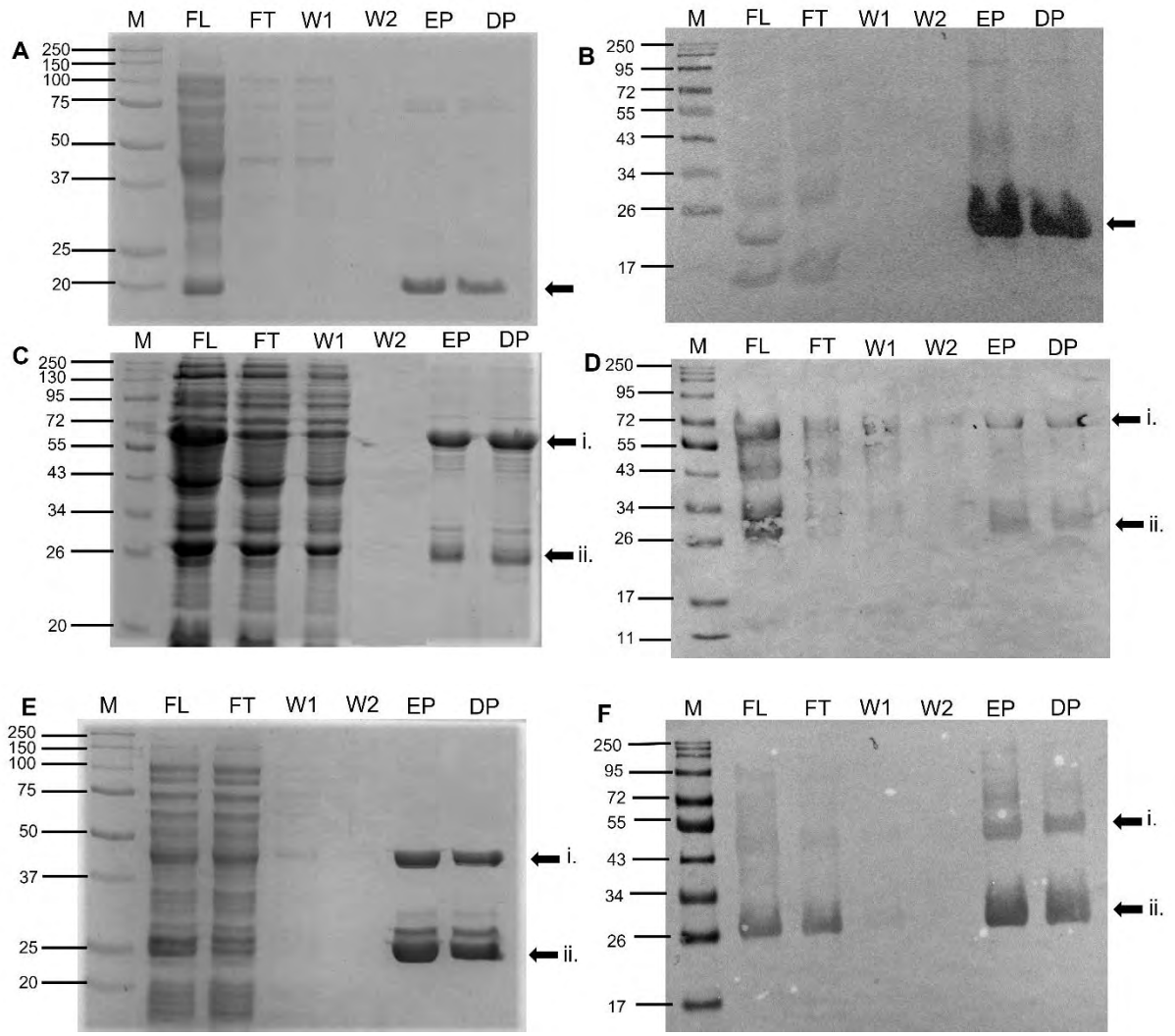

Figure 8: Protein purification profiles and western blot analysis of the recombinant proteins required for the establishment of an ELISA-based *in vitro* Arf1-GGA3 interaction assay. (A) Purification profile for His-*Pf*Arf1$^{N\Delta17}$ resolved on a 12% Coomassie-stained SDS-PAGE gel. (B) Corresponding western blot using HisDetector nickel-HRP. (C) Purification profile for GST-GGA3^{PBD} resolved on an 8% Coomassie-stained SDS-PAGE gel. (D) Corresponding western blot using anti-GST antibodies. (E) Purification profile of GST-GGA3^{GAT} resolved on an 8% Coomassie-stained SDS-PAGE gel. (F) Corresponding western blot using anti-GST antibodies. **Key.** M: Molecular weight marker in kDa, FL: Filtered lysate; FT: Flow through; W1: Wash 1; W2: Wash 2; EP: Eluted protein; DP: Desalted protein.

The purification of His-tagged *Pf*Arf1$^{N\Delta17}$ using the Ni-NTA column was successful and is evident by the presence of an intensely stained protein band in the elution fraction (EP) and desalted fraction (DP) at approximately 20 kDa in **Figure 8A** (*indicated by arrow)*. Due to the low concentration obtained for GST-GGA3^{PDB} in the induced soluble fraction (ISF) during the analytical-scale expression studies (**Figure 8B**), the large-scale expression cultures for this construct were scaled up to 500 mL, instead of the usual 250 mL used for the other proteins. The scaling up and subsequent purification of GST-GGA3^{PDB} using a glutathione-agarose column yielded a higher protein concentration in the eluted (EP) and desalted fractions (DP)

as observed in **Figure 8C** at approximately 61 kDa (*indicated by top arrow*). Purification of GST-GGA3^{GAT} conducted with the glutathione-agarose column was also successful as observed by a distinct protein band in both the EP and DP at approx. 48 kDa (**Figure 8E**). There were, however, substantial amounts of truncated GST proteins in the purification profiles for both the GST-GGA3 constructs which is evident by the protein bands observed at approximately 26 kDa in the elution and desalted fractions of **Figure 8C** and **Figure 8E** (*indicated by bottom arrows)*. In order to validate whether the correct recombinant proteins were expressed, anti-GST and Ni-HRP detection was conducted using western blot analysis. It was determined that all three recombinant proteins were appropriately purified where a band for *Pf*Arf1 $^{N\Delta17}$ was observed at the expected molecular weight of 21 kDa (**Figure 8B**) in the EP and DP (*indicated by arrow*), a protein band for the GST-GGA3^{PBD} construct was observed at the predicted molecular weight of 64 kDa (**Figure 8D**) in the EP and DP, and finally a distinctive band for GST-GGA3^{GAT} was observed at 44 kDa (**Figure 8F**) in the EP and DP (*indicated by arrows*). The detection of the lower molecular weight bands (*indicated by the bottom arrows*) by the anti-GST antibody, in addition to its co-purification during glutathione-agarose chromatography, suggests that these bands represent truncated proteins containing GST, as opposed to an *E. coli* contaminant. The purified proteins were subsequently stored in glycerol at -20°C to maintain protein stability and utilised to develop the ELISA-based GGA3-*Pf*Arf1 interaction assay.

3.3.3. Nucleotide exchange preparation of PfArf1-GTP and -GDP

As described previously, the nucleotide exchange whereby *Pf*Arf1 is activated and deactivated causes conformational changes to the structure of *Pf*Arf1. This conformational change can be monitored by native tryptophan fluorescence which is based on the disruption of mutual quenching occurring on two specific tryptophan residues located at positions 66 and 78 (Richardson and Fromme, 2015). To develop an *in vitro* GGA3-*Pf*Arf1 interaction assay it was necessary to prepare both active (GTP-bound) and inactive (GDP-bound) *Pf*Arf1$^{N\Delta17}$ and monitor its activation status. This required the aforementioned native tryptophan fluorescence methodology to measure the nucleotide-bound state of *Pf*Arf1 (adapted from T. Swart (PhD)). These nucleotide-bound *Pf*Arf1 complexes were prepared with EDTA-mediated nucleotide exchange where 5 µM of His-tagged *Pf*Arf1$^{N\Delta17}$ was incubated with 2 mM EDTA and 25 µM GDP/GTP at 25°C for an hour. The nucleotide bound *Pf*Arf1 complexes were immediately stabilised with the addition of 3 mM $MgCl_2$ and left to incubate for 10 minutes at 25°C. Nucleotide exchange was determined by native tryptophan fluorescence (excitation at 297 nm

and emission at 340 nm). The activation of *Pf*Arf1$^{N\Delta17}$ was displayed as an increase in fluorescence while deactivation was observed as a decrease in fluorescence (**Figure 9**).

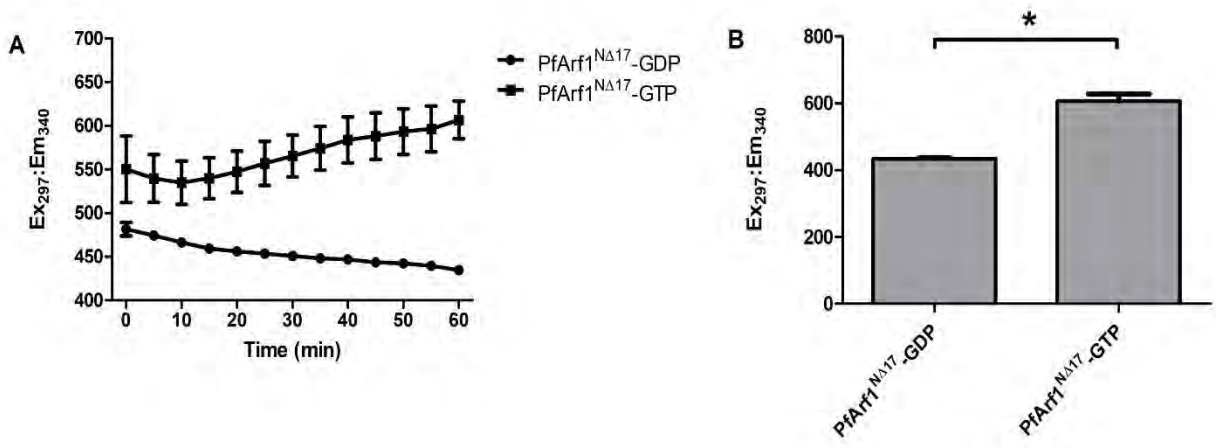

Figure 9: Detecting the activation status of *Pf*Arf1 $^{N\Delta17}$ with tryptophan fluorescence after EDTA-mediated nucleotide exchange. (A) Intrinsic tryptophan fluorescence was measured over 60 minutes at one-minute intervals with excitation and emission wavelengths of 297 nm and 340 nm, respectively. (B) After EDTA induced nucleotide exchange, the resulting complexes were stabilised with $MgCl_2$ and native tryptophan fluorescence was measured as an end-point reading at an excitation wavelength of 297 nm and emission wavelength of 340 nm. Both graphs represent the mean and standard deviation of the samples conducted in technical triplicate; * p=0.0014.

A study conducted by Pan *et al* determined that intrinsic tryptophan fluorescence measurements serve as a sensitive detection method for local conformational changes that occur during GDP/GTP nucleotide exchange (Pan *et al.,* 1995). This detection method is possible for two reasons: a blue shift in the emission spectra for both tryptophan residues present on the *Pf*Arf1$^{N\Delta17}$ protein is expected to result in fluorescence emission, and because tryptophan fluorescence intensity is quenched by approximately 25% in the GTP-bound form relative GDP-bound *Pf*Arf1$^{N\Delta17}$, an observable difference in fluorescence is expected between the two conformations. Since a significant difference in tryptophan fluorescence was observed between the *Pf*Arf1$^{N\Delta17}$-GDP and -GTP complexes (p=0.0014; *indicated by * in* **Figure 9)** it was determined that EDTA-mediated nucleotide exchange was successful so the complexes were immediately used to conduct a Ni-NTA immobilised Arf1-GGA3^{GAT} interaction assay.

3.3.4. Ni-NTA immobilised Arf1-GGA3^{GAT} interaction assay

The establishment of an immobilisation assay for *Pf*Arf1$^{N\Delta17}$ activation status was achieved by T. Swart, where the assay could be used detect and measure the activation of Arf1 by Sec7 and

its deactivation by ArfGAP domains *in vitro* (Swart *et al*., 2020). Briefly, the assay relies on the immobilisation of histidine-tagged *Pf*Arf1$^{N\Delta17}$ on a Ni-NTA 96-well plate, followed by incubation with GST-GGA3^{GAT}. Selective binding of the GGA3 GAT domain to activated Arf1 is subsequently quantified by adding a colorimetric GST enzyme substrate. This assay was conducted in the present study to determine whether the longer GGA3^{PBD} GST fusion protein (GST-GGA3^{PBD}) could detect the activation status of *Pf*Arf1$^{N\Delta17}$ and whether it could do so more efficiently than the GAT domain of GGA3 used in the original methodology (GST-GGA3^{GAT}). The GDP or GTP-loaded *Pf*Arf1$^{N\Delta17}$ proteins (prepared in *section 3.3.3*) were diluted to a final concentration of 1 µM in assay buffer supplemented with BSA and transferred to a 96 well Ni-NTA plate where they were left to incubate for 30 minutes at 4°C. Both the purified GST-GGA3^{GAT} and GST-GGA3^{PBD} proteins were diluted separately to final concentrations of 1 µM in assay buffer, added to the Ni-NTA plates, and left to incubate for a further 60 minutes at 4°C. After several washing steps, a colorimetric GST substrate containing CDNB and GSH was added to the respective sample reactions and left to incubate at room temperature for 30 minutes. The resulting formation of a GS-DNB conjugation product produced by active immobilised GST was measured as an end point reading at an absorbance of 340 nm. The positive control consisted of a His-tagged GST (prepared previously and donated by T. Swart) and was used to confirm that the Ni-NTA plates could immobilise His-tagged proteins and the GST enzyme reaction could be detected (*results not included*). In addition, a background control consisting of either GST-GGA3^{GAT} or GST-GGA3^{PBD} in the absence of immobilised GTP/GDP loaded $^{N\Delta17}$*Pf*Arf1 was included in each experiment and subtracted from the GST absorbance values to correct the data. It was observed that both of the GGA3 constructs selectively bound to the immobilised active (GTP-bound) $^{N\Delta17}$*Pf*Arf1 proteins (**Figure 10**). In addition, the results suggested that the GGA3^{PBD} construct produced higher absorbance readings when compared to the GAT domain of GGA3 alone. When comparing the absorbances observed with GGA3^{GAT} binding to *Pf*Arf1$^{N\Delta17}$-GTP vs. -GDP, a p-value of 0.0013 (*indicated by *)* was obtained, whereas the corresponding absorbances obtained with GGA3^{PBD} produced a p-value of 0.0003 (*indicated by* **). Even though both GGA3 constructs could discriminate between active and inactive *Pf*Arf1$^{N\Delta17}$ forms, this data suggested that GGA3^{PBD} produces more robust absorbance values and would thus be better suited to distinguish between active and inactive *Pf*Arf1$^{N\Delta17}$ forms.

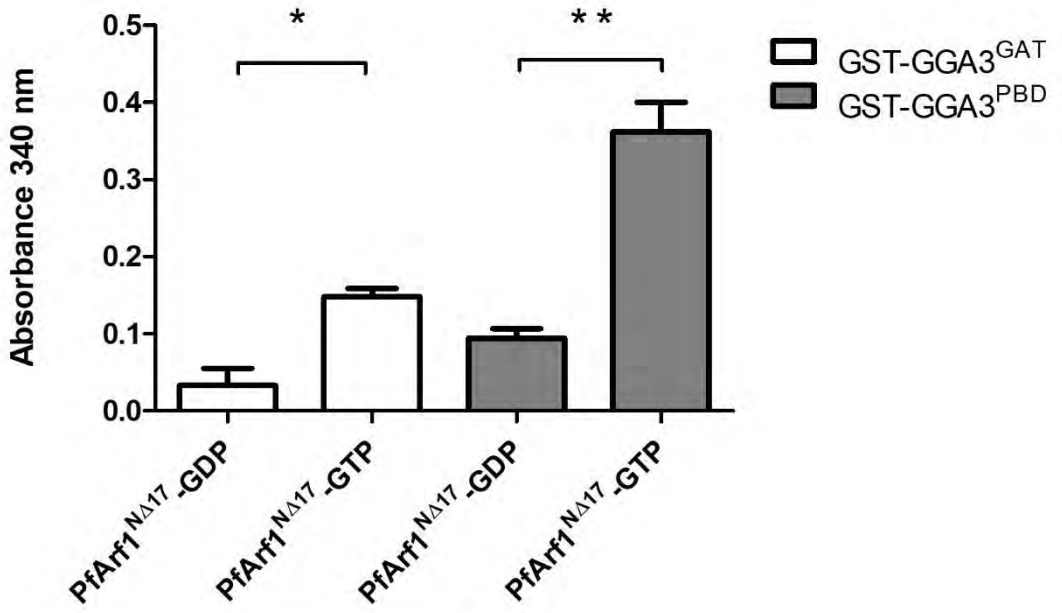

Figure 10: Investigating the selective binding of GST-GGA3^{GAT} and GST-GGA3^{PBD} to active *Pf*Arf1^{NΔ17} immobilised onto nickel-coated plates. A final concentration of 1 µM of GDP-/GTP-loaded His-tagged *Pf*Arf1^{NΔ17} was immobilised on a 96-well nickel-NTA plate by incubating for 60 minutes at 4°C, followed by incubation with 1 µM GST-GGA3^{PBD} or GST-GGA3^{GAT} for 60 minutes at 4°C. After several washing steps to remove any unbound proteins, a GST substrate solution containing CDNB and GSH was added and left to incubate for a further 30 minutes. The resulting GS-DNB conjugation product formed by interacting with active GST and was measured as an end point reading at an absorbance of 340 nm. Background readings obtained from wells devoid of immobilised *Pf*Arf1^{NΔ17} were subtracted from all absorbance readings. The assay was conducted in technical triplicate and the error bars denote standard deviation. The p-values were calculated by two-tailed t-tests where * p=0.0013 ** p= 0.0003.

3.3.5. Glutathione plate-based PfArf1^{NΔ17} GST-GGA3 interaction assay

Using the previously established Arf1 assay, both GST-GGA3 constructs were found to selectively bind to active (GTP-bound) *Pf*Arf1^{NΔ17} immobilised on a nickel-coated plate and to produce robust measurable absorbance readings which could differentiate between the active and inactive *Pf*Arf1^{NΔ17} forms, with GGA3^{PBD} showing more efficient binding. However, the concept ELISA-based assay to detect active Arf1 in malaria parasite lysates (**Figure 6**) required a reversal of the assay format – the binding of Arf1 to GST-GGA3 immobilised on glutathione-coated plates. The next step was therefore to use the purified recombinant proteins to determine whether selective binding of the GST-GGA3 proteins to active PfArf1^{NΔ17} was maintained in the reversed format.

3.3.5.1. Exploring the binding of GST-GGA3 proteins to the glutathione coated plate.

Before the establishment of the concept *Pf*Arf1$^{N\Delta17}$ GST-GGA3 interaction assay, it was necessary to verify the binding and immobilisation of the GST-GGA3 proteins to the glutathione plates. Therefore, an experiment was conducted where both GST-GGA3 constructs were diluted to a final concentration of 1 µM in assay buffer and incubated in a glutathione coated plate for 1 hour at 27°C. After washing away unbound protein, the wells were incubated with a primary rabbit anti-GST antibody, followed by a secondary goat anti-rabbit IgG-HRP antibody and lastly SureBlue Reserve HRP substrate. The absorbance values were read at 650 nm and all experiments were conducted in technical triplicate. The negative control wells contained assay buffer in the absence of immobilised GST-GGA3, whilst the positive control wells were incubated with 1 µM histidine-tagged GST.

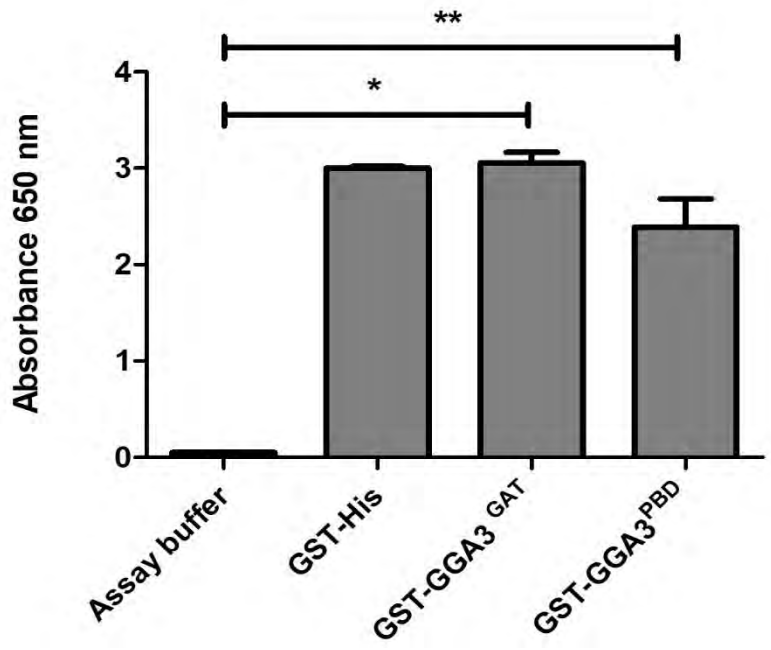

Figure 11: Verification of the binding of GST-GGA3 proteins to the glutathione coated plate. After incubating glutathione-coated plate wells with GST-GGA3^{GAT} or GST-GGA3^{PBD}, protein binding was detected using an anti-GST antibody and an HRP-conjugated secondary antibody, followed by the addition of a chromogenic HRP substrate. Once colour was observed, absorbance readings were read at 650 nm. A negative control containing assay buffer in the absence of GST was included as well as a positive control consisting of GST-His. The data is shown as the standard deviation of the samples in technical triplicate replicates; *p<0.0001, **p= 0.0013.

The results (**Figure 11**) showed that the wells containing the GST-GGA3 constructs produced binding absorbances similar to those obtained with the positive GST-His control. This suggested that the GST tag, fused to both GGA3 constructs, was successfully captured by the

glutathione coated plate and not prohibited from doing so by the fusion partner. The results also suggested sufficient binding integrity regarding the glutathione plates used in this study.

3.3.5.2. Investigating the selective binding of PfArf1$^{N\Delta17}$-GTP to GGA3 using HisDetector Ni-HRP reagent.

Prior to conducting the assay using parasite lysates, purified recombinant *Pf*Arf1$^{N\Delta17}$ was used to determine whether the selective binding of *Pf*Arf1 $^{N\Delta17}$-GTP vs. -GDP to the two respective GST-GGA3 constructs was maintained in the reversed assay format. Moreover, it was used to determine which of the GST-GGA3 constructs could best discriminate between pre-loaded *Pf*Arf1$^{N\Delta17}$-GDP and *Pf*Arf1$^{N\Delta17}$-GTP. To do this, an assay was conducted where both GST-GGA3^{GAT} and GST-GGA3^{PBD} recombinant proteins were diluted to 1 µM and added to the glutathione coated plate where they were left to incubate for 1 hour at 27°C. To remove any unbound proteins, the plate was washed multiple times before diluting and transferring 5µM of GTP and GDP pre-loaded His-*Pf*Arf1 $^{N\Delta17}$. After additional wash steps, HisDetector Ni-HRP (horseradish peroxidase conjugated to nickel) was added to each well and left to incubate for 30 minutes to bind to the His-tags of captured *Pf*Arf1 $^{N\Delta17}$. Binding of the HisDetector Ni-HRP protein was detected through the chromogenic output produced by the reporter enzyme HRP when absorbances were read at an absorbance of 650 nm following the addition of SureBlue Reserve HRP substrate. Background absorbance readings of pre-loaded *Pf*Arf1$^{N\Delta17}$-GDP and -GTP incubated in wells the absence of immobilised GGA3 were included and subtracted from the experimental wells to correct the results. The experimental data obtained suggests that the GST-GGA3^{GAT} domain maintained its ability to discriminate between GDP- (Abs_{650} 0.0263 ± 0.0015) and -GTP bound $^{N\Delta17}$*Pf*Arf1 (Abs_{650} 0.0367 ± 0.000231) (p=0.0203; *indicated by * in* **Figure 12**) in this reversed assay format. However, consistent with the results previously obtained with the nickel plate assay (*section 3.3.4*), GST-GGA3^{PBD} displayed more efficient binding and discrimination between active and inactive $^{N\Delta17}$*Pf*Arf1 (**Figure 12**). The GST-GGA3^{PBD} protein was able to discriminate between the GDP- (Abs_{650} 0.029 ± 0.0027) and GTP-bound *Pf*Arf1$^{N\Delta17}$ (Abs_{650} 0.062 ± 0.004) by selectively binding active *Pf*Arf1 (p= 0.0023; *indicated by* ** in **Figure 12**). For this reason, subsequent experiments were conducted with GST-GGA3^{PBD} in preference to GST-GGA3^{GAT}.

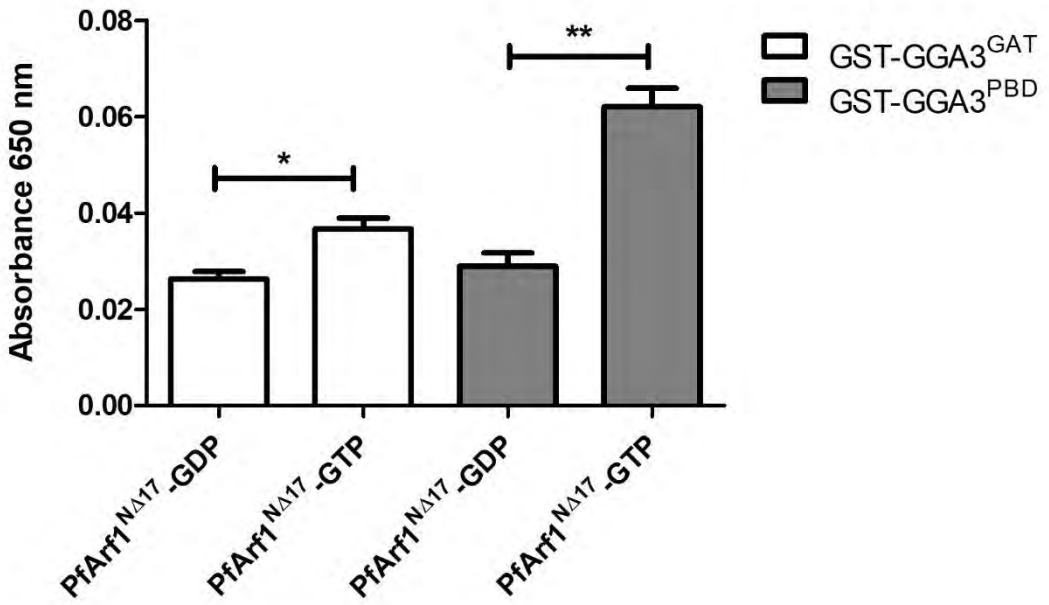

Figure 12: Exploring the selective binding of *Pf*Arf1 $^{N\Delta17}$-GTP to immobilised GST-GGA3 with HisDetector Ni-HRP. Both GST-GGA3 proteins were diluted to 1 µM in assay buffer and transferred to a glutathione coated plate and incubated for 1 hour at 27°C. After sequential washing steps, 5 µM GDP or GTP pre-loaded *Pf*Arf1$^{N\Delta17}$ were added to the immobilised GST-fusion samples and left to incubate for another hour at 27°C. Any unbound proteins were removed with several rinse steps. HisDetector Ni-HRP was added and left to incubate at room temperature for 30 minutes and after washing it was detected by adding SureBlue Reserve peroxidase substrate for 5-10 minutes and reading absorbance at 650 nm. Background controls consisted of *Pf*Arf1, pre-loaded with GDP and GTP, and incubated in wells lacking immobilised GST fusion proteins. The average of the readings obtained from these results were subtracted from the experimental wells containing immobilised GST-GGA3^{GAT}/GST-GGA3^{PBD}. The data is shown as the standard deviation of technical triplicate replicates; * p=0.0203; ** p=0.0023.

While it was verified that GST-GGA3^{PBD} could selectively bind active *Pf*Arf1$^{N\Delta17}$ when immobilised on a glutathione-coated plate, the absorbances obtained from the data portrayed in **Figure 12** were too low for the development of a robust assay. More importantly, the conceptual ELISA assay for the detection of endogenous active *Pf*Arf1 (that doesn't contain a His-tag) in parasite lysates (**Figure 6**) requires the use of antibodies. Therefore, the above assay was repeated with a higher concentration of GST-GGA3^{PBD} in the immobilisation step and detection was carried out with primary and secondary antibodies instead of the HisDetector Ni-HRP. The assumption was that the use of a peroxidase-conjugated polyclonal secondary antibody that recognises multiple epitopes on a primary antibody should amplify the signal produced.

3.3.5.3. Investigating the selective binding of PfArf1$^{N\Delta17}$-GTP to GGA3 using anti-Arf1 antibodies

The immunodetection assay was conducted using the same experimental parameters as described above with two additional incubation steps with monoclonal mouse anti-Arf1 primary antibodies, diluted to 1:5000, and HRP-conjugated goat anti-mouse Ig secondary antibodies diluted to 1:10 000. The use of a primary antibody raised for human Arf1 was done under the assumption that it would recognise and bind to *Pf*Arf1$^{N\Delta17}$ given that the amino acid sequences between *Hs*Arf1 and *Pf*Arf1 are highly conserved. The concentration of GST-GGA3 was also increased to 2 µM. The results demonstrated that there was a two-fold increase in the observed absorbances for both GDP-loaded *Pf*Arf1$^{N\Delta17}$ (0.191 ± 0.0022) and GTP-loaded *Pf*Arf1$^{N\Delta17}$ (0.283 ± 0.004) at 650 nm (**Figure 13**) when compared to the absorbance values detected by the Hisdetector Ni-HRP in the previous experiment (**Figure 12**). This difference could be seen as evidence that *Pf*Arf1, through selective binding, has been immobilised by GST-GGA3 ^{PBD} ($p<0.0001$) which correlates with the results obtained from the previous experiment depicted in **Figure 12.** However, it should be noted that fresh aliquots of *Pf*Arf1-GDP & -GTP were prepared for each experiment, which means the result could also have been due to differences in the efficiency of nucleotide exchange between experiments. Nevertheless, based on the data shown in **Figure 13**, monoclonal mouse anti-human Arf1 antibodies were successfully used to cross-react with *Pf*Arf1.

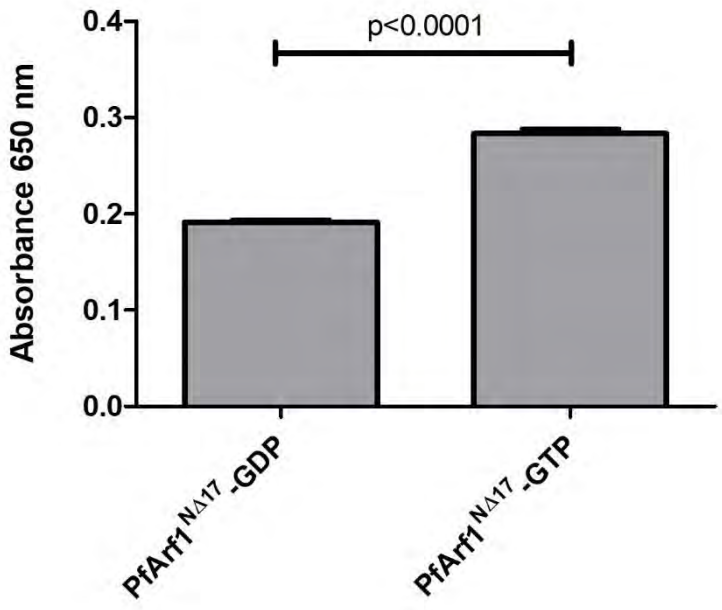

Figure 13: Investigating the selective binding of $^{N\Delta17}$*Pf*Arf1-GTP to immobilised GST-GGA3^{PBD} via immunodetection. GST-GGA3^{PBD} was diluted to 2 µM in assay buffer and

transferred to the glutathione coated plate where it was left to incubate for 1 hour at 27°C. After washing, 5 µM GDP or GTP pre-loaded *Pf*Arf1$^{N\Delta17}$ was added to the immobilised GST-GGA3^{PBD} and left to incubate for another hour at 27°C. Unbound proteins were removed by washing before sequential 1-hour incubations interspersed with washing steps with mouse anti-Arf1 primary antibodies and HRP-conjugated goat anti-mouse Ig secondary antibodies. To detect the selective binding of active *Pf*Arf1 to GST-GGA3, SureBlue Reserve peroxidase substrate was added, and the absorbance read at 650 nm once a colour change was observed. Background control wells contained either GDP or GTP pre-loaded *Pf*Arf1 incubated in wells absent of immobilised GST-GGA3^{PBD} and their absorbance readings subtracted from the experimental wells. The data is shown as the standard deviation of technical triplicate replicates; $p<0.0001$.

Since the assay demonstrated the ability of glutathione plate-immobilised GST-GGA3^{PBD} to discriminate between GDP- and GTP- loaded recombinant *Pf*Arf1 using immunodetection, the next step was to implement it using *Plasmodium falciparum* parasite lysates and determine whether it could discriminate between endogenous GDP/GTP-loaded *Pf*Arf1.

3.3.6. Endogenous Plasmodium falciparum Arf1-GGA3 GST interaction assay

Before the assay could be implemented to verify the inhibition of *Pf*Arf1GAP1 by novel inhibitory compounds previously discovered by a member in our research group, it was necessary to determine whether the assay using immobilised GST-GGA3^{PBD} could capture endogenous *Pf*Arf1 present in a parasite lysate and whether it would be sufficiently detectable using anti-Arf1 and secondary antibodies. This led to the implementation of the assay described in the previous section but using cultured 3D7 *Plasmodium falciparum* parasite lysates instead of using purified recombinant *Pf*Arf1$^{N\Delta17}$.

3.3.6.1. Exploring the binding of active endogenous PfArf1 using the Arf1-GGA3 assay

In preparation for the assay, parasite pellets were prepared. Infected erythrocytes containing mature parasites (trophozoites and schizonts) from cultures were pelleted and resuspended in PBS containing saponin to lyse the erythrocyte membranes. The remaining intact parasites were pelleted, washed by centrifugation, and stored at -80°C. Subsequently, a parasite pellet was thawed, lysed with 0.5% Triton X-100 in assay buffer, and cellular debris and hemozoin crystals removed by centrifugation. The clarified lysate was determined to have a protein concentration of 0.584 mg/mL as quantified by a BCA assay. The parasite lysate was divided into two equal portions incubated with 5 µM GDP and GTP, respectively. Since nucleotide loading could not be monitored by tryptophan fluorescence, the presumption was made that the two lysates would contain predominantly inactive and active *Pf*Arf1, respectively. The lysates

were incubated in a glutathione coated plate containing 2 µM immobilised GST-GGA3^{PBD} and captured *Pf*Arf1 detected with antibodies as described above. Background controls consisted of lysates incubated in wells lacking GST-GGA3^{PBD}, and the absorbance readings subtracted from those obtained in the experimental wells.

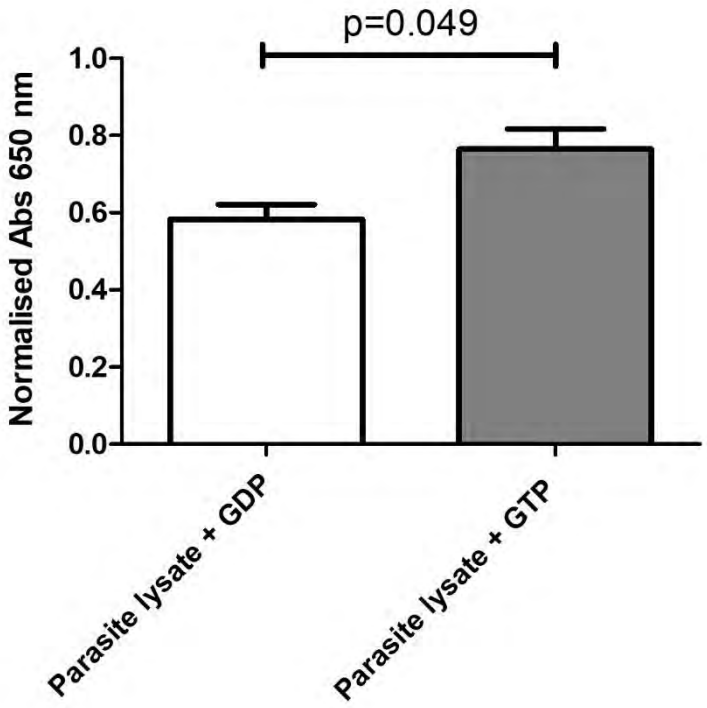

Figure 14: Investigating the binding of endogenous *Pf*Arf1-GTP in *Plasmodium falciparum* parasite lysates to immobilised GST-GGA3^{PBD}. The GST-GGA3 construct was diluted to 2 µM in assay buffer and transferred to the glutathione coated plate where it was left to incubate for 1 hour. Simultaneously, nucleotide exchange was promoted using parasite lysates incubated with 5 µM GDP or GTP and 20 µM EDTA, followed by the addition of 25 µM $MgCl_2$. Once the GGA3 construct was immobilised onto the plate and nucleotide exchange was complete, the parasite lysate was transferred to the plate and left to incubate for 1 hour. *Pf*Arf1 binding was detected via immunodetection by sequential incubations with mouse anti-*Hs*Arf1, goat anti-mouse Ig-HRP and SureBlue Reserve peroxidase substrate before reading the absorbance at 650 nm once a colour change was observed. Background control wells contained either GDP or GTP pre-loaded parasite lysates incubated in wells without immobilised GST-GGA3^{PBD}. The absorbance readings were normalised by dividing with the protein concentrations in the respective lysates. The data is shown as the standard deviation of technical triplicate replicates; p=0.049

It is essential to note that this experiment as well as the one conducted in *section 3.3.6.2* relied on two important assumptions: the first was that, via nucleotide exchange, incubations conducted using *Plasmodium falciparum* parasite lysates with GDP and GTP would result in both active and inactive endogenous *Pf*Arf1. The second assumption was that *Pf*Arf1 could be detected using monoclonal mouse antibodies raised against human Arf1 (for reasons previously stated). Based on the results depicted in **Figure 14**, immobilised GST-GGA3^{PBD} was able to capture *Pf*Arf1 present in the parasite lysate, and that the anti-Arf1 and secondary antibodies were able to detect the captured *Pf*Arf1 (p=0.049) with negligible non-specific background in the wells lacking GST-GGA3^{PBD} (*results not shown*). Nevertheless, the quality of the assay (p=0.049) in **Figure 14** indicated that the current experimental parameters weren't sufficient for the development of a robust assay and thus required re-evaluation. Therefore, the above assay was conducted again with higher concentrations of GDP and GTP.

3.3.6.2. Binding of endogenous PfArf1in Plasmodium falciparum lysates treated with 5 µM and 25 µM of GDP and GTP, respectively

A fresh parasite lysate was prepared and determined to have a protein concentration of 0.208 mg/mL as quantified by a BCA assay. The parasite lysate was divided into two equal portions and incubated with 25 µM GDP and GTP, respectively. The rest of the assay was conducted as described above. Control wells were incubated with either GDP or GTP pre-incubated parasite lysates lacking immobilised GST-GGA3^{PBD}.

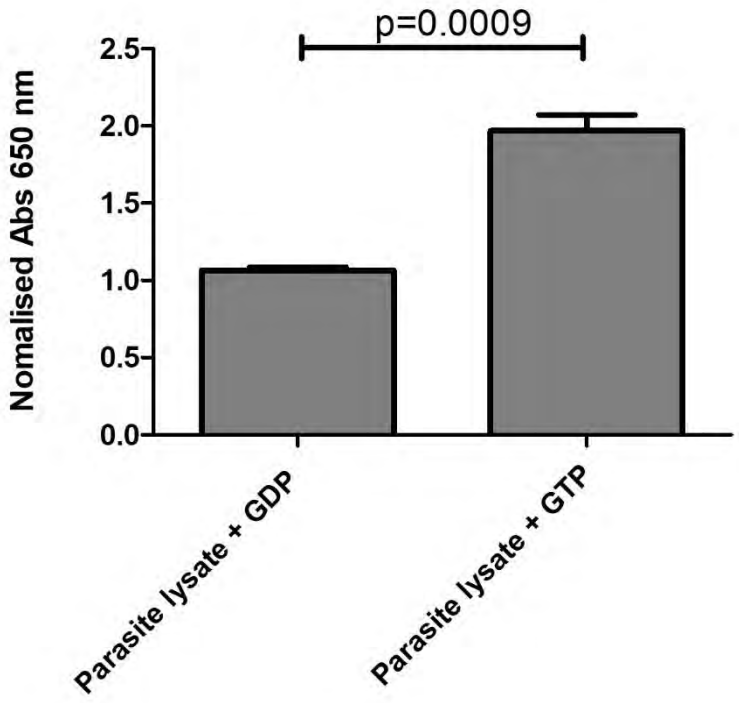

Figure 15: Optimising the experimental parameters of the Arf-GGA3 assay to determine the binding ability of endogenous *Pf*Arf1-GTP in *Plasmodium falciparum* parasite lysates to immobilised GST-GGA3^{PBD}. The GST-GGA3 construct was diluted to 2 µM in assay buffer and transferred to the glutathione coated plate where it was left to incubate for 1 hour. Simultaneously, nucleotide exchange was promoted using 3D7 parasite lysates incubated with 25 µM GDP or GTP and 20 µM EDTA, followed by the addition of25 µM $MgCl_2$. Once the GGA3 construct was immobilised onto the plate and nucleotide exchange was complete, the parasite lysate was transferred to the plate and left to incubate for 1 hour. *Pf*Arf1 binding was detected via immunodetection by sequential incubations with mouse anti-*Hs*Arf1, goat anti-mouse Ig-HRP, and SureBlue Reserve peroxidase substrate before reading the absorbance at 650 nm once a colour change was observed. Background control wells contained either GDP or GTP pre-loaded *Pf*Arf1 incubated in wells without immobilised GST-GGA3^{PBD}. The absorbance readings were normalised by dividing with the protein concentrations in the respective lysates. The data is shown as the standard deviation of technical triplicate replicates; p=0.0009.

The data obtained in **Figure 15** suggested that the Arf-GGA3 assay could discriminate between endogenous active (0.410 ± 0.0209) and inactive *Pf*Arf1 (0.222 ± 0.004) in *P. falciparum* parasite lysates and that the increase in both GDP and GTP concentrations improved the quality of the assay (p=0.0009), comparative to **Figure 14** which had reduced GDP and GTP concentrations and produced a lower p-value of 0.049.

3.3.7. Validation of the PfArf1-GGA3 GST interaction assay by treatment of P. falciparum cultures with Arf1 inhibitors

Having established the ELISA-based assay to detect active *Pf*Arf1 in parasite lysates, the final objective was to determine whether it could fulfil its designed role of detecting the capture of endogenous *Pf*Arf1 via immobilised GGA3 by testing the assay with known *Pf*ArfGAP1 inhibitors.

3.3.7.1. The exploration of the inhibition of endogenous PfArf1 activation in P. falciparum cultures treated with the Arf1-GEF inhibitor, BFA.

As mentioned in Chapter 1, brefeldin A (BFA) inhibits Arf1 by obstructing Arf1-GEF activity and has been categorised as an 'interfacial inhibitor' of Arf activation (Zeghouf *et al*., 2005). Since BFA targets the transient, low affinity complex that initiates the dissociation of GDP from Arf1 for GTP, it traps Arf1 in its inactive state by stabilising the Arf-Sec7 interaction (Zeghouf *et al*., 2005). It can therefore be further exploited to selectively inhibit Arf1 activation in cells. To validate the screening potential of the GGA3-Arf1 interaction assay developed in this study, an experiment was conducted where parasites were cultured in the presence of BFA. Theoretically, there should be a detectable decrease in active Arf1 observed in the BFA-treated

parasite cultures compared to those that are left untreated. The GGA3-Arf1 assay was conducted as previously detailed but with the parasites cultured in the presence of 20 µM BFA for 90 minutes in a total culture volume of 5 mL. Parasites cultured in the absence of BFA were included as a control. After the BFA incubation, cultures were centrifuged to obtain the infected erythrocytes, the erythrocytes lysed with saponin and subsequent pelleted parasites lysed with Triton X-100. The BFA-treated and control lysates were incubated with immobilised GST-GGA3^{PBD}, followed by immunodetection with anti-Arf1 and secondary antibodies as described in preceding sections. The *Pf*Arf1 absorbances were corrected by subtracting readings from background control wells incubated with parasite lysates in the absence of immobilised GST-GGA3^{PBD} from the experimental wells. Assuming that the binding of endogenous *Pf*Arf1 to GST-GGA3 was directly proportional to total parasite lysate protein, to further correct for possible deviations in protein content in the BFA-treated and control lysates during the culture period and sample preparation, the protein concentrations in the two lysates were determined using a BCA assay and the absorbance readings divided by the concentration to normalise the data.

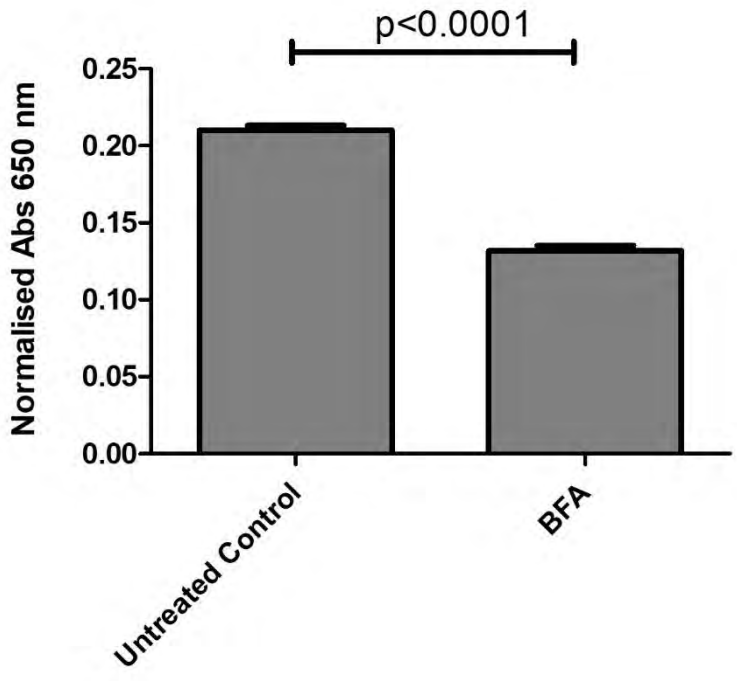

Figure 16: The detection of BFA-mediated inhibition of nucleotide exchange of *Pf*Arf1 in cultured *P. falciparum* parasites using the Arf1-GGA3 interaction assay. *P. falciparum* cultures (5 mL) were left untreated (control) or incubated with 20 µM BFA for 90 minutes. Parasite lysates prepared from the cultures were incubated with immobilised GST-GGA3^{PBD} in a glutathione-coated plate. Detection of bound *Pf*Arf1 was carried out with primary mouse anti-Arf1 and goat anti-mouse Ig-HRP secondary antibodies, followed by the addition of SureBlue reserve peroxidase substrate. Absorbance was read at 650 nm. The background

control wells contained parasite lysates incubated in wells absent of immobilised GST-GGA3^{PBD} and the readings subtracted from the absorbances obtained in experimental wells. The absorbance readings were normalised by dividing with the protein concentrations in the respective lysates. The data is shown as the mean and standard deviation of technical triplicate replicates; $p<0.0001$.

The results depicted in **Figure 16** suggests that BFA selectively inhibits endogenous *Pf*Arf1 activation which is evident by the statistically significant decrease in absorbance ($p<0.0001$) observed at 650 nm for parasites treated with BFA compared to the untreated control. The successful detection of the inhibition of *Pf*Arf1 activation by BFA demonstrates that the GGA3-Arf1 interaction assay developed in this study can provide a means by which to discover/validate potential *Pf*Arf1 inhibitors targeting the activation or deactivation of *Pf*Arf1 via GEF or GAP regulatory proteins.

3.3.7.2. Investigating the inhibition of endogenous PfArf1 deactivation in P. falciparum cultures treated with PfArfGAP1 inhibitors

The next step was to verify whether Chem1099 and Chem3050, two compounds previously shown to inhibit *Pf*Arf1 deactivation by *Pf*ArfGAP1 in a protein-based assay and to inhibit cultured *P. falciparum* viability (Swart et al., 2020), are responsible for the decrease in parasite viability due to the inhibition of *Pf*ArfGAP1 in parasites. Consequently, the next validation experiment was conducted as described above, but instead of treatment with BFA, 5 mL parasite cultures were treated with 20 µM Chem1099 and Chem3050 for 90 minutes, respectively, alongside an untreated control culture. Following protein concentration quantification by a BCA assay, the parasite lysates treated with Chem1099 and Chem3050 had protein concentrations of 0.194 mg/mL and 0.151 mg/mL, respectively, whereas the control was found to be 0.296 mg/mL.

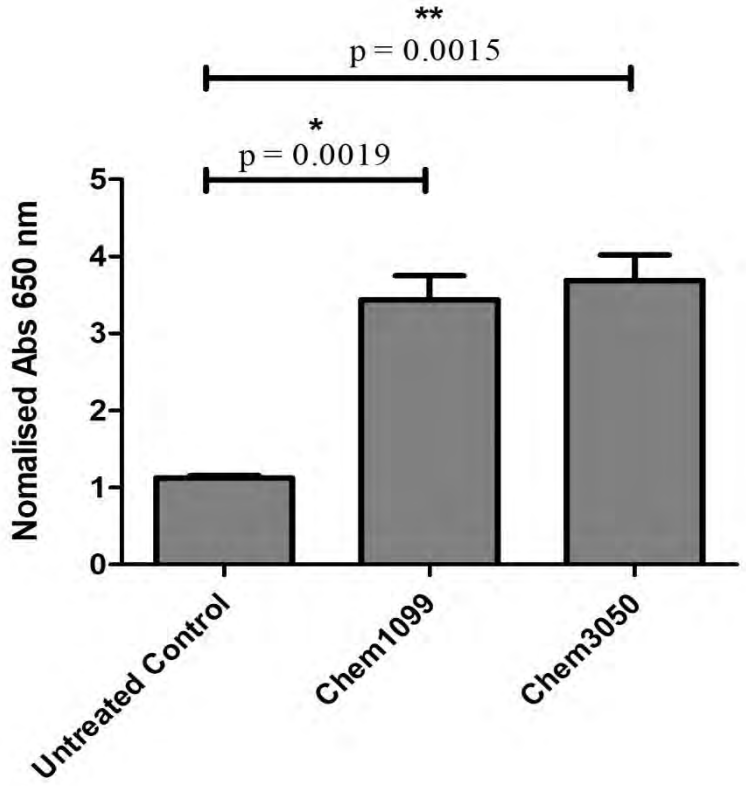

Figure 17: Investigating the inhibition of endogenous *Pf*Arf1 deactivation in *P. falciparum* cultures treated with the *Pf*ArfGAP1 inhibitors Chem1099 and Chem3050. *P. falciparum* cultures (5 mL) were left untreated (control) or incubated with 20 µM Chem1099 and Chem3050 for 90 minutes. Parasite lysates prepared from the cultures were incubated with immobilised GST-GGA3^{PBD} in a glutathione-coated plate. Detection of bound *Pf*Arf1 was carried out with primary mouse anti-Arf1 and goat anti-mouse Ig-HRP secondary antibodies, followed by the addition of SureBlue reserve peroxidase substrate and the absorbance read at 650 nm. The background control wells contained parasite lysates incubated in wells absent of GST-GGA3^{PBD} and their absorbance readings were subtracted from the experimental absorbances. The absorbances measured at 650 nm were normalised with the lysate protein concentration for each sample. The data is shown as the mean and standard deviation of technical triplicate replicates; *p=0.0019. **p=0.0015.

If the inhibitors did indeed inhibit the deactivation of endogenous *Pf*Arf1, we expected to observe an increase in active *Pf*Arf1-GTP relative to the untreated control following treatment with *Pf*ArfGAP1 inhibitors. The results in **Figure 17**, where statistical analysis using two-tailed unpaired t-tests produced a p-value of 0.0019 (indicated by *) for Chem1099 and 0.0015 for Chem3050 (indicated by **), show that there was a marked increase in active *Pf*Arf1-GTP compared to the control. This led to the conclusion that the assay could detect the inhibition of deactivation of endogenous *Pf*Arf1 in parasite lysates.

3.3.8. Validation of PfArf1-GGA3 GST interaction assay by treatment of HeLa cultures with the Arf1 activation inhibitor BFA

The previous experiments showed that the ELISA-based Arf1-GGA3 interaction assay could be used to investigate the activation status of *Pf*Arf1 subsequent to treatment of parasite cultures with potential inhibitory compounds. The next experiment was conducted to determine whether this assay could also be used to investigate the activation status of human Arf1 in human cells treated with Arf1 inhibitors, using the standard Arf1 activation inhibitor, BFA. This was achieved by treating a 5 mL culture of HeLa cells according to the protocol described in *section 2.8.1* with 20 µM BFA for 90 minutes, in parallel with an untreated control culture. After the incubation, the cells were detached using Trypsin-EDTA, pelleted, and lysed by adding Triton X-100. The lysates were subsequently incubated with immobilised GST-GGA3^{PBD} and the ELISA-based detection of captured Arf1 carried out as described previously.

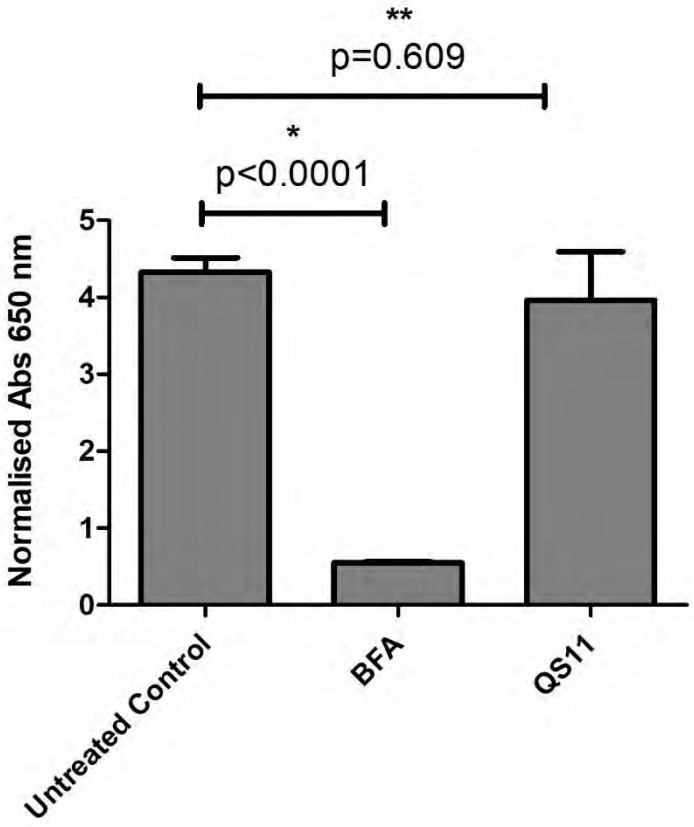

Figure 18: Detecting the inhibition of human Arf1 activation by BFA in HeLa cells using the ELISA-based Arf1-GGA3 interaction assay. HeLa cell cultures (5 mL) were left untreated (control) or incubated with 20 µM BFA/QS11 for 90 minutes. Cell lysates prepared from the cultures were incubated with immobilised GST-GGA3^{PBD} in a glutathione-coated plate. Detection of bound Arf1 was carried out with primary mouse anti-Arf1 and goat anti-mouse Ig-HRP secondary antibodies, followed by the addition of SureBlue reserve peroxidase substrate. The absorbance was read at 650 nm. The background control wells contained HeLa

cell lysates incubated in wells absent of GST-GGA3^{PBD} and their absorbance values were subtracted from the experimental readings. The absorbances read at 650 nm were normalised with the lysate protein concentration for each sample. The data is shown as the mean and standard deviation of technical triplicate replicates; *p<0.0001, **p=0.609.

The results depicted in **Figure 18** suggests that the *Pf*Arf1-GGA3 interaction assay established in this study was capable of detecting the activation of human Arf1, evident by the marked decrease in captured Arf1 in the lysate of HeLa cells treated with BFA compared to the untreated control (p<0.0001). Due to the inhibition of endogenous GEF-mediated activation of human Arf1 by BFA, the expected decrease in GTP-loaded Arf1 was robustly detected. However, the expected increase in GTP-loaded Arf1 following treatment with QS11 (reported to be an ArfGAP1 inhibitor; Singh *et al*., 2015) was not detected. Instead, no significant difference was observed (p=0.609) between the *Hs*Arf1 activation status of the untreated control cells and cells treated with QS11.

Chapter 4: Discussion and future work

In this study, a robust and sensitive *Pf*Arf1-GGA3 GST interaction assay was established that can detect changes in endogenous active (GTP-bound) and inactive (GDP-bound) *Pf*Arf1 levels following incubation with lysates of compound-exposed parasites and ultimately assisted in validating *Pf*Arf1 and, by extension, its GEF and GAP modulators, as antimalarial drug targets. Even though this study is centralised on malaria, given the ubiquitous nature of Arf1 in eukaryotes, the assay mentioned above was also conducted using Arf1 present in the lysates of HeLa cells. Assuming our preliminary findings aren't a false-positive, they suggest that our assay could be optimised and explored as a tool in the identification of potential anti-cancer compounds targeting *Hs*Arf1 and its mediators.

EDTA-mediated nucleotide exchange of GDP and GTP on *Pf*Arf1$^{N\Delta17}$ was successfully conducted and analysed using tryptophan fluorescence assays. The conformational transition from *Pf*Arf1$^{N\Delta17}$-GDP to -GTP was observed in **Figure 9** as an increase in fluorescence over time whereas the transition from GTP-loaded *Pf*Arf1$^{N\Delta17}$ to GDP-loaded protein was observed as a decrease in fluorescence (Goody, 2016). The endpoint and kinetic tryptophan measurements obtained in this study were also indicative that the original preparation of the *Pf*Arf1$^{N\Delta17}$ protein was purified from *E. coli* as a composite of both GDP- and GTP-bound *Pf*Arf1$^{N\Delta17}$, supported by the simultaneous increase and decrease in fluorescence during incubations with GTP and GDP, respectively. These experimental parameters and results align

with those used and obtained in another study that established a Ni-NTA Arf GTPase assay (T. Swart *et al.,* 2020).

Conceptually, the *Pf*Arf1-GGA3 GST assay format, illustrated in **Figure 6**, exploits the transient interaction that occurs between GTP-bound *Pf*Arf1 and its GGA3 effector (Takatsu *et al*., 2002). While several studies have exploited this same interaction in the development of plate-based and pull-down assays for active Arf1, some used a GGA3 construct lacking the VHS domain (Takatsu *et al*., 2002, T. Swart *et al.,* 2020) while others utilised a GGA3 construct containing both the VHS and GAT domains (referred to as $GGA3^{PBD}$ in this study) (Dell'Angelica *et al*., 2000, Cohen and Donaldson, 2010). Preceding the establishment of an *in vitro* biochemical *Pf*Arf1-GGA3 GST assay, a Ni-NTA immobilised Arf1-GGA3 assay developed by T. Swart was conducted and confirmed that preloaded GTP-*Pf*$Arf1^{N\Delta17}$ was capable of selectively capturing both the GST-$GGA3^{GAT}$ and GST-$GGA3^{PBD}$ proteins. These results (depicted in **Figure 10**) further indicated that, while both GGA3 constructs could bind *Pf*$Arf1^{N\Delta17}$, there was more efficient binding between *Pf*$Arf1^{N\Delta17}$ and GST-$GGA3^{PBD}$ when compared to incubations with GST-$GGA3^{GAT}$. This is probably because the less truncated version of GGA3 maximises its binding capacity for GTP-loaded *Pf*$Arf1^{N\Delta17}$. There is a possibility that, at least to some extent, the GST tag fused to the N-terminus of $GGA3^{GAT}$ obstructed the interaction between *Pf*Arf1 and the GAT domain of GGA3 more significantly than when it was fused to the $GGA3^{PBD}$ domain, which has a more extensive N-terminal extension in front of the GAT domain.

The implementation of our *in vitro* biochemical *Pf*Arf1-GGA3 GST assay where the GST-GGA3 was immobilised on the plate and interacted with Arf1 in solution (as opposed to the original assay developed by T. Swart where immobilised Arf1 interacts with soluble GST-GGA3) verified that not only does active *P. falciparum* $Arf1^{N\Delta17}$ bind to both forms of GGA3 while maintaining its selective nucleotide-dependent binding ability, but it was also determined that GST-$GGA3^{PBD}$ was better suited to develop robust absorbance readings that discriminate between active and inactive *Pf*$Arf1^{N\Delta17}$ when compared to GST-$GGA3^{GAT}$ in a plate-based colorimetric assay format which is shown in **Figures 12 & 13**. This further correlated with the results obtained in the previous experiment illustrated in **Figure 11**. While the results implied that the GST tag fused to both GGA3 constructs was successfully captured by the glutathione-coated plate, The presence of truncated proteins in the purification profiles of both GGA3 constructs was noted, which is a common occurrence with GST fusion proteins. Its presence does, however, raise the possibility that the contaminating GST-containing proteins may have

competed with the full-length GST-GGA3 proteins and effectively reduced the binding efficiency of both constructs to the glutathione-coated plate. In addition, it also suggests that the concentrations of the GST-GGA3 proteins, determined using a BCA assay, were overestimated. In this regard, the conclusion that GST-GGA3^{PBD} provides superior discrimination between GTP- and GDP-loaded *Pf*Arf1 compared to GST-GGA3^{GAT} is subject to the assumption that similar concentrations of the two GGA3 proteins were immobilised in the plate wells. Though not attempted in this study, two possible solutions would be to include protease inhibitors during *E. coli* expression to prevent the cleavage of the GST from the fusion protein or, alternatively, one could improve protein translation by inducing expression at lower temperatures for a prolonged period of time in an attempt to reduce premature translation that could result in the formation of truncated GST fusion proteins. In initial experiments described in *section 3.3.5.1*, capture of *Pf*Arf1$^{N\Delta17}$ by immobilised GST-GGA3 was assessed with HisDetector Ni-HRP to detect the His tag on the Arf1 protein. Though detection of *Pf*Arf1$^{N\Delta17}$ by HisDetector was successful, the weak absorbance readings observed in **Figure 12** indicated poor sensitivity. Since the HisDetector consists of horseradish peroxidase conjugated to Ni^{2+} as a transition metal, which is known to have a high affinity for the imidazole rings present in consecutive histidines, it was expected that more robust absorbances would be obtained. However, there is a possibility that the HisDetector Ni-HRP was spatially obstructed by the *Pf*Arf1$^{N\Delta17}$ protein from allowing the Ni^{2+} ion to effectively bind to the polyhistidine tag, which would explain the weak absorbances obtained. Therefore, in an attempt to obtain more robust absorbance readings, anti-Arf1 primary antibodies and complementary HRP-conjugated secondary antibodies were used to assess the capture of *Pf*Arf1$^{N\Delta17}$ by immobilised GST-GGA3. It was reasoned that, if the polyhistidine tag was indeed being obstructed, perhaps the *Pf*Arf1$^{N\Delta17}$ protein would provide a more accessible surface area for anti-Arf1 antibodies to bind. In addition, the recognition of multiple epitopes on the primary antibodies by the polyclonal secondary antibodies should result in signal amplification due to the capture of several peroxidase reporter proteins by a single Arf1 protein. Indeed, the results indicated that immunodetection had a higher specificity in the detection of the target protein and was better suited at discriminating between GDP- and GTP-loaded *Pf*Arf1$^{N\Delta17}$ *in vitro* with negligible background absorbance readings. An aspect that wasn't addressed but could be explored in further assay optimisation experiments is the availability of immobilised GST-GGA3 in the experimental wells. Titration of the GST-GGA3 concentration used could be employed to determine the amount of GST-GGA3 that is required to saturate the glutathione plate wells.

While the results obtained using the biochemical format of the *Pf*Arf1-GGA3 GST assay were promising, it was borne in mind that biochemical *in vitro* experimentation was not an exact representation of the physiological conditions and interactions within the cell. Similar to other publications investigating Arf1, the biochemical *in vitro* design of this assay utilised a *Plasmodium* Arf1 mutant lacking the first 17 amino-terminal residues (*Pf*Arf1$^{N\Delta17}$). The main reason for using a truncated adaptation of *Pf*Arf1 as opposed to the wild type is to improve protein solubility during expression in *E. coli*. However, the absence of the amphipathic helix results in a biologically non-functional *Pf*Arf1 given that, in the cellular context, these residues are post-translationally myristoylated and necessary for membrane recruitment (Yorimitsu *et al*., 2014). Despite loss of function, this study suggests that *Pf*Arf1$^{N\Delta17}$ is still capable of binding nucleotides and maintaining these nucleotides, and the consequent conformational changes, during subsequent experimentation. These findings were consistent with those described by several studies using lipid-independent Arf1$^{N\Delta17}$ mutants (Swart *et al*., 2020, Goldberg, 1998). Our observations should, however, be considered in light of the findings presented by Seidel *et al*. (2004) who found that truncated Arf1 $^{N\Delta17}$ had a higher binding affinity for GTP while full-length Arf1 had a higher affinity for GDP. In addition, it was unclear to what extent the presence of the 17-residue N-terminal extension of native *Pf*Arf1 might affect its interaction with immobilised GST-GGA3 in our assay format. Moreover, it was possible that the concentration of *Pf*Arf1 in parasite lysates would be insufficient to produce robust detection absorbance values, comparable to those obtained with the purified protein. Potentially, these considerations could compromise the ability of our biochemical *Pf*Arf1-GGA3 GST assay format to discriminate between endogenous active and inactive forms of *Pf*Arf1. Therefore, to further explore the sensitivity of our assay design and validate our initial findings, the *Pf*Arf1-GGA3 GST interaction assay was conducted with endogenous *Pf*Arf1 from 3D7 *P. falciparum* parasite lysates to investigate the suitability of this assay in the cellular context. The results shown in **Figure 14** suggests that the *Pf*Arf1-GGA3 GST assay can successfully discriminate between endogenous *Pf*Arf1 GTP- and GDP-loaded proteins with negligible background noise. While these observations don't disprove the findings described by Seidel *et al*., 2004, it does suggest that the difference in binding affinities of the Arf1$^{N\Delta17}$ mutant and the Arf1 wild type for GDP and GTP, the presence of an intact N-terminal amphipathic α-helix in cellular Arf1, and the concentration of Arf1 in the lysate didn't affect the selectivity and sensitivity of either the biochemical or cell-based *Pf*Arf1-GGA3 GST assay formats established in this study.

Although, as mentioned before the normalisation of the concentrations between the BFA-treated and the control lysates were conducted to correct for possible deviations in protein content under the assumption that the binding of *Pf*Arf1 to GST-GGA3 is directly proportional to total parasite lysate protein, this may be an erroneous assumption. In future studies, it is recommended that the total protein concentration of the parasite lysates before conducting the assay is determined and equalised, instead of normalising the concentrations after the fact.

Following the successful discrimination between endogenous GDP- and GTP-loaded *Pf*Arf1 from *P. falciparum* lysates, the *Pf*Arf1-GGA3 GST assay was tested using known inhibitors of *Pf*Arf1 activation and deactivation to provide further evidence that the assay is capable of detecting the capture of endogenous *Pf*Arf1 by immobilised GGA3. The observable decrease in *Pf*Arf1-GTP absorbance (**Figure 16)** following the incubation of malarial lysates with the known GEF inhibitor, BFA, demonstrated that our assay could detect changes in the activation status of *Pf*Arf1, and thus has the potential to be exploited in the discovery of novel *Pf*Arf1 activation inhibitors that target *Pf*Arf1GEF in drug screening campaigns. It was also found that the assay was applicable in the identification and validation of compounds that target *Pf*Arf1 deactivation by obstructing *Pf*ArfGAP1 activity, represented by a marked increase in *Pf*Arf1-GTP absorbance following incubation with known *Pf*Arf1GAP inhibitors, Chem1099 and Chem3050. These results align with the findings published by T. Swart *et al*., 2020, that describe the identification of the compounds in screens conducted using purified *Pf*Arf1 and *Pf*ArfGAP1 proteins.

Based on the assay's success in detecting and measuring the effects that Arf signalling inhibitors have on the activation status of *Pf*Arf1, it was hypothesised that it was likely that results would be seen when probing human Arf1 (*Hs*Arf1) activation status in cells incubated in the presence of known human GEF and GAP inhibitors. In this respect, the findings were inconclusive, because even though a decrease in active *Hs*Arf1 (sourced from HeLa cells) following treatment with the GEF inhibitor BFA was observed and was synonymous with the results obtained using *P. falciparum* cultures in the preceding experiment, an expected increase in active *Hs*Arf1 in the lysates of HeLa cells incubated with the human ArfGAP1 inhibitor, QS11, was not found. Though preliminary, our findings showed no significant difference between the *Hs*Arf1 activation status of the untreated control cells and cells treated with QS11, which is inconsistent with the expected increase in GTP-bound *Hs*Arf1 following the targeted inhibition of *Hs*Arf1 deactivation. Though this incongruency was not further investigated, one speculative possibility is that there is redundancy in ArfGAP activity in the HeLa cells. Based

on sequence homology, there are approx. 30 ArfGAP proteins in mammalian cells (Sztul *et al*., 2019). QS11 was reported as an ArfGAP1 inhibitor (Singh *et al*., 2015), and this inhibition may be compensated for by other ArfGAPs. Thus, it is important that any future studies intent on extending the Arf1-GGA3 GST assay established in this study as a tool for the identification or confirmation of potential anti-cancer compounds targeting *Hs*Arf1 and its mediators, include validations of the assay described above with alternative GEF and GAP inhibitors known to target *Hs*Arf1. Examples could include SecinH3 and Golgicide A, commercially available ArfGEF inhibitors (Hafner *et al*., 2006; Sáenz *et al*., 2009). QS11 is the only available ArfGAP inhibitor; however, screens are being conducted in the research group to identify novel human ArfGAP inhibitors (N. Mqwathi, MSc study).

Another challenge experienced during this study included the expression and purification of GST-GGA3^{PBD}. Initially, T7 Express lysY/Iq *E. coli* cells were transformed with the relevant pGEX construct. However, since the initial results from analytical scale expression indicated poor protein expression and solubility even after expressing GST-GGA3^{PBD} at varying temperatures and IPTG concentrations (*results not shown*), it was speculateded that codon bias (Quax *et al*., 2015) may have contributed to reduced translational efficiency and affected protein folding during initial attempts at expressing GST-GGA3^{PBD}. Therefore T7 Express lysY/Iq *E. coli* cells were substituted with Rosetta cells (DE3) to supplement tRNAs for rare codons that may have been absent in the former expression system, to improve protein folding and protein solubility. This procedural change resulted in the successful overexpression of soluble GST-GGA3^{PBD} in the induced soluble fraction illustrated in **Figure 7B,** thus suggesting that Rosetta (DE3) cells are more appropriate for the expression of this protein. Another observation was that a GST-GGA3^{GAT} protein band was observed in the induced insoluble fraction of the host *E. coli* during analytical scale expression, which was indicative of incomplete bacterial lysis. In an attempt to improve the protein solubility, the duration of physical lysis by sonication was extended. While this adaptation reduced the amount of insoluble protein, it did not result in its complete solubilisation, evident by the presence of the protein band in the induced insoluble fraction in **Figure 7C**. Nonetheless, since sufficient soluble protein was purified for the establishment of the assay in this study, optimisation of the expression parameters for this construct was not further explored. Nevertheless, possible solutions to further improve protein solubility would be to conduct expression at lower IPTG concentrations and/or at lower temperatures (Galloway *et al*., 2003). Alternatively, one could solubilise the inclusion bodies *via* treatment with strong denaturing agents such as guanidium

chloride or urea, followed by attempted refolding and purification of GST-GGA3^{PBD} (Schlager *et al*., 2012).

In summary, the findings of this study contribute to the validation of *Pf*Arf1 deactivation as a possible malaria drug target, by confirming that *Pf*ArfGAP1 inhibitors that inhibit *P. falciparum* viability, discovered in a previous screen, also increase the levels of active *Pf*Arf1 in treated parasites. It also suggests that the *Pf*Arf1-GGA3 GST assay reported here can effectively be exploited to quantitatively measure the effects that compounds have on the activation status of *Pf*Arf1 and by extension, serve as a validation technique for the identification of novel *Pf*ArfGAP and *Pf*ArfGEF inhibitors. On the other hand, the efficiency of the adapted *Pf*Arf1-GGA3 GST assay, using mammalian HeLa cell lysates, remains inconclusive due to the conflicting results obtained following treatment with BFA and QS11. In its current form, the assay requires parasite and HeLa cell biomass obtained from 5 mL cultures and is more useful as a secondary assay to confirm the mode of action of Arf1 inhibitors discovered by other means. However, it would be worthwhile exploring the lower detection limits of the assay in terms of input culture volumes and determining if it could fulfil the role of a higher throughput primary screen for Arf1 inhibitors. Further experimentation is required to verify this conjecture by using progressively smaller cell cultures and calculating the assay Z-factor (Zhang *et al.*,1999), a statistical measurement that is often used to confirm the screening potential of pilot assays.

References

Abdin, M.Z., Israr, M., Rehman, R.U., Jain, S.K., (2003). Artemisinin, a novel antimalarial drug: biochemical and molecular approaches for enhanced production. Planta Med 69, 289–299.

Achan, J., Talisuna, A., Erhart, A., Yeka, A., Tibenderana, J., Baliraine, F., Rosenthal, P. and D'Alessandro, U. (2011). Quinine, an old anti-malarial drug in a modern world: role in the treatment of malaria. Malaria Journal, 10(1).

Afonso, A., Hunt, P., Cheesman, S., Alves, A.C., Cunha, C.V., Rosário, V. do, Cravo, P. (2006). Malaria Parasites Can Develop Stable Resistance to Artemisinin but Lack Mutations in Candidate Genes atp6 (Encoding the Sarcoplasmic and Endoplasmic Reticulum Ca2+ ATPase), tctp, mdr1, and cg10. Antimicrobial Agents and Chemotherapy.

Al-Olayan, E.M., Beetsma, A.L., Butcher, G.A., Sinden, R.E., Hurd, H. (2002). Complete development of mosquito phases of the malaria parasite in vitro. Science 295, 677–679.

Aly, A.S.I., Vaughan, A.M., Kappe, S.H.I. (2009). Malaria Parasite Development in the Mosquito and Infection of the Mammalian Host. Annu Rev Microbiol 63, 195–221.

Arkin, M.R., Randal, M., DeLano, W.L., Hyde, J., Luong, T.N., Oslob, J.D., Raphael, D.R., Taylor, L., Wang, J., McDowell, R.S., Wells, J.A., Braisted, A.C. (2003). Binding of small molecules to an adaptive protein–protein interface. PNAS 100, 1603–1608.

Baird, J. (2005). Effectiveness of Antimalarial Drugs. New England Journal of Medicine, 352(15), pp.1565-1577.

Barr, F. and Lambright, D. (2010). Rab GEFs and GAPs. Current Opinion in Cell Biology, 22(4), pp.461-470.

Bartoloni, A., Zammarchi, L. (2012). Clinical aspects of uncomplicated and severe malaria. Mediterr J Hematol Infect Dis 4, e2012026.

Baumgartner, F., Wiek, S., Paprotka, K., Zauner, S., Lingelbach, K. (2001). A point mutation in an unusual Sec7 domain is linked to brefeldin A resistance in a *Plasmodium falciparum* line generated by drug selection. Mol Microbiol 41, 1151–1158. .

Blasco, B., Leroy, D., Fidock, D.A. (2017). Antimalarial drug resistance: linking *Plasmodium falciparum* parasite biology to the clinic. Nat Med 23, 917–928.

Boman, A.L., Salo, P.D., Hauglund, M.J., Strand, N.L., Rensink, S.J., Zhdankina, O. (2002). ADP-Ribosylation Factor (ARF) Interaction Is Not Sufficient for Yeast GGA Protein Function or Localization. Mol Biol Cell 13, 3078–3095.

Bonifacino, J.S. (2004). The GGA proteins: adaptors on the move. Nat Rev Mol Cell Biol 5, 23–32.

Bonifacino, J.S., Jackson, C.L., (2003). Endosome-Specific Localization and Function of the ARF Activator GNOM. Cell 112, 141–142.

Boulay, P., Cotton, M., Melançon, P. and Claing, A. (2008). ADP-ribosylation Factor 1 Controls the Activation of the Phosphatidylinositol 3-Kinase Pathway to Regulate Epidermal Growth Factor-dependent Growth and Migration of Breast Cancer Cells. Journal of Biological Chemistry, 283(52), pp.36425-36434.

Bykov, Y.S., Schaffer, M., Dodonova, S.O., Albert, S., Plitzko, J.M., Baumeister, W., Engel, B.D., Briggs, J.A. (2017). The structure of the COPI coat determined within the cell. eLife 6, e32493.

Cabrera-Vera, T.M., Vanhauwe, J., Thomas, T.O., Medkova, M., Preininger, A., Mazzoni, M.R., Hamm, H.E. (2003). Insights into G Protein Structure, Function, and Regulation. Endocrine Reviews 24, 765–781.

Cai, H., Reinisch, K., Ferro-Novick, S. (2007). Coats, Tethers, Rabs, and SNAREs Work Together to Mediate the Intracellular Destination of a Transport Vesicle. Developmental Cell 12, 671–682.

Casalou, C., Ferreira, A., Barral, D.C. (2020). The Role of ARF Family Proteins and Their Regulators and Effectors in Cancer Progression: A Therapeutic Perspective. Frontiers in Cell and Developmental Biology 8.

Casanova, J.E. (2007). Regulation of Arf Activation: the Sec7 Family of Guanine Nucleotide Exchange Factors. Traffic 8, 1476–1485.

Chardin, P., McCormick, F., 1999. Brefeldin A: The Advantage of Being Uncompetitive. Cell 97, 153–155.

Chavrier, P., Ménétrey, J. (2010). Toward a Structural Understanding of Arf Family:Effector Specificity. Structure 18, 1552–1558.

Cherfils, J., Zeghouf, M. (2013). Regulation of Small GTPases by GEFs, GAPs, and GDIs. Physiological Reviews 93, 269–309.

Claude, A., Zhao, B.-P., Kuziemsky, C.E., Dahan, S., Berger, S.J., Yan, J.-P., Armold, A.D., Sullivan, E.M., Melançon, P. (1999). Gbf1: A Novel Golgi-Associated Bfa-Resistant Guanine Nucleotide Exchange Factor That Displays Specificity for Adp-Ribosylation Factor 5. Journal of Cell Biology 146, 71–84.

Codd, A., Teuscher, F., Kyle, D.E., Cheng, Q., Gatton, M.L. (2011). Artemisinin-induced parasite dormancy: a plausible mechanism for treatment failure. Malar J 10, 56.

Cohen, L.A., Donaldson, J.G., 2010. Analysis of Arf GTP-Binding Protein Function in Cells. Current Protocols in Cell Biology 48, 14.12.1-14.12.17.

Collins, B.M., Watson, P.J., Owen, D.J. (2003). The Structure of the GGA1-GAT Domain Reveals the Molecular Basis for ARF Binding and Membrane Association of GGAs. Developmental Cell 4, 321–332.

Colvin, H.N., Cordy, R.J. (2020). Insights into malaria pathogenesis gained from host metabolomics. PLOS Pathogens 16, e1008930.

Combrinck, J.M., Mabotha, T.E., Ncokazi, K.K., Ambele, M.A., Taylor, D., Smith, P.J., Hoppe, H.C., Egan, T.J. (2013). Insights into the Role of Heme in the Mechanism of Action of Antimalarials. ACS Chem Biol 8, 133–137.

Cook, W. J., Smith, C. D., Senkovich, O., Holder, A. A. & Chattopadhyay, D. (2010). Structure of *Plasmodium falciparum* ADP-ribosylation factor 1. Acta Cryst. F66, 1426-1431.

Cook, W.J., Senkovich, O., Chattopadhyay, D. (2011). Structure of the catalytic domain of *Plasmodium falciparum* ARF GTPase-activating protein (ARFGAP). Acta Cryst F 67, 1339–1344.

Corrêa, A.P.S.A., Galardo, A.K.R., Lima, L.A., Câmara, D.C.P., Müller, J.N., Barroso, J.F.S., Lapouble, O.M.M., Rodovalho, C.M., Ribeiro, K.A.N., Lima, J.B.P. (2019). Efficacy of insecticides used in indoor residual spraying for malaria control: an experimental trial on various surfaces in a "test house." Malaria Journal 18, 345.

Crary, J. L. & Haldar, K. (1992). Brefeldin A inhibits protein secretion and parasite maturation in the ring stage of *Plasmodium falciparum*. Mol. Biochem. Parasitol. 53, 185-192

Croston, G.E. (2017). The utility of target-based discovery. Expert Opinion on Drug Discovery 12, 427–429.

Cukuroglu, E., Engin, H.B., Gursoy, A., Keskin, O. (2014). Hot spots in protein–protein interfaces: Towards drug discovery. Progress in Biophysics and Molecular Biology 116, 165–173.

D'Souza, J., Nderitu, D. (2021). Ethical considerations for introducing RTS,S/AS01 in countries with moderate to high *Plasmodium falciparum* malaria transmission. The Lancet Global Health 9, e1642–e1643.

D'Souza-Schorey, C., Chavrier, P. (2006). ARF proteins: roles in membrane traffic and beyond. Nat Rev Mol Cell Biol 7, 347–358.

Davis, J.E., Xie, X., Guo, J., Huang, W., Chu, W.-M., Huang, S., Teng, Y., Wu, G. (2016). ARF1 promotes prostate tumorigenesis via targeting oncogenic MAPK signaling. Oncotarget 7, 39834–39845.

Davis, T.M.E., Karunajeewa, H.A., Ilett, K.F. (2005). Artemisinin-based combination therapies for uncomplicated malaria. Med J Aust 182, 181–185.

Dhangadamajhi, G., Kar, S.K., Ranjit, M. (2010). The Survival Strategies of Malaria Parasite in the Red Blood Cell and Host Cell Polymorphisms. Malar Res Treat 2010, 973094.

Dogovski, C., Xie, S.C., Burgio, G., Bridgford, J., Mok, S., McCaw, J.M., Chotivanich, K., Kenny, S., Gnädig, N., Straimer, J., Bozdech, Z., Fidock, D.A., Simpson, J.A., Dondorp, A.M., Foote, S., Klonis, N., Tilley, L. (2015). Targeting the Cell Stress Response of *Plasmodium falciparum* to Overcome Artemisinin Resistance. PLOS Biology 13, e1002132.

Donaldson, J.G., Finazzi, D., Klausner, R.D. (1992). Brefeldin A inhibits Golgi membrane-catalysed exchange of guanine nucleotide onto ARF protein. Nature 360, 350–352.

Donaldson, J.G., Jackson, C.L. (2011). ARF family G proteins and their regulators: roles in membrane transport, development and disease. Nature Reviews Molecular Cell Biology 12, 362–375.

Doray, B., Misra, S., Qian, Y., Brett, T.J., Kornfeld, S. (2012). Do GGA adaptors bind internal DXXLL motifs? Traffic 13, 1315–1325.

Eaton, L. (2009). Mefloquine has more adverse effects than other drugs for malaria prophylaxis. BMJ, 339 (oct13 2), pp.4167-4167.

Fairhurst, R.M., Dondorp, A.M. (2016). Artemisinin-resistant *Plasmodium falciparum* malaria. Microbiol Spectr 4, 10.1128/microbiolspec.EI10-0013–2016.

Feng, Y., Wang, Q., Wang, T. (2017). Drug Target Protein-Protein Interaction Networks: A Systematic Perspective. BioMed Research International 2017, e1289259.

Fiedler, K., Veit, M., Stamnes, M.A., Rothman, J.E. (1996). Bimodal interaction of coatomer with the p24 family of putative cargo receptors. Science 273, 1396–1399.

Foley, M., Tilley, L. (1997). Quinoline antimalarials: Mechanisms of action and resistance. International Journal for Parasitology, Australian and New Zealand Societies for Parasitology Scientific Meeting 27, 231–240.

Frigerio, G., Grimsey, N., Dale, M., Majoul, I., Duden, R. (2007). Two human ARFGAPs associated with COP-I-coated vesicles. Traffic 8, 1644–1655.

Galloway, C.A., Sowden, M.P., Smith, H.C. (2003). Increasing the Yield of Soluble Recombinant Protein Expressed in *E. coli* by Induction during Late Log Phase. BioTechniques 34, 524–530.

Gamo, F., Sanz, L., Vidal, J., de Cozar, C., Alvarez, E., Lavandera, J., Vanderwall, D., Green, D., Kumar, V., Hasan, S., Brown, J., Peishoff, C., Cardon, L. and Garcia-Bustos, J. (2010). Thousands of chemical starting points for antimalarial lead identification. Nature, 465(7296), pp.305-310.

Ghosh, D.K., Kumar, A., Ranjan, A. (2021). Cellular targets of mefloquine. Toxicology 464, 152995.

Gillingham, A.K., Munro, S. (2007). The small G proteins of the Arf family and their regulators. Annu Rev Cell Dev Biol 23, 579–611.

Goldberg, D.E., Slater, A.F.G. (1992). The pathway of hemoglobin degradation in malaria parasites. Parasitology Today 8, 280–283.

Goldberg, J. (1998). Structural basis for activation of ARF GTPase: mechanisms of guanine nucleotide exchange and GTP-myristoyl switching. Cell 95, 237–248.

Goody, P.R. (2016). Intrinsic protein fluorescence assays for GEF, GAP and post-translational modifications of small GTPases. Anal Biochem 515, 22–25.

Gu, G., Chen, Y., Duan, C., Zhou, L., Chen, C., Chen, J., Cheng, J., Shi, N., Jin, Y., Xi, Q., Zhong, J. (2017). Overexpression of ARF1 is associated with cell proliferation and migration through PI3K signal pathway in ovarian cancer. Oncology Reports 37, 1511–1520.

Guan, X. (2015). Cancer metastases: challenges and opportunities. Acta Pharm Sin B 5, 402–418.

Gunjan, S., Singh, S.K., Sharma, T., Dwivedi, H., Chauhan, B.S., Imran Siddiqi, M., Tripathi, R. (2016). Mefloquine induces ROS mediated programmed cell death in malaria parasite: *Plasmodium*. Apoptosis 21, 955–964.

Gurwitz, D. (2009). Malaria drugs: clues from malaria resistance genetics. Drug Development Research

Hafner, M., Schmitz, A., Grüne, I., Srivatsan, S.G., Paul, B., Kolanus, W., Quast, T., Kremmer, E., Bauer, I., Famulok, M. (2006). Inhibition of cytohesins by SecinH3 leads to hepatic insulin resistance. Nature 444, 941–944.

Haldar, K., Bhattacharjee, S., Safeukui, I. (2018). Drug resistance in *Plasmodium*. Nat Rev Microbiol 16, 156–170.

Haldar, K., Mohandas, N. (2009). Malaria, erythrocytic infection, and anemia. Hematology Am Soc Hematol Educ Program 87–93.

Han, Y.S., Thompson, J., Kafatos, F.C., Barillas-Mury, C. (2000). Molecular interactions between Anopheles stephensi midgut cells and *Plasmodium* berghei: the time bomb theory of ookinete invasion of mosquitoes. EMBO J 19, 6030–6040.

Hashimoto, S., Onodera, Y., Hashimoto, A., Tanaka, M., Hamaguchi, M., Yamada, A., Sabe, H. (2004). Requirement for Arf6 in breast cancer invasive activities. Proc Natl Acad Sci U S A 101, 6647–6652.

Helms, J.B., Rothman, J.E., 1992. Inhibition by brefeldin A of a Golgi membrane enzyme that catalyses exchange of guanine nucleotide bound to ARF. Nature 360, 352–354.

Herraiz, T., Guillén, H., González-Peña, D., Arán, V.J., 2019. Antimalarial Quinoline Drugs Inhibit β-Hematin and Increase Free Hemin Catalyzing Peroxidative Reactions and Inhibition of Cysteine Proteases. Sci Rep 9, 15398.

Hirst, J., Lindsay, M.R., Robinson, M.S. (2001). GGAs: roles of the different domains and comparison with AP-1 and clathrin. Mol Biol Cell 12, 3573–3588.

Hongu, T., Yamauchi, Y., Funakoshi, Y., Katagiri, N., Ohbayashi, N., Kanaho, Y. (2016). Pathological functions of the small GTPase Arf6 in cancer progression: Tumor angiogenesis and metastasis. Small GTPases 7, 47–53.

Ibraheem, Z., Abd Majid, R., Noor, S., Sedik, H. and Basir, R. (2014). Role of Different Pfcrt and Pfmdr-1 Mutations in Conferring Resistance to Antimalaria Drugs in *Plasmodium falciparum*. Malaria Research and Treatment, 2014, pp.1-17.

Jackson, C.L. (2014). Arf Proteins and Their Regulators: At the Interface Between Membrane Lipids and the Protein Trafficking Machinery. Ras Superfamily Small G Proteins: Biology and Mechanisms 2 151–180.

Jelínková, L., Jhun, H., Eaton, A., Petrovsky, N., Zavala, F., Chackerian, B., 2021. An epitope-based malaria vaccine targeting the junctional region of circumsporozoite protein. Vaccines 6, 1–10.

Josling, G.A., Llinás, M. (2015). Sexual development in *Plasmodium* parasites: knowing when it's time to commit. Nat Rev Microbiol 13, 573–587.

Kahn, R.A., Bruford, E., Inoue, H., Logsdon, J.M., Jr., Nie, Z., Premont, R.T., Randazzo, P.A., Satake, M., Theibert, A.B., Zapp, M.L., Cassel, D. (2008). Consensus nomenclature for the human ArfGAP domain-containing proteins. Journal of Cell Biology 182, 1039–1044.

Kapishnikov, S., Staalsø, T., Yang, Y., Lee, J., Pérez-Berná, A.J., Pereiro, E., Yang, Y., Werner, S., Guttmann, P., Leiserowitz, L., Als-Nielsen, J. (2019). Mode of action of quinoline antimalarial drugs in red blood cells infected by *Plasmodium falciparum* revealed in vivo. Proceedings of the National Academy of Sciences 116, 22946–22952.

Keiser, J., Singer, B.H., Utzinger, J. (2005). Reducing the burden of malaria in different eco-epidemiological settings with environmental management: a systematic review. The Lancet Infectious Diseases 5, 695–708.

Khan, A.R., Ménétrey, J. (2013). Structural Biology of Arf and Rab GTPases' Effector Recruitment and Specificity. Structure 21, 1284–1297.

Killeen, G.F., Masalu, J.P., Chinula, D., Fotakis, E.A., Kavishe, D.R., Malone, D., Okumu, F. (2017). Control of Malaria Vector Mosquitoes by Insecticide-Treated Combinations of Window Screens and Eave Baffles. Emerg Infect Dis 23, 782–789.

Klonis, N., Crespo-Ortiz, M.P., Bottova, I., Abu-Bakar, N., Kenny, S., Rosenthal, P.J., Tilley, L. (2011). Artemisinin activity against *Plasmodium falciparum* requires hemoglobin uptake and digestion. PNAS 108, 11405–11410.

Knizhnik, A.V., Kovaleva, O.V., Laktionov, K.K., Mochalnikova, V.V., Komelkov, A.V., Tchevkina, E.M., Zborovskaya, I.B. (2011). Arf6, RalA, and BIRC5 protein expression in nonsmall cell lung cancer. Mol Biol 45, 275–282.

Kumar, S., Bhardwaj, T.R., Prasad, D.N., Singh, R.K., 2018. Drug targets for resistant malaria: Historic to future perspectives. Biomedicine & Pharmacotherapy 104, 8–27.

Laishram, D.D., Sutton, P.L., Nanda, N., Sharma, V.L., Sobti, R.C., Carlton, J.M., Joshi, H. (2012). The complexities of malaria disease manifestations with a focus on asymptomatic malaria. Malaria Journal 11, 29.

Lancet, T. (2021). Malaria vaccine approval: a step change for global health. The Lancet 398, 1381.

Larson, B. (2019). Origin of Two Most Virulent Agents of Human Malaria: *Plasmodium falciparum* and *Plasmodium vivax*, Malaria.

Larsson, D., Lövborg, H., Rickardson, L., Larsson, R., Oberg, K., Granberg, D., 2006. Identification and evaluation of potential anti-cancer drugs on human neuroendocrine tumor cell lines. Anticancer research 26, 4125–9.

Laurens, M.B. (2020). RTS,S/AS01 vaccine (Mosquirix™): an overview. Human Vaccines & Immunotherapeutics 16, 480–489.

Leber, W., Skippen, A., Fivelman, Q. L., Bowyer, P. W., Cockroft, S. & Baker, D. A. (2009). A unique phosphatidylinositol 4-phosphate 5-kinase is activated by ADP-ribosylation factor in *Plasmodium falciparum*. Int. J. Parasitol. 39, 654-653.

Lee, F., Patton, W., Yi Lin, C., Moss, J., Vaughan, M., Goldman, N. and Syin, C. (1997). Identification and characterization of an ADP-ribosylation factor in *Plasmodium falciparum*. Molecular and Biochemical Parasitology, 87(2), pp.217-223.

Lee, M.C.S., Miller, E.A., Goldberg, J., Orci, L., Schekman, R. (2004). Bi-directional protein transport between the ER and Golgi. Annu Rev Cell Dev Biol 20, 87–123.

Levi, S., Rawet, M., Kliouchnikov, L., Parnis, A., Cassel, D., (2008). Topology of Amphipathic Motifs Mediating Golgi Localization in ArfGAP1 and Its Splice Isoforms *. Journal of Biological Chemistry 283, 8564–8572.

Li, R., Peng, C., Zhang, X., Wu, Y., Pan, S. and Xiao, Y. (2017). Roles of Arf6 in cancer cell invasion, metastasis and proliferation. Life Sciences, 182, pp.80-84.

Liu, Y., Kahn, R.A., Prestegard, J.H. (2010). Dynamic structure of membrane-anchored Arf•GTP. Nat Struct Mol Biol 17, 876–881.

Lohi, O., Poussu, A., Mao, Y., Quiocho, F., Lehto, V.-P. (2002). VHS domain – a longshoreman of vesicle lines. FEBS Letters, Protein Domains 513, 19–23.

Lu, H., Zhou, Q., He, J., Jiang, Z., Peng, C., Tong, R., Shi, J. (2020). Recent advances in the development of protein–protein interactions modulators: mechanisms and clinical trials. Sig Transduct Target Ther 5, 1–23.

Luchsinger, C., Aguilar, M., Burgos, P.V., Ehrenfeld, P., Mardones, G.A. (2018). Functional disruption of the Golgi apparatus protein ARF1 sensitizes MDA-MB-231 breast cancer cells to the antitumor drugs Actinomycin D and Vinblastine through ERK and AKT signaling. PLoS One 13, e0195401.

Lui, W.W.Y., Collins, B.M., Hirst, J., Motley, A., Millar, C., Schu, P., Owen, D.J., Robinson, M.S. (2003). Binding Partners for the COOH-Terminal Appendage Domains of the GGAs and γ-Adaptin. Mol Biol Cell 14, 2385–2398.

Lundmark, R., Doherty, G.J., Vallis, Y., Peter, B.J., McMahon, H.T. (2008). Arf family GTP loading is activated by, and generates, positive membrane curvature. Biochemical Journal 414, 189–194.

Lundquist, E.A. (2006). Small GTPases. WormBook 1–18.

Mabonga, L., Kappo, A.P. (2019). Protein-protein interaction modulators: advances, successes and remaining challenges. Biophys Rev 11, 559–581.

Martin, R.E., Kirk, K. (2004). The malaria parasite's chloroquine resistance transporter is a member of the drug/metabolite transporter superfamily. Mol Biol Evol 21, 1938–1949.

Martins, A.C., Paoliello, M.M.B., Docea, A.O., Santamaria, A., Tinkov, A.A., Skalny, A.V., Aschner, M. (2021). Review of the mechanism underlying mefloquine-induced neurotoxicity. Crit Rev Toxicol 51, 209–216.

Mbacham, W.F., Ayong, L., Guewo-Fokeng, M., Makoge, V. (2019). Current Situation of Malaria in Africa, in: Ariey, F., Gay, F., Ménard, R. (Eds.), Malaria Control and Elimination, Methods in Molecular Biology. Springer, New York, NY, pp. 29–44.

Mbengue, A., Bhattacharjee, S., Pandharkar, T., Liu, H., Estiu, G., Stahelin, R.V., Rizk, S.S., Njimoh, D.L., Ryan, Y., Chotivanich, K., Nguon, C., Ghorbal, M., Lopez-Rubio, J.-J., Pfrender, M., Emrich, S., Mohandas, N., Dondorp, A.M., Wiest, O., Haldar, K. (2015). A molecular mechanism of artemisinin resistance in Plasmodium falciparum malaria. Nature 520, 683–687.

Mbugi, E.V., Mutayoba, B.M., Malisa, A.L., Balthazary, S.T., Nyambo, T.B., Mshinda, H. (2006). Drug resistance to sulphadoxine-pyrimethamine in Plasmodium falciparum malaria in Mlimba, Tanzania. Malaria Journal 5, 94.

Menard, D., Koula, M., Talarmin, A., Madji, N., Manirakiza, A. And Djalle, D. (2005). Efficacy of Chloroquine, Amodiaquine, Sulfadoxine-Pyrimethamine, Chloroquine-Sulfadoxine-Pyrimethamine combination, and Amodiaquine-Sulfadoxine-Pyrimethamine combination in central African children with noncomplicated malaria. The American Journal of Tropical Medicine and Hygiene, 72(5), pp.581-585.

Meshnick, S. (2002). Artemisinin: mechanisms of action, resistance and toxicity. International Journal for Parasitology, 32(13), pp.1655-1660.

Mesmin, B., Drin, G., Levi, S., Rawet, M., Cassel, D., Bigay, J., Antonny, B. (2007). Two lipid-packing sensor motifs contribute to the sensitivity of ArfGAP1 to membrane curvature. Biochemistry 46, 1779–1790.

Miller, G.J., Mattera, R., Bonifacino, J.S., Hurley, J.H. (2003). Recognition of accessory protein motifs by the γ-adaptin ear domain of GGA3. Nature Structural & Molecular Biology 10, 599–606.

Miller, L.H., Baruch, D.I., Marsh, K., Doumbo, O.K. (2002). The pathogenic basis of malaria. Nature 415, 673–679.

Mondal, S., Hsiao, K., Goueli, S.A. (2015). A Homogenous Bioluminescent System for Measuring GTPase, GTPase Activating Protein, and Guanine Nucleotide Exchange Factor Activities. Assay and Drug Development Technologies 13, 444–455.

Moorthy, V.S., Okwo-Bele, J.-M. (2015). Final results from a pivotal phase 3 malaria vaccine trial. The Lancet 386, 5–7.

Morgan, C., Lewis, P.D., Hopkins, L., Burnell, S., Kynaston, H., Doak, S.H. (2015). Increased expression of ARF GTPases in prostate cancer tissue. SpringerPlus 4, 342.

Morishige, M., Hashimoto, S., Ogawa, E., Toda, Y., Kotani, H., Hirose, M., Wei, S., Hashimoto, A., Yamada, A., Yano, H., Mazaki, Y., Kodama, H., Nio, Y., Manabe, T., Wada, H., Kobayashi, H., Sabe, H. (2008). GEP100 links epidermal growth factor receptor signalling to Arf6 activation to induce breast cancer invasion. Nat Cell Biol 10, 85–92.

Mota, M.M., Pradel, G., Vanderberg, J.P., Hafalla, J.C.R., Frevert, U., Nussenzweig, R.S., Nussenzweig, V., Rodríguez, A. (2001). Migration of *Plasmodium* Sporozoites Through Cells Before Infection. Science.

Müller, I. and Hyde, J. (2010). Antimalarial drugs: modes of action and mechanisms of parasite resistance. Future Microbiology, 5(12), pp.1857-1873.

Müller, M.P., Goody, R.S. (2017). Molecular control of Rab activity by GEFs, GAPs and GDI. Small GTPases 9, 5–21.

Mutabingwa, T.K. (2005). Artemisinin-based combination therapies (ACTs): Best hope for malaria treatment but inaccessible to the needy! Acta Tropica, Malaria Research in Africa - Multilateral Initiative on Malaria 95, 305–315.

Mwai, L., Ochong, E., Abdirahman, A., Kiara, S., Ward, S., Kokwaro, G., Sasi, P., Marsh, K., Borremann, S., Mackinnon, M., Nzila, A. (2009). Chloroquine resistance before and after its withdrawal in Kenya. *Malar J* **8**, 106.

Nawrotek, A., Zeghouf, M., Cherfils, J. (2016). Allosteric regulation of Arf GTPases and their GEFs at the membrane interface. Small GTPases 7, 283–296.

Nie, Z. (2006). Arf GAPs and membrane traffic. Journal of Cell Science, 119(7), pp.1203-1211.

Nogi, T., Shiba, Y., Kawasaki, M., Shiba, T., Matsugaki, N., Igarashi, N., Suzuki, M., Kato, R., Takatsu, H., Nakayama, K., Wakatsuki, S. (2002). Structural basis for the accessory protein recruitment by the gamma-adaptin ear domain. Nat Struct Biol 9, 527–531.

O'Neill, P., Barton, V. and Ward, S. (2010). The Molecular Mechanism of Action of Artemisinin—The Debate Continues. Molecules, 15(3), pp.1705-1721.

O'Neill, P.M., Bray, P.G., Hawley, S.R., Ward, S.A., Park, B.K. (1998). 4-Aminoquinolines—Past, present, and future; A chemical perspective. Pharmacology & Therapeutics 77, 29–58.

Ohashi, Y., Iijima, H., Yamaotsu, N., Yamazaki, K., Sato, S., Okamura, M., Sugimoto, K., Dan, S., Hirono, S., Yamori, T., (2012). AMF-26, a Novel Inhibitor of the Golgi System, Targeting ADP-ribosylation Factor 1 (Arf1) with Potential for Cancer Therapy. J Biol Chem 287, 3885–3897.

Olafson, K.N., Ketchum, M.A., Rimer, J.D., Vekilov, P.G. (2015). Mechanisms of hematin crystallization and inhibition by the antimalarial drug chloroquine. Proceedings of the National Academy of Sciences 112, 4946–4951.

Ooi, C.E., Dell'Angelica, E.C., Bonifacino, J.S. (1998). ADP-Ribosylation Factor 1 (ARF1) Regulates Recruitment of the AP-3 Adaptor Complex to Membranes. Journal of Cell Biology 142, 391–402.

Osaka, N., Hirota, Y., Ito, D., Ikeda, Y., Kamata, R., Fujii, Y., Chirasani, V., Campbell, S., Takeuchi, K., Senda, T., Sasaki, A. (2021). Divergent Mechanisms Activating RAS and Small GTPases Through Post-translational Modification. Frontiers in Molecular Biosciences 8.

Owoloye, A., Olufemi, M., Idowu, E.T., Oyebola, K.M. (2021). Prevalence of potential mediators of artemisinin resistance in African isolates of Plasmodium falciparum. Malaria Journal 20, 451.

Pacheco-Rodriguez, G., Moss, J., Vaughan, M. (2002). BIG1 and BIG2: brefeldin A-inhibited guanine nucleotide-exchange proteins for ADP-ribosylation factors. Methods Enzymol 345, 397–404.

Paek, S.-M. (2018). Recent Synthesis and Discovery of Brefeldin A Analogs. Mar Drugs 16, 133.

Paloque, L., Ramadani, A.P., Mercereau-Puijalon, O., Augereau, J.-M., Benoit-Vical, F. (2016). Plasmodium falciparum: multifaceted resistance to artemisinins. Malaria Journal 15, 149.

Pan, J.Y., Sanford, J.C., Wessling-Resnick, M. (1995). Effect of Guanine Nucleotide Binding on the Intrinsic Tryptophan Fluorescence Properties of Rab5. Journal of Biological Chemistry 270, 24204–24208.

Park, S.Y., Guo, X. (2014). Adaptor protein complexes and intracellular transport. Biosci Rep 34, e00123.

Pearson, R.D., Hewlett, E.L. (1987). Use of Pyrimethamine-Sulfadoxine (Fansidar) in Prophylaxis Against Chloroquine-Resistant Plasmodium falciparum and Pneumocystis carinii. Ann Intern Med 106, 714–718.

Pennetier, C., Costantini, C., Corbel, V., Licciardi, S., Dabiré, R.K., Lapied, B., Chandre, F., Hougard, J.-M. (2008). Mixture for Controlling Insecticide-Resistant Malaria Vectors. Emerg Infect Dis 14, 1707–1714.

Petersen, I., Eastman, R., Lanzer, M. (2011). Drug-resistant malaria: Molecular mechanisms and implications for public health. FEBS Letters, Turin Special Issue: Biochemistry for Tomorrow's Medicine 585, 1551–1562.

Peyroche, A., Antonny, B., Robineau, S., Acker, J., Cherfils, J., Jackson, C.L. (1999). Brefeldin A Acts to Stabilize an Abortive ARF–GDP–Sec7 Domain Protein Complex: Involvement of Specific Residues of the Sec7 Domain. Molecular Cell 3, 275–285.

Phillips, L.R., Wolfe, T.L., Malspeis, L., Supko, J.G. (1998). Analysis of brefeldin A and the prodrug breflate in plasma by gas chromatography with mass selective detection. J Pharm Biomed Anal 16, 1301–1309.

Pimenta, P.F., Touray, M., Miller, L. (1994). The journey of malaria sporozoites in the mosquito salivary gland. J Eukaryot Microbiol 41, 608–624.

Pou, S., Winter, R.W., Nilsen, A., Kelly, J.X., Li, Y., Doggett, J.S., Riscoe, E.W., Wegmann, K.W., Hinrichs, D.J., Riscoe, M.K. (2012). Sontochin as a guide to the development of drugs against chloroquine-resistant malaria. Antimicrob Agents Chemother 56, 3475–3480.

Puertollano, R., Randazzo, P.A., Presley, J.F., Hartnell, L.M., Bonifacino, J.S. (2001). The GGAs Promote ARF-Dependent Recruitment of Clathrin to the TGN. Cell 105, 93–102.

Quax, T.E.F., Claassens, N.J., Söll, D., van der Oost, J. (2015). Codon Bias as a Means to Fine-Tune Gene Expression. Mol Cell 59, 149–161.

Quiñones, M.L., Norris, D.E., Conn, J.E., Moreno, M., Burkot, T.R., Bugoro, H., Keven, J.B., Cooper, R., Yan, G., Rosas, A., Palomino, M., Donnelly, M.J., Mawejje, H.D., Eapen, A., Montgomery, J., Coulibaly, M.B., Beier, J.C., Kumar, A. (2015). Insecticide Resistance in Areas under Investigation by the International Centers of Excellence for Malaria Research: A Challenge for Malaria Control and Elimination. Am J Trop Med Hyg 93, 69–78.

Ramasamy, R. (2014). Zoonotic Malaria – Global Overview and Research and Policy Needs. Frontiers in Public Health 2.

Reiner, D.J., Lundquist, E.A. (2018). Small GTPases, WormBook: The Online Review of *C. elegans* Biology

Ren, X., Farías, G.G., Canagarajah, B.J., Bonifacino, J.S., Hurley, J.H. (2013). Structural Basis for Recruitment and Activation of the AP-1 Clathrin Adaptor Complex by Arf1. Cell 152, 755–767.

Richardson, B.C., Fromme, J.C., (2015). Biochemical methods for studying kinetic regulation of Arf1 activation by Sec7. Methods Cell Biol 130, 101–126.

Rosano, G.L., Ceccarelli, E.A. (2009). Rare codon content affects the solubility of recombinant proteins in a codon bias-adjusted *Escherichia coli* strain. Microbial Cell Factories 8, 41.

Sáenz, J.B., Sun, W.J., Chang, J.W., Li, J., Bursulaya, B., Gray, N.S., Haslam, D.B. (2009). Golgicide A reveals essential roles for GBF1 in Golgi assembly and function. Nat Chem Biol 5, 157–165.

Samarasekera, U. (2021). Cautious optimism for malaria vaccine roll-out. The Lancet 398, 1394.

Sato, S. (2021). *Plasmodium*-a brief introduction to the parasites causing human malaria and their basic biology. J Physiol Anthropol 40, 1.

Sawyer, A. (2020). Developing drugs for the 'undruggable.' BioTechniques 69, 239–241.

Sayang, C., Gausseres, M., Vernazza-Licht, N., Malvy, D., Bley, D., Millet, P. (2009). Treatment of malaria from monotherapy to artemisinin-based combination therapy by health professionals in rural health facilities in southern Cameroon. Malar J 8, 174.

Scheffzek, K., Ahmadian, M.R., Kabsch, W., Wiesmüller, L., Lautwein, A., Schmitz, F., Wittinghofer, A. (1997). The Ras-RasGAP complex: structural basis for GTPase activation and its loss in oncogenic Ras mutants. Science 277, 333–338.

Schuster, F.L. (2002). Cultivation of *Plasmodium* spp. Clin Microbiol Rev 15, 355–364.

Schlager, B., Straessle, A., Hafen, E. (2012). Use of anionic denaturing detergents to purify insoluble proteins after overexpression. BMC Biotechnology 12, 95.

Seidel, R., Amor, J., Kahn, R., Prestegard, J. (2004). Conformational Changes in Human Arf1 on Nucleotide Exchange and Deletion of Membrane-binding Elements. The Journal of biological chemistry 279, 48307–18

Severe *falciparum* malaria. World Health Organization, Communicable Diseases Cluster. (2000). Transactions of the Royal Society of Tropical Medicine and Hygiene 94 Suppl 1, S1-90.

Shandilya, A., Chacko, S., Jayaram, B., Ghosh, I. (2013). A plausible mechanism for the antimalarial activity of artemisinin: A computational approach. Sci Rep 3, 2513.

Shiba, T., Kawasaki, M., Takatsu, H., Nogi, T., Matsugaki, N., Igarashi, N., Suzuki, M., Kato, R., Nakayama, K., Wakatsuki, S. (2003). Molecular mechanism of membrane recruitment of GGA by ARF in lysosomal protein transport. Nature Structural & Molecular Biology 10, 386–393.

Shibeshi, M.A., Kifle, Z.D., Atnafie, S.A. (2020). Antimalarial Drug Resistance and Novel Targets for Antimalarial Drug Discovery. Infect Drug Resist 13, 4047–4060.

Sidhu, A., Uhlemann, A., Valderramos, S., Valderramos, J., Krishna, S. and Fidock, D. (2006). Decreasingpfmdr1Copy Number inPlasmodium falciparumMalaria Heightens Susceptibility to Mefloquine, Lumefantrine, Halofantrine, Quinine, and Artemisinin. The Journal of Infectious Diseases, 194(4), pp.528-535.

Singh, M.K., Gao, H., Sun, W., Song, Z., Schmalzigaug, R., Premontand, R.T., Zhang, Q. (2015). Structure-activity Relationship Studies of QS11, a Small Molecule Wnt Synergistic Agonist. Bioorg Med Chem Lett 25, 4838–4842.

Sinka, M.E., Bangs, M.J., Manguin, S., Rubio-Palis, Y., Chareonviriyaphap, T., Coetzee, M., Mbogo, C.M., Hemingway, J., Patil, A.P., Temperley, W.H., Gething, P.W., Kabaria, C.W., Burkot, T.R., Harbach, R.E., Hay, S.I. (2012). A global map of dominant malaria vectors. Parasites & Vectors 5, 69.

Slater, A.F. (1993). Chloroquine: mechanism of drug action and resistance in *Plasmodium falciparum*. Pharmacol Ther 57, 203–235.

Stafford, W., Stockley, R., Ludbrook, S. and Holder, A. (1996). Isolation, Expression and Characterization of the Gene for an ADP-Ribosylation Factor from the Human Malaria Parasite, *Plasmodium falciparum*. European Journal of Biochemistry, 242(1), pp.104-113.

Stoddart, L.A., White, C.W., Nguyen, K., Hill, S.J., Pfleger, K.D.G. (2016). Fluorescence- and bioluminescence-based approaches to study GPCR ligand binding. Br J Pharmacol 173, 3028–3037.

Straimer, J., Gnädig, N.F., Witkowski, B., Amaratunga, C., Duru, V., Ramadani, A.P., Dacheux, M., Khim, N., Zhang, L., Lam, S., Gregory, P.D., Urnov, F.D., Mercereau-Puijalon, O., Benoit-Vical, F., Fairhurst, R.M., Ménard, D., Fidock, D.A. (2015). K13-propeller mutations confer artemisinin resistance in *Plasmodium falciparum* clinical isolates. Science 347, 428–431.

Su, X., Miller, L.H. (2015). The discovery of artemisinin and Nobel Prize in Physiology or Medicine. Sci China Life Sci 58, 1175–1179.

Sullivan, D.J., Gluzman, I.Y., Russell, D.G., Goldberg, D.E. (1996). On the molecular mechanism of chloroquine's antimalarial action. PNAS 93, 11865–11870.

Sullivan, D.J., Matile, H., Ridley, R.G., Goldberg, D.E. (1998). A Common Mechanism for Blockade of Heme Polymerization by Antimalarial Quinolines*. Journal of Biological Chemistry 273, 31103–31107.

Sun, W., Vanhooke, J., Sondek, J. and Zhang, Q. (2011). High-Throughput Fluorescence Polarization Assay for the Enzymatic Activity of GTPase-Activating Protein of ADP-Ribosylation Factor (ARFGAP). Journal of Biomolecular Screening, 16(7), pp.717-723.

Swart, T., Khan, F.D., Ntlantsana, A., Laming, D., Veale, C.G.L., Przyborski, J.M., Edkins, A.L., Hoppe, H.C. (2020). Detection of the in vitro modulation of *Plasmodium falciparum* Arf1 by Sec7 and ArfGAP domains using a colorimetric plate-based assay. Sci Rep 10, 4193.

Sztul, E., Chen, P.-W., Casanova, J.E., Cherfils, J., Dacks, J.B., Lambright, D.G., Lee, F.-J.S., Randazzo, P.A., Santy, L.C., Schürmann, A., Wilhelmi, I., Yohe, M.E., Kahn, R.A. (2019). ARF GTPases and their GEFs and GAPs: concepts and challenges. Mol Biol Cell 30, 1249–1271.

Sztul, E., Chen, P.-W., Casanova, J.E., Cherfils, J., Dacks, J.B., Lambright, D.G., Lee, F.-J.S., Randazzo, P.A., Santy, L.C., Schürmann, A., Wilhelmi, I., Yohe, M.E., Kahn, R.A. (2019). ARF GTPases and their GEFs and GAPs: concepts and challenges. MBoC 30, 1249–1271.

Takatsu, H., Yoshino, K., Toda, K., Nakayama, K. (2002). GGA proteins associate with Golgi membranes through interaction between their GGAH domains and ADP-ribosylation factors. Biochem J 365, 369–378.

Takatsu, H., Yoshino, K., Toda, K., Nakayama, K. (2002). GGA proteins associate with Golgi membranes through interaction between their GGAH domains and ADP-ribosylation factors. Biochem J 365, 369–378.

Targett, G. (2015). Phase 3 trial with the RTS,S/AS01 malaria vaccine shows protection against clinical and severe malaria in infants and children in Africa. BMJ Evidence-Based Medicine 20, 9–9.

Tilley, L., Straimer, J., Gnädig, N.F., Ralph, S.A., Fidock, D.A. (2016). Artemisinin action and resistance in *Plasmodium falciparum*. Trends Parasitol 32, 682–696.

Tizifa, T.A., Kabaghe, A.N., McCann, R.S., van den Berg, H., Van Vugt, M., Phiri, K.S. (2018). Prevention Efforts for Malaria. Curr Trop Med Rep 5, 41–50.

Toé, K.H., Jones, C.M., N'Fale, S., Ismail, H.M., Dabiré, R.K., Ranson, H. (2014). Increased Pyrethroid Resistance in Malaria Vectors and Decreased Bed Net Effectiveness, Burkina Faso. Emerg Infect Dis 20, 1691–1696.

Toda, T., Watanabe, M., Kawato, J., Kadin, M.E., Higashihara, M., Kunisada, T., Umezawa, K., Horie, R. (2015). Brefeldin A exerts differential effects on anaplastic lymphoma kinase positive anaplastic large cell lymphoma and classical Hodgkin lymphoma cell lines. Br J Haematol 170, 837–846.

Toma-Fukai, S., Shimizu, T. (2019). Structural Insights into the Regulation Mechanism of Small GTPases by GEFs. Molecules 24, 3308.

Tuteja, R. (2007). Malaria − an overview. The FEBS Journal 274, 4670–4679.

Van Acker, T., Tavernier, J., Peelman, F. (2019). The Small GTPase Arf6: An Overview of Its Mechanisms of Action and of Its Role in Host–Pathogen Interactions and Innate Immunity. Int J Mol Sci 20, 2209.

von Einem, B., Wahler, A., Schips, T., Serrano-Pozo, A., Proepper, C., Boeckers, T.M., Rueck, A., Wirth, T., Hyman, B.T., Danzer, K.M., Thal, D.R., von Arnim, C.A.F. (2015). The Golgi-Localized γ-Ear-Containing ARF-Binding (GGA) Proteins Alter Amyloid-β Precursor Protein (APP) Processing through Interaction of Their GAE Domain with the Beta-Site APP Cleaving Enzyme 1 (BACE1). PLoS One 10, e0129047.

Wang, J., Xu, C., Lun, Z.-R., Meshnick, S.R. (2017). Unpacking 'Artemisinin Resistance.' Trends in Pharmacological Sciences 38, 506–511.

Wang, J., Zhang, C.-J., Chia, W.N., Loh, C.C.Y., Li, Z., Lee, Y.M., He, Y., Yuan, L.-X., Lim, T.K., Liu, M., Liew, C.X., Lee, Y.Q., Zhang, J., Lu, N., Lim, C.T., Hua, Z.-C., Liu, B., Shen, H.-M., Tan, K.S.W., Lin, Q. (2015). Haem-activated promiscuous targeting of artemisinin in *Plasmodium falciparum*. Nat Commun 6, 10111.

West, P.A., Protopopoff, N., Wright, A., Kivaju, Z., Tigererwa, R., Mosha, F.W., Kisinza, W., Rowland, M., Kleinschmidt, I. (2014). Indoor Residual Spraying in Combination with Insecticide-Treated Nets Compared to Insecticide-Treated Nets Alone for Protection against Malaria: A Cluster Randomised Trial in Tanzania. PLOS Medicine 11, e1001630.

Westrip, C.A.E., Zhuang, Q., Hall, C., Eaton, C.D., Coleman, M.L. (2021). Developmentally regulated GTPases: structure, function and roles in disease. Cell. Mol. Life Sci. 78, 7219–7235.

World Health Organization. (2021). World malaria report 2021.

Wiek, S., Cowman, A.F., Lingelbach, K. (2004). Double cross-over gene replacement within the sec 7 domain of a GDP-GTP exchange factor from *Plasmodium falciparum* allows the generation of a transgenic brefeldin A-resistant parasite line. Mol Biochem Parasitol 138, 51–55.

Witkowski, B., Amaratunga, C., Khim, N., Sreng, S., Chim, P., Kim, S., Lim, P., Mao, S., Sopha, C., Sam, B., Anderson, J.M., Duong, S., Chuor, C.M., Taylor, W.R.J., Suon, S., Mercereau-Puijalon, O., Fairhurst, R.M., Menard, D. (2013). Novel phenotypic assays for the detection of artemisinin-resistant *Plasmodium falciparum* malaria in Cambodia: in-vitro and ex-vivo drug-response studies. The Lancet Infectious Diseases 13, 1043–1049.

Witkowski, B., Lelièvre, J., Barragán, M.J.L., Laurent, V., Su, X., Berry, A., Benoit-Vical, F. (2010). Increased Tolerance to Artemisinin in *Plasmodium falciparum* Is Mediated by a Quiescence Mechanism. Antimicrobial Agents and Chemotherapy.

Wong, W., Bai, X.-C., Sleebs, B.E., Triglia, T., Brown, A., Thompson, J.K., Jackson, K.E., Hanssen, E., Marapana, D.S., Fernandez, I.S., Ralph, S.A., Cowman, A.F., Scheres, S.H.W., Baum, J. (2017). The antimalarial Mefloquine targets the *Plasmodium falciparum* 80S ribosome to inhibit protein synthesis. Nat Microbiol 2, 17031.

Xu, R., Zhang, Y., Gu, L., Zheng, J., Cui, J., Dong, J., Du, J. (2015). Arf6 regulates EGF-induced internalization of E-cadherin in breast cancer cells. Cancer Cell Int 15, 11.

Yamauchi, L.M., Coppi, A., Snounou, G., Sinnis, P. (2007). *Plasmodium* sporozoites trickle out of the injection site. Cell Microbiol 9, 1215–1222.

Yang, J., He, Y., Li, Y., Zhang, X., Wong, Y.-K., Shen, S., Zhong, T., Zhang, J., Liu, Q., Wang, J. (2020). Advances in the research on the targets of anti-malaria actions of artemisinin. Pharmacology & Therapeutics, Youyou Tu 90th Birthday Tribute 216, 107697.

Yeung, S. (2018). Malaria – Update on Antimalarial Resistance and Treatment Approaches. The Pediatric Infectious Disease Journal, p.1.

Yorimitsu, T., Sato, K., Takeuchi, M. (2014). Molecular mechanisms of Sar/Arf GTPases in vesicular trafficking in yeast and plants. Frontiers in Plant Science 5.

Zeghouf, M., Guibert, B., Zeeh, J.-C., Cherfils, J. (2005). Arf, Sec7 and Brefeldin A: a model towards the therapeutic inhibition of guanine nucleotide-exchange factors. Biochem Soc Trans 33, 1265–1268.

Zhang, M., Wang, C., Otto, T., Oberstaller, J., Liao, X., Adapa, S., Udenze, K., Bronner, I., Casandra, D., Mayho, M., Brown, J., Li, S., Swanson, J., Rayner, J., Jiang, R. and Adams, J. (2018). Uncovering the essential genes of the human malaria parasite *Plasmodium falciparum* by saturation mutagenesis. Science, 360(6388).

Zhao, L., Helms, J.B., Brügger, B., Harter, C., Martoglio, B., Graf, R., Brunner, J., Wieland, F.T. (1997). Direct and GTP-dependent interaction of ADP ribosylation factor 1 with coatomer subunit β. Proc Natl Acad Sci U S A 94, 4418–4423.

Zhao, L., Helms, J.B., Brügger, B., Harter, C., Martoglio, B., Graf, R., Brunner, J., Wieland, F.T. (1997). Direct and GTP-dependent interaction of ADP ribosylation factor 1 with coatomer subunit β. Proc Natl Acad Sci U S A 94, 4418–4423.

Zhou, L., Gao, W., Wang, K., Huang, Z., Zhang, L., Zhang, Z., Zhou, J., Nice, E.C., Huang, C. (2019). Brefeldin A inhibits colorectal cancer growth by triggering Bip/Akt-regulated autophagy. The FASEB Journal 33, 5520–5534.